STEADY-STATE ANALYSIS OF DYNAMICALLY DISORDERED ASYMMETRIC SIMPLE EXCLUSION PROCESS

A Thesis

submitted in partial fulfillment of the requirements for the award of the degree of

Doctor of Philosophy

in

Mathematics

by

Shaweta Garg

Reg no: 901811004

under the supervision of

Dr. Isha Dhiman

Assistant Professor

and

Dr. Sapna Sharma

Associate Professor

THAPAR INSTITUTE
OF ENGINEERING & TECHNOLOGY
(Deemed to be University)

Department of Mathematics

Thapar Institute of Engineering and Technology
Patiala-147004, Punjab, India

January 2024

To

my parents and husband

Certificate

I hereby certify that the work, which is being presented in the thesis, entitled **"Steady-state analysis of dynamically disordered asymmetric simple exclusion process"**, in partial fulfillment of the requirements for the award of degree of *Doctor of Philosophy* in Department of Mathematics, Thapar Institute of Engineering and Technology, Patiala is an authentic record of my own work carried out during the period of degree, under the supervision of *Dr. Isha Dhiman*, and *Dr. Sapna Sharma*, Department of Mathematics, Thapar Institute of Engineering and Technology, Patiala.

Date: May 07, 2024

Shaweta Garg

Shaweta Garg

It is to certify that the above statement made by the candidate is correct and true to the best of my knowledge.

Date: May 07, 2024

Dr. Isha Dhiman

Assistant Professor

Date: 08/05/2024

Dr. Sapna Sharma

Associate Professor

Acknowledgements

First and foremost, I would like to thank almighty for granting perseverance. He has always blessed me in countless ways, for which words are short to describe. I would like to express my deepest gratitude to my honorable supervisors Dr. Isha Dhiman and Dr. Sapna Sharma for giving me the opportunity to work on this project, providing valuable guidance and feedback. I am extremely grateful to them for always being there when I needed their support, reviewing my progress constantly and continued to have faith in me over the time.

In addition, I would like to mention Dr. Mahesh Kumar Sharma, Head, SOM, Thapar Institute of Engineering and Technology, Patiala, for providing all the necessary facilities in the school. I also could not have undertaken this journey without my doctoral committee members, Dr. Kavita Goyal, Dr. Parimita Roy and Dr. Debabrata Deb, who generously provided knowledge and expertise. My sincere thanks to Dr. Harish Garg for his valueable words of motivation and help at various times during the period.

I am heartfelt to my lab mates and friends- Nishtha, Daljeet, Rajvinder and Bhavna for being a great bunch of people in and out of the lab and keeping me sane throughout the whole process. I greatly value their friendship and deeply appreciate their belief in me.

Last, but not the least, I would like to highlight truly exceptional people- my parents for supporting me spiritually throughout the entire process. Without their support and hope, this thesis would not have been possible. Special thanks to my brother- Rohit Garg, uncle- Narinder Garg and husband- Pankaj Bansal, for always being so supportive and helping me every step of the way. Their belief in me has kept my spirits and motivation high during the journey. Thank you!

Abstract

This thesis focuses primarily on comprehending the intricacies of stochastic transport systems, in motivation with the increasing scientific needs for optimized and efficient traffic. A significant number of real world processes include directed movement of particles along the lattice channels. Several randomly evolving analogous processes include traffic on highways which involve vehicle motion between different lanes and molecular motors moving along multi-lane microtubules. The motion in such processes may comprise different hopping rates and boundary conditions. The particular problem of congestion caused by dynamic defects in transport systems is gaining attraction of researchers and scientists in the growing field of statistical physics.

Totally asymmetric simple exclusion process (TASEP) belongs to a special class of the driven lattice gas model and is considered to be a paradigmatic non-equilibrium model to study stochastic transport processes. We focus to analyze collective properties of diffusive systems with open boundaries in single-channel as well as two-channel, in which the lattice is connected to boundary reservoirs at either ends. The particles obey hard-core exclusion principle, in which no two particles can occupy same lattice site. There also exists dynamic defects in the system which can stochastically bind and unbind from a lattice site with certain rates. For theoretical investigations, we adopt simple mean-field approximation theory and its variant- vertical cluster mean-field theory to derive continuum master equations. The continuum equations are solved using finite difference numerical scheme. To further validate the theoretical findings, we run extensive Monte Carlo simulation which shows a good agreement with theoretical findings. The study provides valuable insights into the underlying mechanisms of physical phenomena

in non-equilibrium and have been identified for the various models examined in this thesis.

In the first model studied in this thesis, we investigate a two-channel asymmetric simple exclusion process with site-wise dynamic disorder under symmetric and asymmetric coupling environment. The study is an extension to literature on disordered systems by analyzing a general coupled TASEP model. The model presented here well explains the hindrance in biological process of gene transcription. We made an attempt to provide a comprehensive depiction of the stationary dynamics of a disordered two-channel exclusion process. The dynamic defects obey un-constrained dynamics, which allows a defect to bind to or unbind from a lattice site regardless of particle presence. It is found that the rich topology of steady-state phase diagram differs qualitatively as well as quantitatively subject to symmetric and fully asymmetric coupling conditions.

The second model deals with a dynamically disordered TASEP model with LK. The inclusion of LK, inspite of adding more realism into the model, brings along many mathematical challenges as well. The analysis is explicitly categorized for two different values of binding constant. The competing interplay between dynamic disorder and LK discovers various non-equilibrium phenomena like phase coexistence and appearance of localised shock which otherwise are not found in ddTASEPs without LK. The shock dynamics are explored through varying defect density and defect strength.

In the last part, we study a coupled two-channel exclusion process with dynamic disorder and LK. The model is inspired from real transport situation like periodic switching of traffic lights on roads and stochastic binding of motor proteins to microtubule. The complex problem considers two different couplings- symmetric and asymmetric environments. Under symmetric coupling conditions, the two-channel ddTASEP with LK behaves similar to its analogue in single-channel. Under fully asymmetric coupling environment, the system is studied for two different values of binding constant. The rich steady-state phase diagram, due to the effect of lane-changing, shows very interesting non-equilibrium feature of mixed phases and

phase reduction. The current-density relation plot infers that the maximum current reduces with an increase in defect density. Further, we observe that the effect of coupling weakens for higher values of attachment rate, signifying LK dominance.

Keywords: Asymmetric simple exclusion process, traffic flow, mathematical modeling, driven diffusive systems, non-equilibrium, stochastic transport, single-channel, two-channel, steady-state, phase diagrams, phase transitions, Langmuir kinetics, dynamic disorder, Monte Carlo simulation, mean-field approximation, vertical cluster theory, continuum, shock, coupling constant, binding constant.

Contents

Acknowledgements iii

Abstract v

List of Figures xii

List of Tables xvii

1 Introduction 1

1.1 Stochastic processes . . . 1

1.2 Non-equilibrium systems . . . 2

1.3 Driven diffusive systems . . . 3

1.3.1 Vehicular Traffic . . . 4

1.3.2 Biological Transportation . . . 5

1.4 Driven Lattice Gas Model- Totally Asymmetric Simple Exclusion Process (TASEP) . . . 6

1.4.1 Mathematical Analysis . . . 7

1.4.1.1 Mean-field theory . . . 8

1.4.1.2 Exact Phase Diagram . . . 10

1.4.2 Monte Carlo simulation . . . 12

1.4.3 Finite-difference approximation . . . 13

1.5 Variants of TASEP . . . 14

1.5.1 Two-lane TASEP . . . 14

1.5.2 Langmuir Kinetics . . . 16

1.5.3 TASEP with dynamic disorder . . . 18

1.6 Aim and Objectives of the thesis . . . 20

1.7 Overview of the thesis 21

2 Symmetric coupling in a two-channel ddTASEP 25

2.1 Model and dynamical rules 25

2.2 Mathematical analysis 27

2.2.1 Particle density evolution 27

2.2.2 Defect density evolution 28

2.2.3 Continuum mean-field equations 28

2.2.4 Re-scaling of system parameters 29

2.2.5 Steady-state solution 31

2.2.6 Monte Carlo simulation 33

2.3 Results and Discussion 33

2.3.1 Shifting of phase boundaries 34

2.3.2 Current Analysis 36

2.3.3 Effect of lane-changing rates 39

2.3.4 Finite-size effect 39

2.4 Conclusion 40

3 Asymmetric coupling in a two-channel ddTASEP 43

3.1 Model Description 44

3.1.1 Definition of the dynamical rules 44

3.2 Theoretical analysis 44

3.2.1 Vertical Cluster Mean-Field Theory 44

3.2.2 Master equations 46

3.2.3 Steady-state solution 49

3.3 Results and Discussion 53

3.3.1 Effect of system parameters on the steady-state properties . 61

3.4 Comparative analysis of symmetric and fully asymmetric coupling in a two-channel ddTASEP 63

3.5 Conclusion 64

4 Particle creation and annihilation in a single-channel ddTASEP 67

4.1 Introduction . . . 67
4.2 Description of model and dynamical rules . . . 68
4.3 Master equations . . . 69
4.3.1 Particle density evolution . . . 69
4.3.2 Defect density evolution . . . 70
4.3.3 Continuum mean-field equations . . . 70
4.4 Steady-State solution and Monte Carlo Simulation . . . 72
4.5 Steady-state phase diagrams and transitions . . . 72
4.5.1 Effect of defect binding and unbinding rates . . . 73
4.5.2 Effect of variation in strength of dynamic defects . . . 82
4.5.3 Elimination of steady-state phases . . . 83
4.6 Shock dynamics . . . 85
4.7 Finite size effect . . . 87
4.8 Conclusion . . . 88

5 Two-lane ddTASEP with Langmuir kinetics 91

5.1 Introduction . . . 91
5.2 Model . . . 92
5.3 Master equations . . . 92
5.3.1 Particle density evolution . . . 92
5.3.2 Defect density evolution . . . 94
5.3.3 Continuum mean-field equations . . . 94
5.4 Steady-state equations and numerical solution . . . 97
5.4.1 Steady-State equation . . . 97
5.4.2 Numerical scheme . . . 97
5.5 Symmetric coupling (C=1) . . . 99
5.6 Fully asymmetric coupling (C=0) . . . 99
5.6.1 Effect of lane-changing rate . . . 103
5.6.2 Effect of Langmuir kinetics . . . 106
5.6.3 Current analysis . . . 108
5.7 Conclusion . . . 109

6 Conclusion **111**

6.1 Summary of results 112

6.2 Future scope 113

Appendices **127**

A 127

B 128

Bibliography **127**

List of Figures

1.1 Systems in statistical mechanics. 3
1.2 Illustration of vehicular traffic flow. 4
1.3 Intracellular transport in an eukaryotic cell carried out by motor proteins moving along microtubule filaments. Right side represents the enlarged view of moving molecular motors along a filament. . . 5
1.4 An illustration of a one-channel TASEP model connected to a reservior of infinite particles at both ends. The red circles represent particles moving along lattice and obeying the hard-core exclusion principle. Particles may enter latticefrom left end with a rate α, and exit from right end with a rate β, and hop forward in bulk with a unit rate. 7
1.5 (a) Exact phase diagram for one-channel open TASEP model in (α, β) space. (b) Fundamental diagram showing current-density relation in TASEP model. 10
1.6 Flowchart representation of Monte Carlo simulation applying random sequential update rule. The input parameters α and β are entry and exit rates of particles respectively and the random number r is generated between 0 and 1. The algorithm is repeated for sufficient long time, ignoring early 5% steps to ensure occurrence of steady-state, the average lattice density is determined by taking time average. 13
1.7 Diagrammatic representation of an open TASEP model with bulk attachment and detachment of particles with rates ω_a and ω_d respectively. 15
1.8 Diagrammatic representation of open TASEP model with bulk attachment and detachment of particles with rates ω_a and ω_d respectively. 17

1.9 (a) A schematic diagram of open-channel TASEP with dynamic defect. A particle hops with rate p_d, if a defect is present at target site. A dynamic defect can stochastically bind and unbind from a lattice site with rates k_+ and k_- respectively, (b) in presence of particle at target site and (c) in absence of particle at target site. 19

2.1 (a) Schematic diagram of a symmetrically coupled two-channel TASEP with dynamic disorder. The defect is represented as a blue shaded site. Crossed arrows indicate forbidden transitions. Illustration of unconstrained defect dynamics with k_+ (defect binding) and k_- (defect unbinding) rates, (b) in the presence and (c) in the absence of a particle at the target site. 27

2.2 For $k_+ = 0.2$, $k_- = 0.6$, $p_d = 1/3$, $\Omega = 0.1L$, $\Omega_d = 0.06L$ (a) Steady-state phase diagram with three phases. The dashed line is the extrapolation of solid phase boundary between (LD-LD) and (MC-MC) phases. Density profiles for (b) (LD-LD)phase $\alpha = 0.3$, $\beta = 0.5$, (c) (MC-MC)phase $\alpha = 0.7$, $\beta = 0.6$ and (d) (HD-HD)phase $\alpha = 0.8$, $\beta = 0.2$. 35

2.3 For $k_+ = 0.15$, $k_- = 0.1$, $\Omega = 0.1$, $\Omega_d = 0.06$, steady-state phase diagram with three phases. 36

2.4 (a) Re-normalized current J/J_{max} as a function of α/α^* for $\beta = 1$. (b) Maximum current J_{max} as a function of slow hopping rate p_d, for $L = 1000$ and varying k_+ and k_-. 38

2.5 Particle current J as a function of particle density ρ for defect density $\rho_d = 0.8$ ($k_+ = 0.8$ and $k_- = 0.2$) and varying slow hopping rate p_d. 39

2.6 Density profiles for L=100, 500 and 1000, fixing $k_+ = 0.15$ and $k_- = 0.1$. The insets in both the figures are results obtained from continuum mean-field. (a) LD phase for $\alpha = 0.4$, $\beta = 0.3$ (b) HD phase for $\alpha = 0.7$, $\beta = 0.1$. 40

3.1 (a) A schematic view of asymmetrically coupled two-channel TASEP with dynamic disorder. Circles describe particles and shaded squares are dynamic defects. An illustration of unconstrained defect dynamic (b) defect binding with rate k_+ and (c) defect unbinding with rate k_-. 45

3.2 Different possible configurations of a vertical cluster representing (a) particles and (b) defects in the system. 45

3.3 Gain terms: Different possible configurations incoming to probability P_{11}. 47
3.4 Loss terms: Different possible configurations outgoing from probability P_{11}. 48
3.5 The horizontal particle transitions in the bulk of lane A. 51
3.6 Steady-state phase diagram with seven different phases for $p_d = 1/3$, $k_+ = 0.4$, $k_- = 0.8$, $\omega_A = 1$ and $\omega_B = 0$. 59
3.7 For $p_d = 1/3$, $k_+ = 0.4$, $k_- = 0.8$, $\omega_A = 1$, (a) (0, LD) phase for $\alpha = 0.05$, $\beta = 0.8$, (b) (0, HD) phase for $\alpha = 0.25$, $\beta = 0.25$, (c) (0, MC) phase for $\alpha = 0.3$, $\beta = 0.9$, (d) (LD,1) phase for $\alpha = 0.5$, $\beta = 0.2$, and (e) (HD, 1) phase for $\alpha = 0.8$, $\beta = 0.05$. 60
3.8 Phase diagram for $p_d = 1/3$, $k_+ = 0.9$, $k_- = 0.1$, $Y = 0.9$ and $\omega_A = 1$. 61
3.9 Density profile in (0, MC) region fixing $\alpha = 0.3$, $\beta = 0.9$, $p_d = 1/3$, $k_+ = 0.4$, $k_- = 0.8$ for $\omega_A = 0.5$ (lines) and $\omega_A = 1$ (markers). . . . 62
3.10 Particle current J as a function of particle density ρ for defect density $Y = 0.9$ ($k_+ = 0.9$ and $k_- = 0.1$) and varying slow hopping rate p_d. 63

4.1 (a) Schematic diagram of a single-channel TASEP with dynamic disorder and Langmuir kinetics. The dynamic defect is represented as a shaded site. Crossed arrows indicate forbidden transitions. Illustration of unconstrained defect dynamic (b) in the presence and (c) in the absence, of a particle at the target site. 69
4.2 Steady-state phase diagram with seven different phases for $k_+ = 0.4$, $k_- = 0.8$, $\rho_d = 1/3$, $p_d = 1/3$, $K = 1$, $\Omega_a = 0.2$ and $\Omega_{ad} = \Omega_a/2$. The LMH region corresponds to LD-MC-HD. 74
4.3 Density profiles for $p_d = 1/3$, $k_+ = 0.4$, $k_- = 0.8$, $\rho_d = 1/3$, $\Omega_a = 0.2$, $\Omega_{ad} = \Omega_a/2$ and $L = 1000$ (a) LD phase for $\alpha = 0.2$, $\beta = 0.8$, (b) LD-MC phase for $\alpha = 0.45$, $\beta = 0.9$, (c) MC phase for $\alpha = 0.9$, $\beta = 0.85$, (d) HD phase for $\alpha = 0.8$, $\beta = 0.1$, (e) MC-HD phase for $\alpha = 0.8$, $\beta = 0.25$, (f) LD-MC-HD phase for $\alpha = 0.4$, $\beta = 0.25$ and (g) S phase for $\alpha = 0.2$, $\beta = 0.1$. 77
4.4 Current profiles for $p_d = 1/3$, $k_+ = 0.4$, $k_- = 0.8$, $\rho_d = 1/3$, $\Omega_a = 0.2$, $\Omega_{ad} = \Omega_a/2$ and $L = 1000$ (a) LD phase for $\alpha = 0.2$, $\beta = 0.8$, (b) LD-MC phase for $\alpha = 0.45$, $\beta = 0.9$, (c) MC phase for $\alpha = 0.9$, $\beta = 0.85$, (d) HD phase for $\alpha = 0.8$, $\beta = 0.1$, (e) MC-HD phase for $\alpha = 0.8$, $\beta = 0.25$, (f) LD-MC-HD phase for $\alpha = 0.4$, $\beta = 0.25$ and (g) S phase for $\alpha = 0.2$, $\beta = 0.1$. 78

4.5 Phase diagram for $p_d = 1/3$, $K = 1$, $\Omega_a = 0.2$, $\Omega_{ad} = \Omega_a/2$, (a) $k_+ = 0.15$, $k_- = 0.1$ ($\rho_d = 0.6$) and (b) $k_+ = 0.9$, $k_- = 0.1$ ($\rho_d = 0.9$). The LMH region corresponds to LD-MC-HD. 79

4.6 Steady-state phase diagram with four different phases for $k_+ = 0.4$, $k_- = 0.8$, $\rho_d = 1/3$, $p_d = 1/3$, $K = 3$, $\Omega_a = 0.2$ and $\Omega_{ad} = \Omega_a/2$. . . 80

4.7 Density profiles for $p_d = 1/3$, $k_+ = 0.4$, $k_- = 0.8$, $\rho_d = 1/3$, $K = 3$, $\Omega_a = 0.2$, $\Omega_{ad} = \Omega_a/2$ and $L = 1000$ (a) LD phase for $\alpha = 0.07$, $\beta = 0.8$, (b) S phase for $\alpha = 0.3$, $\beta = 0.4$, (c) MC phase for $\alpha = 0.8$, $\beta = 0.9$, (d) HD phase for $\alpha = 0.8$, $\beta = 0.1$. 81

4.8 Phase diagram for $p_d = 1/3$, $K = 3$, $\Omega_a = 0.2$, $\Omega_{ad} = \Omega_a/2$, (a) $k_+ = 0.15$, $k_- = 0.1$ ($\rho_d = 0.6$) and (b) $k_+ = 0.9$, $k_- = 0.1$ ($\rho_d = 0.9$). . . 82

4.9 Density profile for $K = 1$, $k_+ = 0.4$, $k_- = 0.8$ and varying pd, (a) $\alpha = 0.2$, $\beta = 0.8$ and (b) $\alpha = 0.8$, $\beta = 0.1$. The figures are results from MCS with the respective insets obtained from CMF. 83

4.10 Phase diagram for $k_+ = 0.4$, $k_- = 0.8$, $\rho_d = 1/3$, $p_d = 1/3$, $K = 1$, $\Omega_{ad} = \Omega_a/2$, (a) $\Omega_a = 0.5$ and (b) $\Omega_a = 1$. The LMH region corresponds to LD-MC-HD. 84

4.11 Phase diagram for $k_+ = 0.4$, $k_- = 0.8$, $\rho_d = 1/3$, $p_d = 1/3$, $K = 3$, $\Omega_{ad} = \Omega_a/2$, (a) $\Omega_a = 0.5$ and (b) $\Omega_a = 1$. 86

4.12 Shock profile for $K = 1$, $\Omega_a = 0.2$, $p_d = 1/3$, $\alpha = 0.2$, $\beta = 0.1$ and varying k_+ and k_-. The results are captured using (a) Monte Carlo simulation and (b) continuum mean-field approximation. 86

4.13 Shock profile for $K = 3$, $\Omega_a = 0.2$, $k_+ = 0.4$, $k_- = 0.8$, $\alpha = 0.3$, $\beta = 0.4$ and varying p_d. The results are captured using (a) Monte Carlo simulation and (b) continuum mean-field approximation. . . . 87

4.14 Effect of system size for $\alpha = 0.2$, $\beta = 0.1$, $k_+ = 0.4$, $k_- = 0.8$, $K = 1$, $\Omega_a = 0.2$, $\Omega_{ad} = \Omega_a/2$ and $L = 500, 1000, 5000$ and 1000. The results are obtained using (a) Monte Carlo simulation and (b) continuum mean field approximations. 88

5.1 (a) Schematic illustration of a two-lane TASEP with dynamic disorder and Langmuir kinetics. Shaded squares indicate the presence of dynamic defect and circles indicate particles. Crossed arrow indicate forbidden transition. An illustration of unconstrained defect dynamics (b) defect binding (c) defect unbinding, at the target site. 93

5.2 Phase diagram consisting five stationary phases for $p_d = 1/3$, $k_+ = 0.4$, $k_- = 0.8$, $\Omega_a = 0.2$, $\Omega_{ad} = \Omega/2$, $C = 0$, $\Omega_A = 0.8$, $\Omega_{AD} = \Omega_A/3$ and $L = 1000$. 101
5.3 For $p_d = 1/3$, $k_+ = 0.4$, $k_- = 0.8$, $\Omega_a = 0.2$, $\Omega_{ad} = \Omega/2$, $\Omega_A = 0.8$, $\Omega_{AD} = \Omega_A/3$ and $L = 1000$ (a) (S, S) phase $\alpha = 0.2$, $\beta = 0.15$, (b) (LD, S) phase $\alpha = 0.3$, $\beta = 0.8$ and (c) (LD, HD) phase $\alpha = 0.9$, $\beta = 0.8$. Figures (d), (e) and (f) are the corresponding current profiles respectively. 102
5.4 Steady-state phase diagram with five different phases for $k_+ = 0.4$, $k_- = 0.8$, $p_d = 1/3$, $K = 3$, $\Omega_a = 0.2$, $\Omega_{ad} = \Omega_a/2$, $\Omega_A = 0.8$ and $\Omega_{AD} = \Omega_A/3$. 104
5.5 Phase diagram for $p_d = 1/3$, $k_+ = 0.4$, $k_- = 0.8$, $\Omega_a = 0.2$, $\Omega_{ad} = \Omega/2$, $\Omega_A = 80$, $\Omega_{AD} = \Omega_A/3$ and $L = 1000$. 105
5.6 Density profile for $\alpha = 0.7$, $\beta = 0.7$, $p_d = 1/3$, $k_+ = 0.4$, $k_- = 0.8$, $\Omega_a = 20$, $\Omega_{ad} = \Omega/2$, $\Omega_A = 0.8$, $\Omega_{AD} = \Omega_A/3$ and $L = 1000$. 107
5.7 Current J as a function of particle density ρ for different values of slow hopping rate p_d. (a)$\rho_d = 0.5$ for $k_+ = 0.4$, $k_- = 0.4$ and (b)$\rho_d = 0.75$ for $k_+ = 0.6$, $k_- = 0.2$, and varying p_d. 108
5.8 Current (J) as a function of defect strength (p_d) for $L = 1000$, $\alpha = 0.8$, $\beta = 0.8$, $\Omega_a = 0.2$, $\Omega_A = 0.8$, $K = 1$, $x = L/2$ and varying defect density ρ_d. 109
5.9 Current (J) as a function of defect strength (p_d) for $L = 1000$, $\alpha = 0.8$, $\beta = 0.8$, $\Omega_a = 0.2$, $\Omega_A = 0.8$, $K = 1$, $x = L/2$ and varying binding constant K. 110

List of Tables

1.1 Summary of characteristic properties (existence of distinct phases, boundary and bulk particle densities and current) of stationary phases in the open TASEP model. The density at boundary sites i=1(L) is denoted by $\rho_1(\rho_L)$ and the corresponding particle current in steady-state is signified by J. 11

3.1 Steady-state properties of each phase in a fully-asymmetric ddTASEP. 58

3.2 Comparison of steady-state properties of symmetric and fully asymmetric coupling in two-channel ddTASEP. 64

Chapter 1

Introduction

1.1 Stochastic processes

The real-world physical and stochastic processes, ranging from vehicle flow, pedestrian flow, granular flow, ant trail movement to biological transport including protein synthesis, molecular motion, and biological species evolution have significant contributions in biophysics, statistics, chemistry, microbiology, and mathematical theory [1–5]. The majority of these processes evolve randomly, which limits us in predicting the future behavior of dynamical systems using knowledge of their current state. To better understand the physical phenomenon, an extensive range of statistical physics tools are used to analyse the class of these evolutionary models, which yields various interesting findings [6]. Statistical physics acts as a strong paradigm for interpreting the characteristics of complex networks that are modeled as systems of heterogeneous components. The term 'statistical' is due to involvement of probabilities to understand collective behavior of systems with large number of particles. Therefore, in order to gain deep insight into the collective phenomenon of interacting species at the macroscopic scale requires the employment of statistical mechanics approach [7–9].

The behavior of physical systems with a large number of particles is mainly categorized into two broad categories, i.e.: (i) Equilibrium systems and (ii) Non-equilibrium systems [10,11]. In equilibrium state, a system tends to move towards a state of balance in the forces acting on it or towards equilibrium where there is no net change in system properties. The equilibrium process is dynamic whereas the total dynamic change of properties becomes zero upon reaching a equilibrium. As an illustration, consider a metal rod with a heat source at one end. Once the heat source has been turned off, heat flows towards an end at lower potential. Given enough time for evolution, the rod will attain a uniform temperature all along

its length. Due to constant temperature, the rod will attain equilibrium where either there is no dissipation of heat (i.e., total dynamic change of properties is zero) or the net heat flow along the rod is balanced (net movement is balanced). Nevertheless, what about the characteristics of open systems, which evolve with time when connected to external energy? Such systems do exist in real life, and are categorized as non-equilibrium systems. [11].

1.2 Non-equilibrium systems

Usually, complex natural systems continuously exchange energy and matter with their surroundings and generally do not reach an equilibrium state. Such systems are said to exhibit a non-equilibrium state. The flow of particles in vehicular traffic to intracellular transport in living organisms are universal complex transport systems that involve stochasticity. Such systems are considered to be far from equilibrium whose collective behavior is rich and diverse which depends critically on various internal parameters and boundary conditions [10, 11]. Consider a tube linking two infinite particle reservoirs kept at various chemical potentials as an illustration of such a system. At an almost constant rate, particles will flow through the tube irreversibly towards the lower chemical potential. Such a system can never attain an equilibrium, but besides a few fluctuations, its properties remain constant with time. Due to the ambiguity involved in the time evolution of such type of systems, it is difficult and worthwhile to forecast their future behavior. There is, so far, no standard theoretical framework to handle non-equilibrium systems, unlike equilibrium systems [12]. Such systems are classified into two broad categories, as shown in fig. 1.1, (i) Systems progressing towards equilibrium steady-state, and (ii) Systems progressing towards a non-equilibrium steady-state.

(i) *Systems progressing towards equilibrium steady-state:* Systems evolving towards thermodynamic equilibrium after an ample long time fall under the category of equilibrium steady-state. Such a steady-state corresponds to time-independent fluctuations. Hamiltonian of a system is the rate at which the state of a dynamical physical system changes with time. Using Onsagar's regression theory and linear response theory, the systems can be analyzed by defining the Hamiltonian. The detailed balance- which is the tendency of the system to switch from one state to another counterbalanced by tendency in switch in reverse direction between same states, holds in such systems. For further information, we refer to references [6, 13].

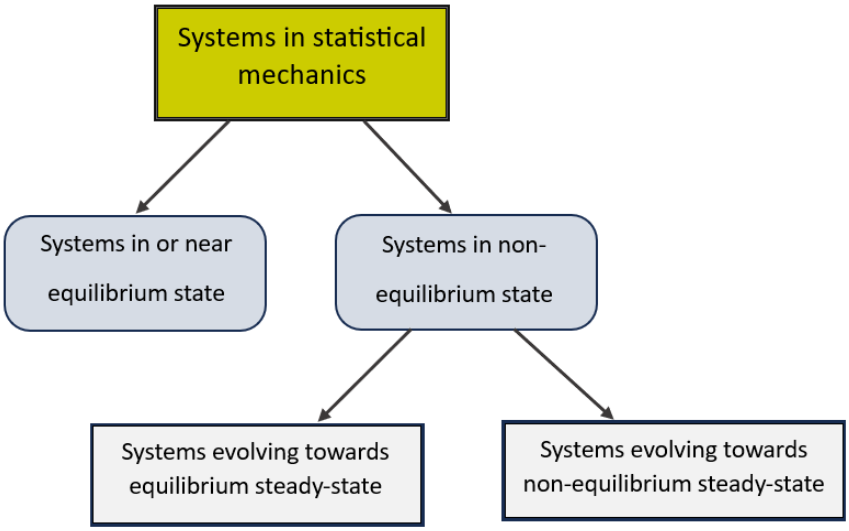

Figure 1.1: Systems in statistical mechanics.

(ii) *Systems progressing towards non-equilibrium steady-state:* Despite various efforts made in the past years, it is difficult to understand the macroscopic state of systems far from equilibrium. No Hamiltonian can be defined for these systems and the dynamics of the system can be defined in terms of rates of transitions between different states. As the system keeps evolving with time, so the detailed balance does not hold, but it eventually reaches a steady-state where the fluctuations become time-independent [14]. Since motion is always occurring in the system, the non-zero current flows through it even in steady-state. The Onsagar's theory fails far from equilibrium. Commonly, the driving force triggers motion of bodies in non-equilibrium systems, which further categorizes them under driven diffusive systems, being discussed in forthcoming sections [10].

1.3 Driven diffusive systems

In non-equilibrium statistical physics, driven diffusive systems are a class reflecting non-equilibrium dynamic mechanisms. The systems constantly exchange energy with the external field such that the time-independent state is no longer an equilibrium state. The condition of detailed balancing no longer holds true, however a non-equilibrium steady-state exists because of the pairwise-balance condition. In pairwise balance condition, the total flux into each configuration of the system is

Figure 1.2: Illustration of vehicular traffic flow.

equal to the flux out of that configuration. Due to pairwise balance between system configurations, the probability of finding the system in that particular configuration becomes independent of time and a steady-state of the system exists. Instead, the system stops evolution over time, the steady-state carries a constant current. Apart from being far from equilibrium, another feature of these systems is being driven by utilising some mechanism. The continuous motion of active species is captured by enforcing a drive biasing the direction of motion. In some models, the bias in the movement of agents is introduced by driving external field, and hence the particles are known as field-driven. However, the particles moving under the influence of internal drive in a system are called self-driven particles. The non-zero particle current in driven diffusive systems characterizes its non-equilibrium steady-state [10]. Such types of systems include pedestrian flow, cellular automata [7], vehicular flow, biological transport [15], and many more [2]. The following sections discuss the importance of real-world self-driven diffusive systems in various physical and biological stochastic transport processes being undertaken in investigation.

1.3.1 Vehicular Traffic

One of the major sociological and economic issues with transportation in developed nations today is the flow of traffic and congestion. Over the years, understanding the principles of optimized and controlled traffic flow has become an enormous interdisciplinary area of research. Due to their pervasive relevance to the natural sciences, the areas of stochastic transport along with statistical physics have gained deeper insight into studying traffic science and phenomena like traffic forecasting, jamming and collective flow [16].

Recently, statistical physicists have been contributing in modeling traffic flow to examine numerous fundamental properties of truly non-equilibrium systems [10]. The main goal is to build a more effective, structured network of roads since inefficient roads can cause human fatalities, leading to various social effects.

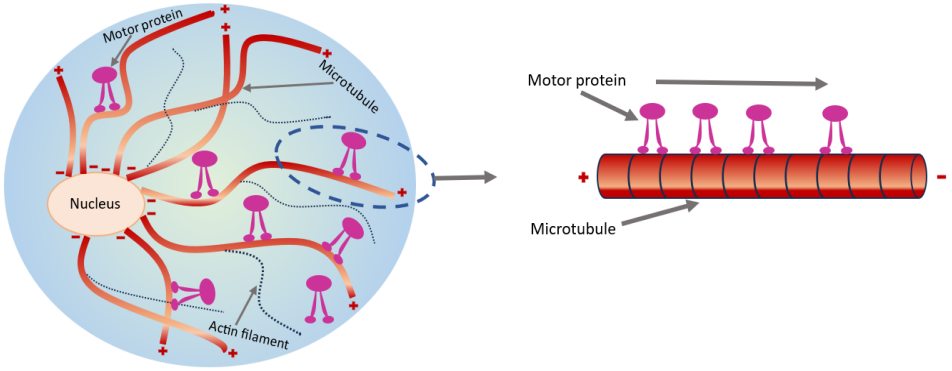

Figure 1.3: Intracellular transport in an eukaryotic cell carried out by motor proteins moving along microtubule filaments. Right side represents the enlarged view of moving molecular motors along a filament.

1.3.2 Biological Transportation

The fundamental structural, functional, and basic unit of all living forms is the tiny package called cell. A cell contains minute factories, transport systems, warehouses, and power plants. In order to survive life forms, a cell must be able to perform all the necessary functions [17]. These functions include the transport of mineral nutrients, water, hormones, energy, disposing of wastes etc [18, 19]. Primarily, there are two types of transport across the cell membranes in living beings: (i) Active transport, and (ii) Passive transport. Both these types emerge based on a concentration gradient across the cell membranes. Active transport requires greater energy in the form of ATP to transmit substances across cell membranes. Here, the movement of substances is against the direction of concentration gradient [20]. Conversely, passive transport does not require any energy from cells and the substances diffuse along the concentration gradient.

Motor proteins are nanoparticles that carry vesicles and intracellular cargoes like organelles, proteins to appropriate locations within the cell. They carry out active transport along the cytoskeleton filaments, either actin or microtubules as presented in fig. 1.3. Motor proteins move via force dependent mechanism that is supplied with energy by hydrolysis of adenosine triphosphate (ATP) [21, 22]. This classifies proteins as self driven diffusive systems.

For the global study of motor protein motion, there have been substantial improvements in experimental and theoretical research. Generally, the motor proteins work in vast groups, and the collective motion of mobile elements play an essential role in the working of cells [15]. Therefore, understanding their mutual behavior is very crucial in complex systems. The functioning of motors play an important role

in sustaining cellular processes, whereas their malfunctioning may lead to many diseases, such as motor neuron disease [23], respiratory diseases, Alzheimers [24], and various others.

1.4 Driven Lattice Gas Model- Totally Asymmetric Simple Exclusion Process (TASEP)

At first sight, terms "lattice" and "gas" may seem contradictory because lattice defines characteristics of crystalline solids, and a true lattice lacks gas phase of matter. The fundamental principle of lattice gas is to discretize the continuous space into a regular array of molecular cells. At any given moment, each cell is able to accommodate atmost one particle and a fraction of cells is accommodated by particles. The particle-hopping models of automotive traffic are essentially the lattice gas models, where every individual particle indicates the active entity performing the transportation phenomenon.

Totally asymmetric simple exclusion process (TASEP) belongs to a special class of the driven lattice gas model and is considered to be a paradigmatic non-equilibrium model to study stochastic transport processes. It was first introduced by MacDonald and Gibbs [3] in 1968 to understand the kinetics of biopolymerization. Ever since the model has been widely used to capture the transport mechanisms of molecules in various fields. This stochastic model has been extensively analyzed and employed in studying transport mechanisms in various fields of physics, chemistry, and biology [2,4,25–27]. Despite the model simplicity, the complex dynamics of multi-particle systems can be captured efficiently. The nature of non-equilibrium state of TASEP model is sensitive to the choice of boundary conditions: (i) Periodic boundary and (ii) Open boundary condition, see fig 1.4. In the former case, the total number of particles in the system remains conserved, and each site has equiprobable average particle density [28]. In contrast, the latter case of the open boundary condition exhibits counterintuitive properties [29–33]. The thesis mainly focuses on the various generalisations of TASEP with open boundaries. Firstly, let us discuss in detail the dynamics and results of the open TASEP model. The dynamical rules governing the model are as follows:

1. On the lattice, the particles move with excluded volume interactions.

2. At the left end of lattice (site 1), particles are injected with a rate α if the target site is empty.

3. In the bulk, a particle may jump to its immediate neighboring vacant site with a unit rate.

4. At the other end of the lattice (site L), a particle may escape with a rate β.

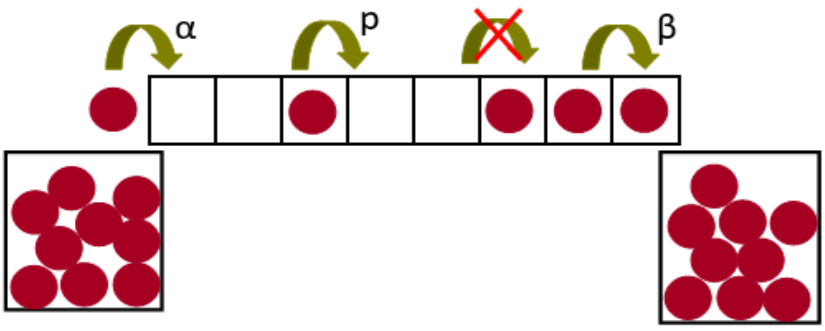

Figure 1.4: An illustration of a one-channel TASEP model connected to a reservior of infinite particles at both ends. The red circles represent particles moving along lattice and obeying the hard-core exclusion principle. Particles may enter lattice-from left end with a rate α, and exit from right end with a rate β, and hop forward in bulk with a unit rate.

The next section of the thesis thoroughly discusses the mathematical analysis of TASEP model and its important results.

1.4.1 Mathematical Analysis

The simplest driven-lattice gas model- one dimensional TASEP is aimed to capture various important features of transportation like particle distribution, average density, particle current, etc. In order to analyse the steady-state, several exact methods have been employed by researchers to obtain model solution. The exact methods reported in literature are namely- recursive relations [29, 34], Bethe ansatz [35, 36], matrix-product ansatz [37, 38], and domain wall theory [10]. Recursive relations method was first introduced by Derrida et al. to obtain exact steady-state solution. The method uses recursion relation using generating function and the stationary probabilities are calculated after performing long calculations. Matrix product ansatz is a very powerful method which represents steady-state probabilities known as configuration weights, in terms of matrices. Bethe ansatz was developed to solve model of interacting quantum spins using concept of integrability. Despite the existing methods for exact solution of TASEP model, their application to various generalisation of TASEP model is of greater concern as one

needs to incorporate much complex and rich dynamics. The exact methods, in such situations are difficult to handle and involves lengthy calculations. Therefore, predicting the steady-state properties might be challenging and sheds light on the use of approximation techniques [10,27]. In this direction, a widely used method of mean-field approximation has proven to be successful to solve several general versions of TASEP, where exact methods fails. This method well justify the findings of exact methods and captures stationary dynamics of TASEP and its variants. Below, we discuss in detail the mean-field approximation method.

1.4.1.1 Mean-field theory

Consider a finite lattice in one-dimension with discrete L sites labelled as $i = 1, 2, \ldots, L$. The system obeys random-sequential dynamics, i.e., a site is randomly chosen, and the state of a single site is updated at each time step. The state of a site i is characterized by occupation number τ_i, which can be 0 and 1, if the site is vacant and occupied by the particle, respectively. The average particle density for each site is defined by $\langle \tau_i \rangle$ where $\langle \ldots \rangle$ denotes the statistical time average. We first begin with the mathematical analysis by formulating the master equation regulated by transition rates. The equation governing the dynamics of occupancy of every bulk site $1 < i < L$ is given by:

$$\frac{d\langle \tau_i \rangle}{dt} = \langle \tau_{i-1}(1-\tau_i) \rangle - \langle \tau_i(1-\tau_{i+1}) \rangle. \tag{1.1}$$

while for boundary sites the time evolution equation is given by,

$$\frac{d\langle \tau_1 \rangle}{dt} = \alpha \langle (1-\tau_1) \rangle - \langle \tau_1(1-\tau_2) \rangle \tag{1.2}$$

$$\frac{d\langle \tau_L \rangle}{dt} = \langle \tau_{L-1}(1-\tau_L) \rangle - \beta \langle \tau_L \rangle \tag{1.3}$$

In the above equations, the first term on R.H.S. represents the particle gain term at site i and the second term describes the loss term of the same i^{th} site. It is easy to see that the above equations involve two-site correlations, which makes it complex in the current form. The fundamental idea is to break the two-site correlations by the use of mean-field approximation theory. This theory neglects the nearest-site correlations between system variables and the occupancy of two successive sites become independent of each other. Therefore, mathematically, we

can write

$$\langle \tau_i \tau_{i+1} \rangle = \langle \tau_i \rangle \langle \tau_{i+1} \rangle \tag{1.4}$$

For large L, this discrete system of equations makes a multiple-body problem as we require to solve large number of equations. Therefore, it is vital to transform multiple-body problem to one-body problem by coarse-graining the discrete lattice in the thermodynamic limit $L \to \infty$ with lattice constant $\epsilon = 1/L$. Further, we rescale the spatial and temporal variables as $x = i/L$ and $t = t/L$ respectively to find the continuum limit. Defining the average particle density, $\langle \tau_i \rangle = \rho_i$ and using Taylor series expansion on eqn. (1.1) with retaining terms up to first order derivative, gives a well-recognized continuity equation.

$$\frac{\partial \rho_i}{\partial t} + \frac{\partial J(\rho_i)}{\partial x} = 0 \tag{1.5}$$

where the particle current in the system is given by

$$J(\rho_i) = \rho_i (1 - \rho_i). \tag{1.6}$$

As, we are typically interested in obtaining the steady-state solution of the open system (ignoring the time derivative term), eqn. (1.5) reduces to,

$$(2\rho - 1)\frac{\partial \rho}{\partial x} = 0 \tag{1.7}$$

along with the following boundary conditions,

$$\begin{aligned} \rho(0) &= \alpha \\ \rho(1) &= 1 - \beta. \end{aligned} \tag{1.8}$$

Now, the eqn. (1.8) has two possible solutions defined as $\rho(x) = constant$ and $\rho(x) = 1/2$. The system is over-determined as the first-order partial differential equation has two boundary conditions provided for it. The boundary conditions at both the boundaries cannot be met by the system simultaneously and the density profile has a boundary layer on one of the boundaries. Henceforth, the boundaries are controlling parameters in determining the steady behavior of the open TASEP model. Hence, the system is sensitive to boundary conditions and exhibits the phenomenon of boundary-induced phase transitions [39, 40]. The solution of the system satisfying the left (right) boundary condition is left (right) boundary controlled.

1.4.1.2 Exact Phase Diagram

Depending on the values of boundary control parameters, the system in steady-state can exist in any of the three phases discussed below :

(i) *Low density phase (LD):* When $\alpha < \beta$, the probability of particle entering a lattice is less than that of leaving, so more number of particles leave the system implying the system to be in low density phase. Thus, the phase is entrance dominated and exists when left boundary condition is matched by the solution. Mathematically, the particle density is given by $\rho = \alpha < 1/2$.

(ii) *High density phase (HD):* This phase is exit dominated phase, when $\alpha > \beta$ more number of particles enter the system as compared to particles leaving, causing high density over the lattice. The solution in this phase satisfies right boundary condition. The particle density in this phase is given by $\rho = 1 - \beta > 1/2$.

(iii) *Maximal current phase (MC):* This phase is independent from values of boundary controlling parameters and achieves smooth flow of particles over the lattice. Hence, the phase is bulk dominated phase with particle density $\rho = 1/2$. The flow of bulk particles becomes constant with a value equal to $1/2$.

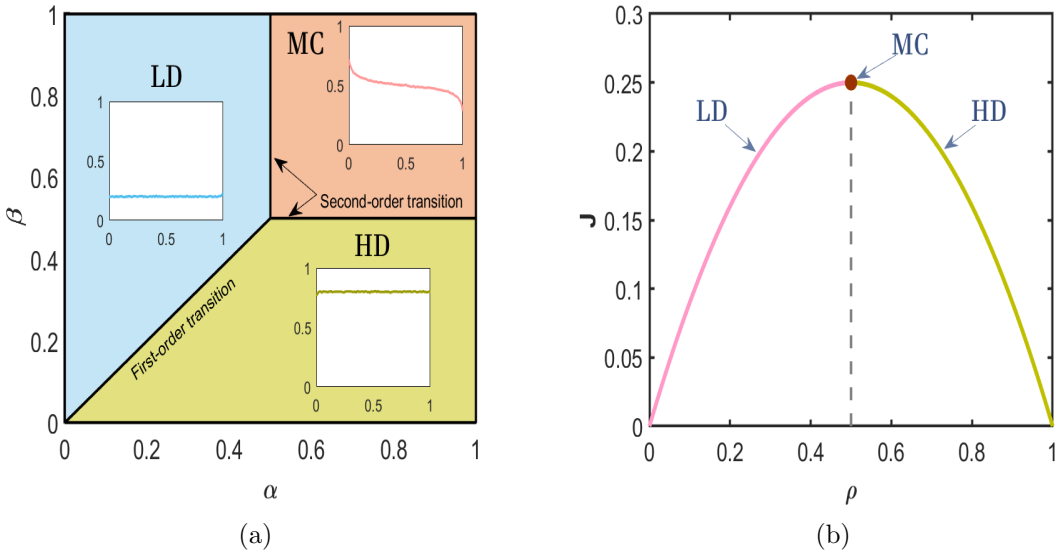

(a) (b)

Figure 1.5: (a) Exact phase diagram for one-channel open TASEP model in (α, β) space. (b) Fundamental diagram showing current-density relation in TASEP model.

The characteristic properties of the distinct stationary phases, expressions of particle density on boundaries and in bulk along with particle current are summarized in table 1.1. Depending upon the boundary controlling parameter values, the phase composition in steady-state is shown in fig. 1.5(a). One can see the existence of two types of phase transitions:

1. *First-order transition:* Along the transition line $\alpha = \beta$, the LD phase jumps into HD phase, suddenly exhibiting a discontinuous phase transition. Such a transition is categorized as first-order transition. On the line of transition, low density regime connects to a high density regime, giving a discontinuous density profile. This type of density profile is named as delocalized shock which has a non-fixed point of discontinuity.

2. *Second-order transition:* The line of transition from LD to MC phase and HD to MC phase exhibits a smooth and continuous phase transition. This type of transition is a second-order transition.

Figure 1.5(b) shows the current-density relation which represents a parabolic curve. The physical significance of the curve is that an increase in particle density increases current in the system depicting the LD phase. At the critical value of $\rho = 1/2$, it attains a maxima representing the MC phase and a further increase in density cause jamming of particles, which reduces the overall flow of particles being in HD phase. With modifications in the dynamical rules of the system (discussed in next section), the current-density curve may acquire a different shape. For example, CDR has single maxima in simple TASEP model, a double-hump in TASEP with interactions, a change in height of parabolic curve in TASEP with slow hopping rate, a symmetry breaking in curve (curve skewing) in closed TASEP with altering dynamic defect rates [10].

Phase	Phase region	ρ_1	ρ_{bulk}	ρ_L	J
Low density (LD)	$\alpha < 1/2,\ \alpha < \beta$	α	α	$\frac{\alpha(1-\alpha)}{\beta}$	$\alpha(1-\alpha)$
High density (HD)	$\beta < 1/2,\ \beta < \alpha$	1- $\frac{\beta(1-\beta)}{\alpha}$	1-β	1-β	$\beta(1-\beta)$
Maximal current (MC)	$\alpha > 1/2,\ \beta > 1/2$	1- $\frac{1}{4\alpha}$	1/2	$\frac{1}{4\beta}$	1/4

Table 1.1: Summary of characteristic properties (existence of distinct phases, boundary and bulk particle densities and current) of stationary phases in the open TASEP model. The density at boundary sites i=1(L) is denoted by $\rho_1(\rho_L)$ and the corresponding particle current in steady-state is signified by J.

Particle-hole symmetry

Particle-hole symmetry means if the particles (occupied sites) in the system are replaced by holes (empty sites), the system current does not change. This is evident in TASEP as every move comprise of exchange in position of particle with the hole ahead of it. As the particles and holes obey the same dynamical rules, the current in the system can be attributed to either forwarding particles or to receding holes. Therefore, there is a symmetry in current-density relation and we have $\rho \leftrightarrow 1-\rho$. Thus, this symmetry implies $J(\rho) = J(1-\rho)$.

1.4.2 Monte Carlo simulation

A stochastic process usually applied in realization of a configuration of system is Monte Carlo simulation (MCS) [41]. This computational tool allows to implement stochastic dynamics of the system by producing transitions with suitable probabilities. One necessary condition to apply Monte Carlo simulation is that the system must be ergodic. In configuration space, every point that is accessible should be attainable from any other point in the space in finite number of Monte Carlo moves. A Monte Carlo simulation will generally proceed as follows: starting with an initial particle configuration in a system, an attempt is made to perform a Monte Carlo move that modifies the particle configuration. An acceptance criterion that ensures that configurations are sampled from a statistical mechanics ensemble distribution in the simulation determines whether or not this move is approved [42]. One determines the value of an interest property when a move is accepted or rejected, and after several such moves, an exact average value of this property may be acquired [43]. In the thesis, to validate the theoretical findings of mean-field equations considering various assumptions and approximations, Monte Carlo simulation are performed extensively based upon the repeated random sequential update rule.

A Monte Carlo step starts by generating a random number to choose a site on the lattice. Further, a random integer r is generated from a uniform distribution in $[0, 1]$ if a process at that site occurs with a certain probability p. The process will take place if $r \leq p$, but not if $r > p$. The simulation steps for standard TASEP model are detailed in a flowchart shown in fig. 1.6. The iterations are repeated for a very large number of time steps and the initial 5% steps are disregarded to ensure occurrence of steady-state. Lastly, the average density is evaluated by considering time average over an interval 10L.

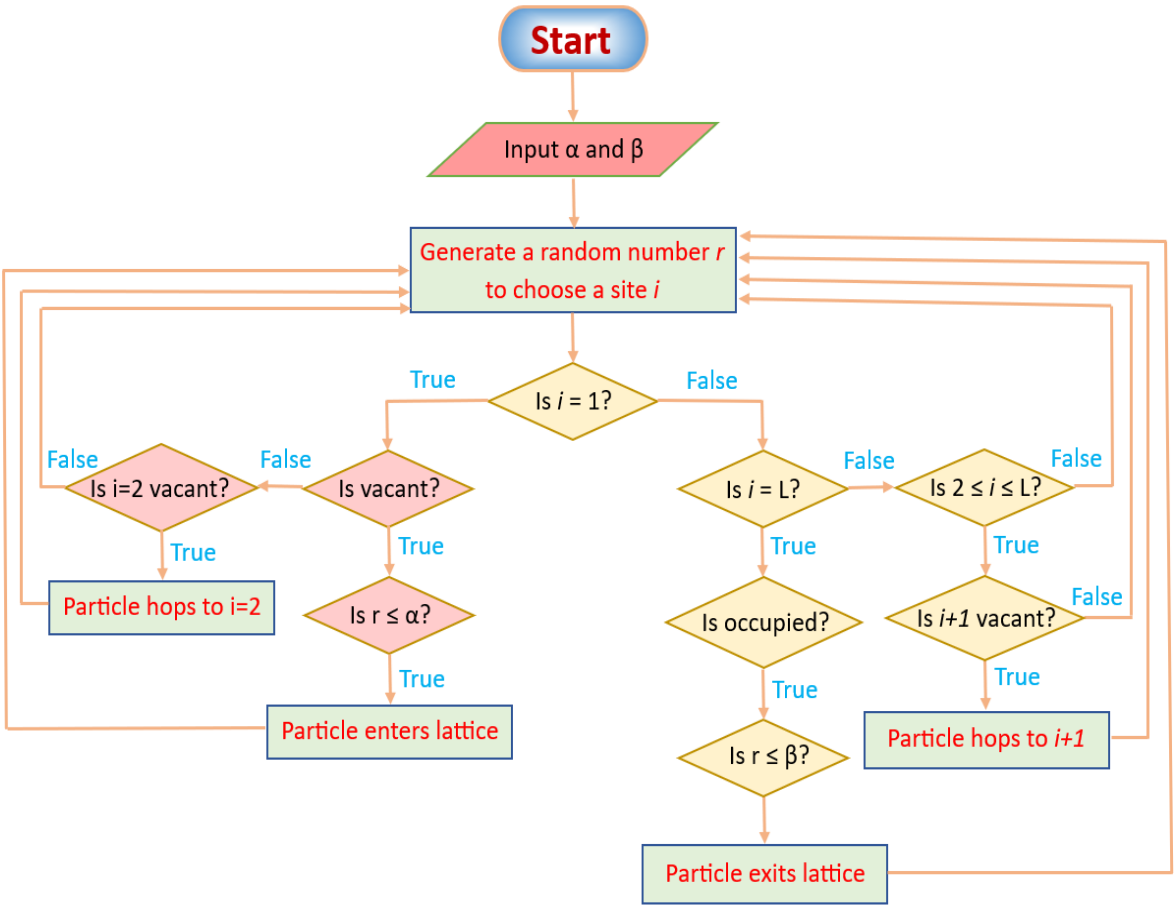

Figure 1.6: Flowchart representation of Monte Carlo simulation applying random sequential update rule. The input parameters α and β are entry and exit rates of particles respectively and the random number r is generated between 0 and 1. The algorithm is repeated for sufficient long time, ignoring early 5% steps to ensure occurrence of steady-state, the average lattice density is determined by taking time average.

1.4.3 Finite-difference approximation

So far we know that an exact solution of one-dimensional TASEP model exists by the use different analytical methods (mentioned earlier) but their application to several generalisation of TASEP model is of considerable concern due to the necessity to include rich and complicated dynamics. The complexity of the system increases and therefore the exact methods in such circumstances are challenging to manage and need extensive computations. Henceforth, one needs to use numerical technique to find the steady-state solution of the complex and multi-dimensional systems. One of the simplest and the most established techniqus in solving differential equations is the implementation of finite difference approximation for deriva-

tives. Finite-difference methods are approximate in the sense that derivatives at a point are approximated by differential quotients [44]. The domain is divided into segments in time and space, and for each segment, approximations of solution are calculated at space and time points. The error between an exact solution and numerically found, is determined by the discrepancy in moving from a differential to a difference operator.

The analytical approximation methods for differential equations provide closed-form formulations that show alteration of the dependant variables over domain. Whereas, numerical solutions based upon finite differences used more frequently and universally, gives the values only at discrete points in domain referred to as grid points.

1.5 Variants of TASEP

In spite of simplicity, TASEP model has become a prominent model in depicting various driven diffusive non-equilibrium systems to study the physics of transport processes. Several generalisations have been examined over past years in the TASEP framework, which take into account many essential aspects of the transport processes. These include systems with dynamic disorder, particle association and dissociation, multi-lane transport model, and many more [45]. The following sections discuss various extensions of the TASEP that are relevant to real-life problems undertaken in the thesis.

1.5.1 Two-lane TASEP

A fundamental one-dimensional ASEP model has proven to be beneficial in studying driven diffusive systems by several researchers. However, most of the real-life transport phenomenon exhibit particle motion in a more complicated framework than one dimension. Evidently, changing lanes is obviously an essential part of any traffic flow strategy. For example: vehicular traffic involves several lane of highways where moving vehicles can change lanes which might either improve traffic capacity or interrupt the flow of traffic or driving speed [10, 46]. Another example to consider is biological intracellular transport in which molecular motors progress along a protofilament. The microtubules appear as a multi-lane track involving different hopping rates and motors progressing in different directions [3, 22, 47]. The two-lane system is more complex as compared to a single-lane system due to the inter-lane coupling and hence exhibits diverse steady-state properties. Over

the years, multiple lane models have gained attention of researchers and are still a matter of research in various fields of the natural sciences. Therefore, in order to have ample understanding of dynamical aspects of many-particle networks, it becomes essential to study multi-lane TASEP systems.

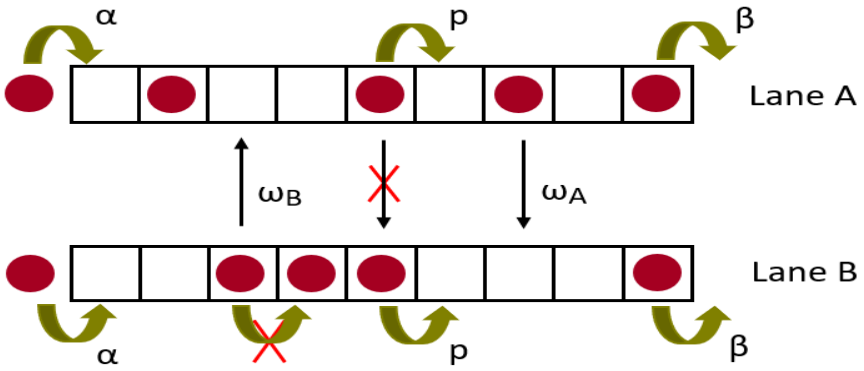

Figure 1.7: Diagrammatic representation of an open TASEP model with bulk attachment and detachment of particles with rates ω_a and ω_d respectively.

The two-lane TASEP system is a generalization of single-lane TASEP, which can be observed as two identically parallel single-lane TASEPs in which a particle can hop forward as well as can switch between the lanes. On the two-lane lattice, the entrance and the exit criteria of a particle from each lane is similar as in standard TASEP with an additional lane-changing rule as shown in fig. 1.7. The steady-state properties of coupled two-lane TASEP model strongly depend on inter-lane coupling leading to phase co-existence phenomenon. Based on the condition on rate of transition of particle from a site in one lane to same site in another lane, the coupling in two-lane TASEP system is classified into three different categories.

1. *Symmetric coupling:* When $\omega_A = \omega_B = \omega$ (say), the inter-lane transition rates become same for each lane, which infers that equal number of particles are allowed to shift between the lanes. The symmetry in coupling rates causes cancellation of lane-changing source terms with the sink terms in the mean-field equation, which leads to two uncoupled ordinary differential equations representing two independent TASEPs. Therefore, the average particle density in both the lanes becomes equal.

2. *Fully asymmetric coupling:* In this particular case, the coupling between the lanes is biased as lane-changing from only one of the lanes is allowed (say $\omega_A \neq 0$), while lane-changing from another lane is restricted (say $\omega_B = 0$). One can map the coupled system into an effective single-channel TASEP

model with effective dynamic rates. The coupling term serves the role of sink term for lane A and source term for another lane B, which leads to accommodation of particles in the lane and eventually gives higher particle density in lane B in steady-state of the system.

3. *Partial asymmetric coupling:* In this general case of coupling, lane-changing with unequal rates between the lanes is allowed, i.e., $\omega_A \neq \omega_B$ and $\omega_A, \omega_B \neq 0$. This particular case of coupling is comparatively complex and difficult from theoretical point of view than the other cases due to lack of any simplified master equations. Here, the coupled system cannot be mapped into an effective one dimensional TASEP model. As a result, the particle densities in the lanes become unequal.

In the literature, several studies have been implemented on two-lane TASEP models [48–57]. Pronina and Kolomeisky [58, 59] investigated a two-lane TASEP model in the limit of weak, strong and no coupling environment. They gave an exact description of system dynamics by mapping the coupled system into an effective one-dimensional system and calculated the steady-state phase diagram and density profiles. Various studies have been carried out in the past in the context of coupled TASEP model such as the dependency of interlane coupling rate on the configuration of parallel lane [60], the role of coupling in symmetric and asymmetric exclusion processes [61–64], inclusion of Langmuir Kinetics in one or both lanes under different coupling conditions [65–68], the study of effect of local inhomogeneity [69, 70]. Additionally, various other aspects, like phase coexistence, symmetry breaking, phase separation, along with bidirectional movement and shock formation have been investigated in multi-lane TASEP models.

1.5.2 Langmuir Kinetics

Biological and physical transport processes typically involves directional progression of active species, which can reversibly or irreversibly associate and dissociate from a lattice site due to various reasons. The vehicular traffic involves such situations arising from on-off ramps, by use of which a vehicle can attach to or leave a highway. Analogously, in intracellular transport, the free diffusing processive motors can reversibly associate and dissociate from the microtubule filament into the cell cytoplasm [71]. In the context of the exclusion process, the characteristics of particle association-dissociation along the lattice is termed as Langmuir Kinetics (LK) [72].

The inclusion of an on-off mechanism in the diffusive system violates the particle conservation property in the bulk, which leads to competing bulk and boundary dynamics. One of the most interesting and novel consequences of introducing LK dynamics is the localization of domain wall (shock) exhibiting critical stationary-state properties [73]. This gives rise to the well known non-equilibrium phenomenon of phase separation, where the domain wall separates the coexisting phases. This sheds light on the study of a hybrid TASEP model with particles hopping along the lattice and permitted to attach and detach from any site. An illustration of Langmuir Kinetics in single-channel TASEP model is shown in fig. 1.8, with ω_a and ω_d as attachment and detachment rates, respectively.

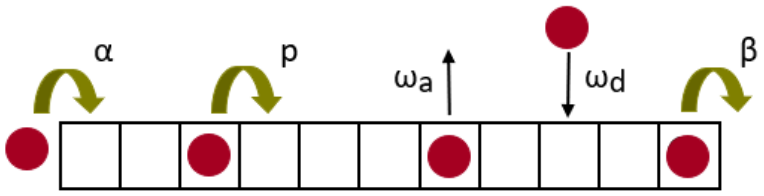

Figure 1.8: Diagrammatic representation of open TASEP model with bulk attachment and detachment of particles with rates ω_a and ω_d respectively.

In this direction, Parmeggiani et al. [74], proposed a TASEP model with LK and presented a theoretical analysis based on mean-field approximation and describe stationary-state and critical domain wall properties of the system. The competing system dynamics lead to phase coexistence phenomenon manifested by a localized domain wall in the bulk of the system [75, 76]. Mirin et al. [77] revealed the appearance of domain wall in the region between sublattices in a single-channel TASEP with irreversible detachments from a specific site in the bulk. A few studies reported in literature [78, 79] explored localized shock dynamics and phase transitions in exclusion process models with LK. In this direction, Jiang [65] studied a two-channel TASEP under symmetrical coupling environment with the presence of LK in one of the two lane. As a consequence, the steady-state densities in the lanes become unequal and one witnesses (S, S) phase in the steady phase diagram, with shock present at two different positions in the lanes. Importantly, the non-equilibrium phenomena of synchronizing shocks was revealed in a two-channel TASEP with particle non-conservation [65]. Various other generalizations of the transport model have been extensively studied by incorporating rich dynamics such as lane-switching in the TASEP model for multi-channels under symmetric and asymmetric lane-changing rules [80, 81], non-conserving dynamics in one of the

two-lane models [66, 82–84], static inhomogeneity [85]. An analogous model has been studied in the past which captures the system with and without correlations in the steady-state [73]. However, various other models have been proposed in the literature using other theoretical analysis to study the complex shock dynamics arising from association and dissociation rules.

1.5.3 TASEP with dynamic disorder

In real-world transportation, the mobility of actively moving particles is frequently impeded by obstructions. Such a situation can be easily observed in regular traffic as a variety of moving vehicles hinder the movement of other moving vehicles, accidents, road construction works and speed limit etc. These obstructions can either be static or dynamic in nature, blocking the path of the particle entirely or allowing it to pass at a slower rate [86–89]. Some classic examples of physical application are obstacles that move randomly and make long range hops [90], and obstacles that bind and unbind randomly to certain lattice sites [91], or periodic switching of traffic lights [92]. In case of static obstruction in the free flow of particles, the position of the defect remains fixed, whereas, on the other side, the case of dynamic hindrance involves a periodic or random hindrance during the movement of particles. In biological transport, some prominent examples of dynamic hindrance include road blocking by DNA-bound proteins in transcription process or microtubule-associated proteins in the cellular cytoskeleton [93, 94]. During transcription of genes, a molecular motor - the RNA polymerase - attaches itself to a specific promoter region of DNA (transcription start site), read off the DNA sequence adding RNA nucleotides to create messenger-RNA (mRNA) sequence and escapes from DNA (transcription end site) [95]. The translation involves decoding of mRNA in a ribosome to produce amino acid chain. The free diffusing transfer-RNA (tRNA) binds to specific mRNA codon and carry the amino acid chain [96]. The rate of translation at each single codon is determined by tRNA concentration in cytoplasm and codon specificity [97, 98]. The slowing down of RNA polymerase by protein roadblocks act as a bottleneck in the transcription process [99]. Additionally, these bound proteins can modulate the motion of active motors along the protein filaments. The randomness involved in the nature of obstruction makes it suitable yet comparatively complex to capture intracellular transport by motor proteins. Apart from this, bottlenecks also occur in many other transport processes such as vehicular accidents [100], narrow highways [51], blood flow [101] and jamming due to road construction [102]. The presence of defects on roads causes

congestion of vehicles impeding the flow rate. Henceforth, it becomes important to analyse the role of dynamic disorder in studying the behavior of particles in non-equilibrium systems.

In mathematical terms, the idea of slowing down of molecular motors or vehicles at some positions due to random obstruction can be viewed in the form of inhomogeneous sites over the lattice. A lattice may have consistent or randomly distributed defects over it, termed as site-wise disorder. A defect can stochastically attach to or detach from a specific site far from the boundaries of lattice, even in the presence of particles at the target site. Figure 1.9 shows the illusion of an exclusion model explaining the hopping rule of particles and defects. Consequently, the model becomes inhomogeneous, which has a significant effect on the steady-state properties of the system. Throughout the thesis, we focus on incorporating site-wise dynamic disorder in TASEP model (ddTASEP), which is more appropriate in transcribing hindrance occurring in transport of vehicles and motor proteins.

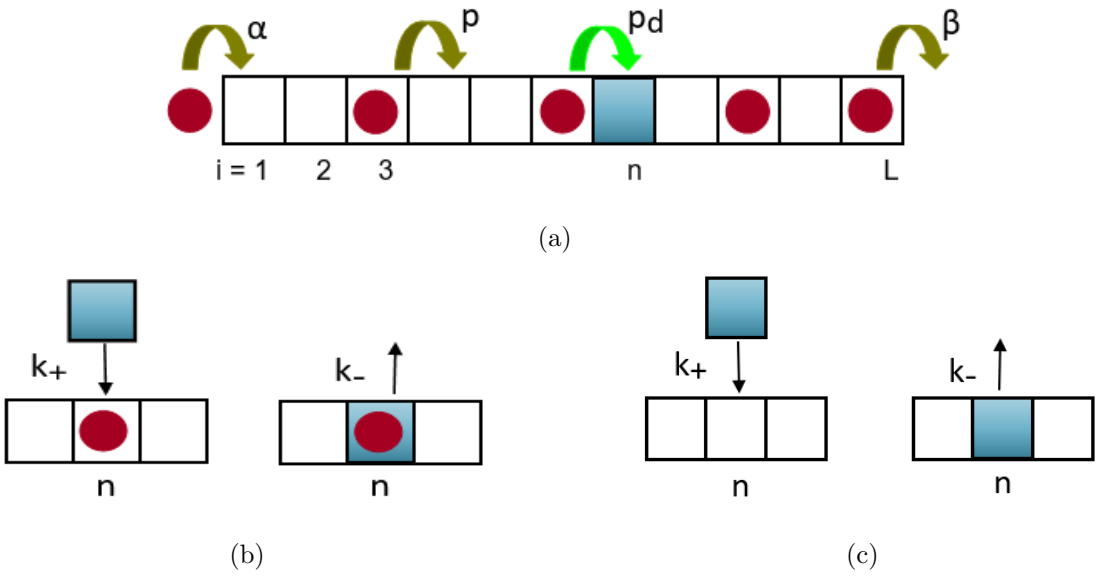

Figure 1.9: (a) A schematic diagram of open-channel TASEP with dynamic defect. A particle hops with rate p_d, if a defect is present at target site. A dynamic defect can stochastically bind and unbind from a lattice site with rates k_+ and k_- respectively, (b) in presence of particle at target site and (c) in absence of particle at target site.

To investigate the impact of disorder on the dynamical features of the system, numerous generalisations of the TASEP model have been investigated. In our opinion, the significant work in this context has been done by a few researchers recently. Turci et al. [103] studied a closed one-dimensional exclusion model with a dynamic

defect which has possibly two configurational states (closed and open) depending upon particle occupancy. They studied the physics of an intermittent regime which strongly influences particle current in the system, and found that severe finite-size effect in the regime has strong consequences on the steady density profile and current. Sahoo et al. [104] thoroughly studied one-channel closed TASEP with dynamic roadblock which can move diffusively (forward as well as backward) and can perform long range jumps to mimick binding-unbinding process. They found that in the long-range jumps by roadblock, the current was proportional to number of particles rather than depending upon particle density in the system with small unbinding rate. The case of purely diffusive roadblock exhibits an asymmetry in current-density relation. Later, they investigated a one-dimensional open TASEP model with a dynamic defect and derived steady phase diagram, and deeply examined the effect of slow and rapid defect dynamics on particle flux [105]. Arita et al. [92] studied a single-channel exclusion model on a ring structure with time-dependent defect rate which take values between zero and one periodically. They derived density profiles and thoroughly studied correlations between system current and waiting time to analyse vehicle queuing and shock formation. Recently, Waclaw et al. [91] conducted mean field theory on one-channel TASEP with site-wise dynamic disorder to analyze steady-state behavior of the system in terms of phase diagram and fundamental diagram.

1.6 Aim and Objectives of the thesis

In the current thesis, motivated by crucial characteristics of the stochastic non-equilibrium transport processes, our major goal is to consolidate the knowledge of several disciplines (Mathematics, Physics, Statistics, Biology) to categorise the properties of the transport systems. An attempt has been made to investigate several generalisations in the framework of principle TASEP model while integrating some rich dynamics into the system. The general aim in studying various versions of TASEP model is to explore the role played by dynamic disorder on the steady-state characteristics of the system. Theoretical as well as numerical approaches have been utilized to derive phase diagrams and current within the context of the governing parameters of the model dynamics. The gaps found in the literature are as follows:

Gap 1: A significant work has been already done on single-channel TASEP with dynamic disorder but to our view point the analogous model in two-channel

has not yet studied. The inclusion of lane-interactions might induce some new steady-state characteristics of the model, thereby making it important to take under consideration. Objective 1 covers the related study.

Gap 2: The coupling between different channels in traffic models has always been an essential part as it calls for complexity and exhibit diverse stationary state properties. To have ample understanding of dynamical aspects of many-particle systems, it would be interesting to uncover the dynamics of coupled TASEP model with dynamic disorder. This analysis has been linked to objective 2 described below.

Gap 3: It has been found in literature that the inclusion of Langmuir kinetics in TASEP models leads to a novel aspect of localized shock in steady-state. It would be more interesting and equally significant to explore dynamically disordered TASEP model with Langmuir Kinetics. As far as we are concerned, TASEP with dynamic disorder with bulk attachment and detachment has not been explored in the past studies, this motivates us to work on it. The related research links to last objective- Objective 3 of the thesis.

The following are the main goals and objectives of the thesis:

Objective 1: To analyze the effect of dynamic disorder in two-lane transport processes.

Objective 2: To study the role of coupling (inter-lane interaction) on the steady-state dynamics of the system.

Objective 3: To examine the interplay between Langmuir kinetics and dynamic disorder.

1.7 Overview of the thesis

In the current thesis, several replications of out-of-equilibrium stochastic transport models using the TASEP paradigm are discussed. The dynamical characteristics of the system are widely investigated by utilising theoretical and computational methodologies. The entire work has been assembled in six chapters, comprising four principal chapters (Chapters 2-5) accompanied by introductory chapter (Chapter 1) and a concluding chapter (Chapter 6). The chapter contents are outlined as follows:

Chapter 1: Introduction

In this chapter, we introduce the exclusion process model and its fundamentals as motivation for the current work. To study and describe various important features of the TASEP model and its variants such as two-channel model, inclusion of LK and dynamic disorder, theoretical and computational approaches are discussed. The pertinent literature survey incites the necessity of studying more generic models and their characteristics.

Chapter 2: Symmetric coupling in a two-channel ddTASEP

In this chapter, we study a two-channel TASEP model under symmetric coupling environment with dynamic disorder, which can reversibly bind and unbind from any lattice site. Theoretically, a suitable finite-difference scheme is utilized on the mean-field equations to study the stationary state properties of the system. The symmetric coupling between the lanes preserves the homogeneity of the model, thus, the system can be scrutinized as two independent single-channel systems with dynamic disorder. The results of the theoretical approach agree well with the results from the Monte Carlo simulation. The defect dynamical rates are found to affect the phase boundaries in the phase plane.

Chapter 3: Asymmetric coupling in a two-channel ddTASEP

In this chapter, a theoretical model is developed which concerns the effect of asymmetric lane changing of particles on a two-channel transport model. Another type of species termed defect is allowed to bind and unbind from any lattice site. Motivated by the collective transport of motor proteins on cytoskeleton, which tend to jump asymmetrically between filaments, our main aim is to understand how asymmetric lane-changing and defect dynamics affects the stationary properties of the system. We map our coupled system into an effective single-channel system with defects. It has been found that the asymmetric lane changing rule introduces correlations that affects stationary phases. Theoretically, cluster mean-field theory is utilized to discover the stationary behavior of the system and the results are found to be in agreement with Monte Carlo simulation.

Chapter 4: Particle creation and annihilation in a single-channel ddTASEP

This chapter establishes a single-channel dynamically disordered TASEP model with bulk particle attachment and detachment. The main aim is to focus on the role played by dynamic disorder in an exclusion model with Langmuir kinetics. The defect dynamics are assumed to be independent of particle hopping and attach-detach mechanism whereas dependency over defect existence holds for particle dynamics. The mean-field theory, along with an appropriate numerical scheme is exploited in examining the steady properties of the system. The stationary system dynamics are studied in terms of phase diagrams and density profiles. One of the important consequence of introducing particle non-conserving dynamics is the appearance of shock in steady-state. In the thermodynamic limit, the system characteristics are analysed through the finite-size effect. Monte Carlo simulation is performed to validate mean field results.

Chapter 5: Two-lane ddTASEP with Langmuir kinetics

In this chapter, we formulated a model of two-channel open transport with dynamic disorder and Langmuir kinetics. We conceptually discussed two distinct scenarios: symmetric coupling and asymmetric coupling conditions. In the former case, it is trivial to examine the stationary behavior, the topological structure of phase diagram of the system is similar to its analogue in single-channel. However, in the latter case, the system dynamics are analysed in terms of the binding constant and effect of variation in several governing parameters on the rich phase diagram, fundamental current-density relation, and the interplay between defect and LK dynamics are examined. We validate the mean-field findings with extensive Monte Carlo simulation.

Chapter 6: Conclusion and future work

This chapter of the thesis provides a summary of the findings discussed in the earlier chapters. Additionally, we detail several intriguing potential extensions of the proposed models for future research problems.

Chapter 2

Symmetric coupling in a two-channel ddTASEP

Similar to dynamically disordered single-lane systems, particles in multi-lane transport systems may also observe hindrance by bottleneck, present in either one or more channels. It is interesting to know whether the steady-state of dynamically disordered two-channel TASEP exhibits similar behavior as its single-channel counterpart or are the system dynamics relatively more complex? In the direction of exploring the underlying physics arising from interlane interactions, we study the role of symmetric coupling in a two-channel ddTASEP.

The chapter is classified as follows. In section 2.1, the model and its governing dynamical rules are defined. The theoretical mean-field approach, steady-state equations and a suitable numerical technique are discussed in section 2.2. A thorough analysis of the effect of various system parameters on the steady-state properties of the model is discussed in section 2.3. The last section 2.4 comprises of brief conclusion of the obtained results.

2.1 Model and dynamical rules

We consider a system of two parallel one-dimensional lattice channels with dynamic disorder under open boundary conditions, each with L sites, denoted by A and B. The dynamic defect can appear and disappear on any lattice site including both bulk and boundary stochastically. The particles in each lane are distributed under the hard-core exclusion principle (see fig. 2.1). The random-sequential update rules are adopted for dynamic evolvement of the system. For each time step, a lattice site (i, j); $(i = 1, 2, 3, ..., L;\ j = A, B)$ is randomly chosen. The state of system is characterized by a set of occupation numbers $\tau_{i,j}$ $(\nu_{i,j})$ $(i = 1, 2, 3, ..., L; j = A, B)$,

each of which is 0 if (i, j) site is vacant and 1 if (i, j) site is occupied by particle (defect). A defect can bind to a site in any of the lanes with a rate k_+ and unbinds with a rate k_-. Furthermore, the unconstrained defect dynamics are adopted, in which a defect can bind-unbind to and from a site regardless of the particle presence at that site. In case of periodic switching of traffic lights, the lights switch between red and green color irrespective of vehicles aligning in front of traffic signal. The particles follow the dynamical rules explained below.

(i) At the entrance ($i = 1$), a particle can enter the lane j with a rate α provided $\nu_{1,j} = 0$ and $\tau_{1,j} = 0$. In other words, if first site is defect free as well as unoccupied by a particle then a particle can enter with a rate α.

(ii) At the exit ($i = L$), a particle can leave the lattice with a rate β when $\tau_{L,j} = 1$ regardless of presence of defect there.

(iii) In the bulk $1 < i < L$, if $\tau_{i,j} = 1$, a particle in lane j moves forward from i^{th} site to $(i + 1)^{th}$ site with a rate $p_{i,j}$ defined as follows

$$p_{i,j} = \begin{cases} p & \text{if } \nu_{i+1,j} = 0 \\ p_d & \text{if } \nu_{i+1,j} = 1 \end{cases}$$

Clearly, the rate $p_{i,j}$ depends on the defect occupancy at target site, i.e., if there is no defect at target site particle hops with a rate p else the hopping rate becomes p_d.

(iv) If the particle at (i, j) site fails to hop forward (when the $(i + 1, j)$ site is occupied, no forward hopping is possible), it attempts to shift to i^{th} site in other lane with a rate ω if the target site is defect free or ω_d if the target site contains a defect.

For the sake of simplicity, the lane-changing rate from lane A to B and from lane B to A is taken as equal (symmetric coupling). The rate p_d termed as defect rate (throughout this thesis) where $0 \leq p_d \leq p$ is the slow hopping rate in the presence of defect at target site in a lane. If $p_d = 0$, the defect represents a physical barrier completely blocking the particle movement. For $p_d = p$, the model becomes homogeneous TASEP which is exactly solvable and studied in detail in literature [58].

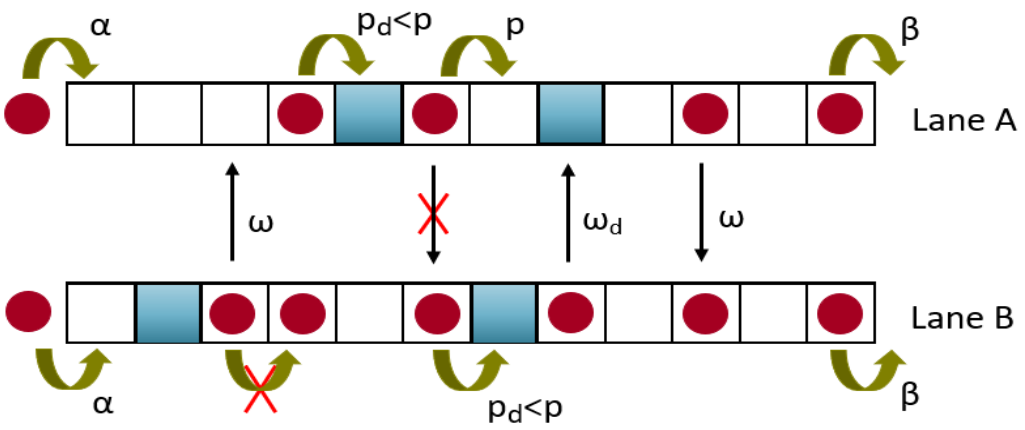

(a)

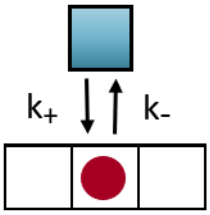

(b)

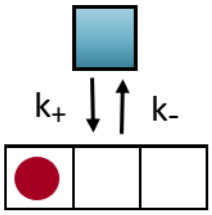

(c)

Figure 2.1: (a) Schematic diagram of a symmetrically coupled two-channel TASEP with dynamic disorder. The defect is represented as a blue shaded site. Crossed arrows indicate forbidden transitions. Illustration of unconstrained defect dynamics with k_+ (defect binding) and k_- (defect unbinding) rates, (b) in the presence and (c) in the absence of a particle at the target site.

2.2 Mathematical analysis

2.2.1 Particle density evolution

Firstly, we compute the temporal evolution of bulk particle densities ($1 < i < L$) in both lanes from the following set of master equations.

$$\begin{aligned}\frac{d\langle\tau_{i,j}\rangle}{dt} &= p\langle\tau_{i-1,j}(1-\tau_{i,j})(1-\nu_{i,j})\rangle + p_d\langle\tau_{i-1,j}(1-\tau_{i,j})(\nu_{i,j})\rangle \\ &- p\langle\tau_{i,j}(1-\tau_{i+1,j})(1-\nu_{i+1,j})\rangle - p_d\langle\tau_{i,j}(1-\tau_{i+1,j})(\nu_{i+1,j})\rangle \\ &\mp \omega\langle\tau_{i,j}\tau_{i+1,j}(1-\tau_{i,j'})(1-\nu_{i,j'})\rangle \mp \omega_d\langle\tau_{i,j}\tau_{i+1,j}(1-\tau_{i,j'})(\nu_{i,j'})\rangle \\ &\pm \omega\langle\tau_{i,j'}\tau_{i+1,j'}(1-\tau_{i,j})(1-\nu_{i,j})\rangle \pm \omega_d\langle\tau_{i,j'}\tau_{i+1,j'}(1-\tau_{i,j})(\nu_{i,j})\rangle\end{aligned} \tag{2.1}$$

where $\langle ... \rangle$ denotes the statistical average and last four terms on the right-hand side take a negative (positive) sign and a positive (negative) sign for lane A (B), respectively. Note that when $j = A$, we have $j' = B$ and when $j = B$, $j' = A$. At the boundaries, the particle density evolves as

$$\begin{aligned}\frac{d\langle \tau_{1,j} \rangle}{dt} &= \alpha\langle (1-\tau_{1,j})(1-\nu_{1,j}) \rangle - p\langle \tau_{1,j}(1-\tau_{2,j})(1-\nu_{2,j}) \rangle \\ &\quad - p_d\langle \tau_{1,j}(1-\tau_{2,j})(\nu_{2,j}) \rangle \end{aligned} \tag{2.2}$$

$$\begin{aligned}\frac{d\langle \tau_{L,j} \rangle}{dt} &= p\langle \tau_{L-1,j}(1-\tau_{L,j})(1-\nu_{L,j}) \rangle + p_d\langle \tau_{L-1,j}(1-\tau_{L,j})(\nu_{L,j}) \rangle \\ &\quad - \beta\langle \tau_{L,j} \rangle \end{aligned} \tag{2.3}$$

2.2.2 Defect density evolution

The defect density for the lattice sites in each lane evolves according to the following equation.

$$\frac{d\langle \nu_{i,j} \rangle}{dt} = k_+\langle 1-\nu_{i,j} \rangle - k_-\langle \nu_{i,j} \rangle \tag{2.4}$$

2.2.3 Continuum mean-field equations

Factorizing the correlations in eqn. (2.1) applying mean-field approximation, we get

$$\langle \tau_{i,j}\tau_{i+1,j} \rangle = \langle \tau_{i,j} \rangle \langle \tau_{i+1,j} \rangle \tag{2.5}$$

To find the continuum limit of the master equations, we coarse-grain the discrete lattice with lattice constant $\epsilon = 1/L$. Writing $x = (i-1)\epsilon$, we replace binary discrete variables $\tau_{i,j}$ and $\nu_{i,j}$ with continuous variables $\rho_{i,j}$ and $\rho_{d_{i,j}} \in [0,1]$ and use the Taylor's series expansion (given below) after retaining the terms up to second-order (for a large system, i.e., $L >> 1$),

$$\rho_{i\pm1,j} = \rho_{i,j} \pm \frac{1}{L}\frac{\partial \rho_{i,j}}{\partial x} + \frac{1}{2L^2}\frac{\partial^2 \rho_{i,j}}{\partial x^2} + O\Big(\frac{1}{L^3}\Big) \tag{2.6}$$

we get

$$\begin{aligned}\frac{\partial \rho_{i,j}}{\partial t} =&\left(\rho_{i,j} - \epsilon\frac{\partial \rho_{i,j}}{\partial x} + \frac{\epsilon^2}{2}\frac{\partial^2 \rho_{i,j}}{\partial x^2}\right)(1-\rho_{i,j})(p(1-\rho_{d_{i,j}}) + p_d\rho_{d_{i,j}}) \\ &- \rho_{i,j}\left(1 - \rho_{i,j} - \epsilon\frac{\partial \rho_{i,j}}{\partial x} - \frac{\epsilon^2}{2}\frac{\partial^2 \rho_{i,j}}{\partial x^2}\right)(p(1-\rho_{d_{i,j}}) + p_d\rho_{d_{i,j}}) \\ &\mp \rho_{i,j}\left(\rho_{i,j} + \epsilon\frac{\partial \rho_{i,j}}{\partial x} + \frac{\epsilon^2}{2}\frac{\partial^2 \rho_{i,j}}{\partial x^2}\right)(1-\rho_{i,j'})(\omega(1-\rho_{d_{i,j'}}) + \omega_d\rho_{d_{i,j'}}) \\ &\pm \rho_{i,j'}\left(\rho_{i,j'} + \epsilon\frac{\partial \rho_{i,j'}}{\partial x} + \frac{\epsilon^2}{2}\frac{\partial^2 \rho_{i,j'}}{\partial x^2}\right)(1-\rho_{i,j})(\omega(1-\rho_{d_{i,j}}) + \omega_d\rho_{d_{i,j}}) \end{aligned} \tag{2.7}$$

$$\begin{aligned}=&\frac{\epsilon^2}{2}(-p\rho_{d_{i,j}} + p + p_d\rho_{d_{i,j}})\frac{\partial^2 \rho_{i,j}}{\partial x^2} + \epsilon(-p + 2p\rho_{i,j} + p\rho_{d_{i,j}} - 2p\rho_{d_{i,j}}\rho_{i,j} \\ &- p_d\rho_{d_{i,j}} + 2p_d\rho_{d_{i,j}}\rho_{i,j})\frac{\partial \rho_{i,j}}{\partial x} \mp [\omega\rho_{i,j}^2(1-\rho_{i,j'})(1-\rho_{d_{i,j'}}) \\ &+ \omega_d\rho_{i,j}^2(1-\rho_{i,j'})\rho_{d_{i,j'}} - \omega\rho_{i,j'}^2(1-\rho_{i,j})(1-\rho_{d_{i,j}}) \\ &- \omega_d\rho_{i,j'}^2(1-\rho_{i,j})\rho_{d_{i,j}}]\end{aligned}$$

2.2.4 Re-scaling of system parameters

At the macroscopic level, the non-conservative part of the system dynamics happens so slowly that the system eventually approaches stationarity with respect to the conservative part of the dynamics. Any finite perturbation arise from the non-conservative dynamics would travel a macroscopic distance and hence disappear before interacting with any another perturbation. Therefore, re-scaling the time variable $t' = t/L$, is necessary to understand involvement of dynamics of particle conserving and non-conserving dynamics.

To ensure the competing interplay between the particle conserving and non-conserving dynamics (lane-changing dynamics), we re-scale the lane-changing rates (ω, ω_d) in such a way that the rates decrease simultaneously with an increase in the system size L, while the rate Ω, Ω_d remain fixed in the limit $L \to \infty$. Thus, we have

$$\Omega = \omega L, \Omega_d = \omega_d L. \tag{2.8}$$

In terms of rescaled variables, eqn. (2.7) becomes

$$\begin{aligned}\frac{\partial \rho_{i,j}}{\partial t'} =& \frac{\epsilon}{2}(-p\rho_{d_{i,j}} + p + p_d\rho_{d_{i,j}})\frac{\partial^2 \rho_{i,j}}{\partial x^2} + (-p + 2p\rho_{i,j} + p\rho_{d_{i,j}} - 2p\rho_{d_{i,j}}\rho_{i,j} \\ & - p_d\rho_{d_{i,j}} + 2p_d\rho_{d_{i,j}}\rho_{i,j})\frac{\partial \rho_{i,j}}{\partial x} \mp [\Omega\rho_j^2(1-\rho_{i,j'})(1-\rho_{d_{i,j'}}) \\ & - \Omega_d\rho_j^2(1-\rho_{i,j'})\rho_{d_{i,j'}} + \Omega\rho_{i,j'}^2(1-\rho_{i,j})(1-\rho_{d_{i,j}}) + \Omega_d\rho_{i,j'}^2(1-\rho_{i,j})\rho_{d_{i,j}}]\end{aligned} \tag{2.9}$$

Since all the lattice sites in the bulk have similar dynamical rules, as dynamical defect can occur anywhere in the lattice irrespective of the site occupancy and their transition rates are site independent, we can drop the subscript i. The average densities (ρ_A and ρ_B) in both lanes, which are the function of continuous time variable t' and space variables $x \in [0,1]$, describe the state of the system as

$$\frac{\partial \rho}{\partial t'} + \frac{\partial J}{\partial x} = S, \tag{2.10}$$

where

$$\rho = \begin{bmatrix} \rho_A \\ \rho_B \end{bmatrix},$$

$$J = \begin{bmatrix} (\frac{\epsilon}{2}p\rho_{dA} - \frac{\epsilon}{2}p - \frac{\epsilon}{2}p_d\rho_{dA})\frac{\partial \rho_A}{\partial x} & + & (p\rho_A - p\rho_A^2 - p\rho_{dA}\rho_A + p\rho_{dA}\rho_A^2 \\ & & +p_d\rho_{dA}\rho_A - p_d\rho_{dA}\rho_A^2) \\ (\frac{\epsilon}{2}p\rho_{dB} - \frac{\epsilon}{2}p - \frac{\epsilon}{2}p_d\rho_{dB})\frac{\partial \rho_B}{\partial x} & + & (p\rho_B - p\rho_B^2 - p\rho_{dB}\rho_B + p\rho_{dA}\rho_B^2 \\ & & +p_d\rho_{dB}\rho_B - p_d\rho_{dB}\rho_B^2) \end{bmatrix},$$

$$S = \begin{bmatrix} -\Omega\rho_A^2(1-\rho_B)(1-\rho_{dB}) - \Omega_d\rho_A^2(1-\rho_B)\rho_{dB} + \Omega\rho_B^2(1-\rho_A)(1-\rho_{dA}) \\ +\Omega_d\rho_B^2(1-\rho_A)\rho_{dA} \\ +\Omega\rho_A^2(1-\rho_B)(1-\rho_{dB}) + \Omega_d\rho_A^2(1-\rho_B)\rho_{dB} - \Omega\rho_B^2(1-\rho_A)(1-\rho_{dA}) \\ -\Omega_d\rho_B^2(1-\rho_A)\rho_{dA} \end{bmatrix}$$

Here S represents the non-conservative terms formed by lane-changing transitions. The components of J are the currents in the particle conservation situation in lanes A and B, respectively. It is to observe that the defect dynamics in both the lanes A and B are similar as k_+ and k_- values for lane A and B are same, which gives equal defect density in each lane, therefore we have, $\rho_{dA} = \rho_{dB} = \rho_d$ (say).

The equations (2.2) and (2.3) in the steady-state reduces to the following equa-

tions.

$$\rho_A(1) = \rho_B(1) = \frac{\alpha(1-\rho_d)}{p(1-\rho_d) + p_d\rho_d}, \tag{2.11}$$

$$\rho_A(L) = \rho_B(L) = 1 - \frac{\beta}{p(1-\rho_d) + p_d\rho_d} \tag{2.12}$$

The system current describing the free flow of particles in the coupled system is given by following expression.

$$J = [p(1-\rho_d) + p_d\rho_d]\rho_j(1-\rho_j), \text{ where j=A, B} \tag{2.13}$$

where the maximum current $J_{max} = J(\rho_{max})$. Also, the defect evolution eqn. (2.4), in continuum limit gives defect density in the system as

$$\rho_d = \frac{k_+}{k_+ + k_-} \tag{2.14}$$

The detailed derivation of the above expressions - particle density at boundaries, system current and defect density are provided in the appendix A. We now determine the steady-state solution of the coupled system (2.10), for which we need to solve the following system along with the boundary conditions given by eqn. (2.11) and (2.12).

$$\begin{aligned}
&\frac{\partial\rho_A}{\partial t'} + \Big(\frac{\epsilon}{2}p\rho_d - \frac{\epsilon}{2}p - \frac{\epsilon}{2}p_d\rho_d\Big)\frac{\partial^2\rho_A}{\partial x^2} + \Big(p - 2p\rho_A - p\rho_d + 2p\rho_d\rho_A + p_d\rho_d \\
&- 2p_d\rho_d\rho_A\Big)\frac{\partial\rho_A}{\partial x} = -\Omega\rho_A^2(1-\rho_B)(1-\rho_d) - \Omega_d\rho_A^2(1-\rho_B)\rho_d \\
&+ \Omega\rho_B^2(1-\rho_A)(1-\rho_d) + \Omega_d\rho_B^2(1-\rho_A)\rho_d, \\
&\frac{\partial\rho_B}{\partial t'} + \Big(\frac{\epsilon}{2}p\rho_d - \frac{\epsilon}{2}p - \frac{\epsilon}{2}p_d\rho_d\Big)\frac{\partial^2\rho_B}{\partial x^2} + \Big(p - 2p\rho_B - p\rho_d + 2p\rho_d\rho_B + p_d\rho_d \\
&- 2p_d\rho_d\rho_B\Big)\frac{\partial\rho_B}{\partial x} = \Omega\rho_A^2(1-\rho_)(1-\rho_d) + \Omega_d\rho_A^2(1-\rho_B)\rho_d \\
&- \Omega\rho_B^2(1-\rho_A)(1-\rho_d) - \Omega_d\rho_B^2(1-\rho_A)\rho_d
\end{aligned} \tag{2.15}$$

2.2.5 Steady-state solution

In order to acquire the steady-state solution of the proposed model, we require to put time derivative of the average particle density equal to zero. In eqn. (5.13), if we equate time derivative terms ($\frac{\partial\rho_A}{\partial t'}$ and $\frac{\partial\rho_B}{\partial t'}$) to zero, we get second-order coupled ordinary differential equations which are difficult to solve analytically. Thus we propose the use of an appropriate numerical scheme to get its steady-state solution by keeping the time derivative term in the equations. Therefore, the solution can

be obtained by capturing the solution over really long time using finite difference scheme discussed below.

The continuous model equations are discretized using finite-difference method and replacing time derivative at site $(i,j);\ i=1,2,\ldots,L;\ j=A,B$ with forward difference formula and first-order and second-order central difference formula for space derivatives. The scheme is applied to model equations represented in eqn. (5.13) along with the boundary conditions given by eqn. (2.11) and (2.12). The following are the difference formulas substituted in eqn. (5.13) to replace time and space derivative terms.

$$\frac{\partial \rho_i^n}{\partial t'} = \frac{\rho_i^{n+1}-\rho_i^n}{\Delta t'} \tag{2.16}$$

$$\frac{\partial \rho_i^n}{\partial x} = \frac{(\rho_{i+1}^n-\rho_{i-1}^n)}{2\Delta x} \tag{2.17}$$

$$\frac{\partial^2 \rho_i^n}{\partial x^2} = \frac{(\rho_{i+1}^n-2\rho_i^n+\rho_{i-1}^n)}{\Delta x^2} \tag{2.18}$$

After substitution, we get the following numerical scheme for the coupled system.

$$\begin{aligned}
&\frac{\rho_{i,j}^{n+1}-\rho_{i,j}^n}{\Delta t'} + \frac{\epsilon}{2}\big(p\rho_d - p - p_d\rho_d\big)\frac{(\rho_{i+1,j}^n - 2\rho_{i,j}^n+\rho_{i-1,j}^n)}{\Delta x^2} + \big(p - 2p\rho_{i,j}^n - p\rho_d \\
&+ 2p\rho_d\rho_{i,j}^n + p_d\rho_d - 2p_d\rho_d\rho_{i,j}^n\big)\frac{(\rho_{i+1,j}^n-\rho_{i-1,j}^n)}{2\Delta x} = \mp\Omega(\rho_{i,j}^n)^2(1-\rho_{i,j'}^n)(1-\rho_d) \\
&\mp \Omega_d(\rho_{i,j}^n)^2(1-\rho_{i,j'}^n)\rho_d \pm \Omega(\rho_{i,j'}^n)^2(1-\rho_{i,j}^n)(1-\rho_d) \pm \Omega_d(\rho_{i,j'}^n)^2(1-\rho_{i,j}^n)\rho_d
\end{aligned}$$

$$\begin{aligned}
\rho_{i,j}^{n+1} &= \rho_{i,j}^n + \frac{\epsilon}{2}\frac{\Delta t'}{\Delta x^2}\big(p - p\rho_d + p_d\rho_d\big)\big(\rho_{i+1,j}^n - 2\rho_{i,j}^n + \rho_{i-1,j}^n\big) \\
&+ \frac{\Delta t'}{2\Delta x}\big(-p + 2p\rho_{i,j}^n + p\rho_d - 2p\rho_d\rho_{i,j}^n - p_d\rho_d + 2p_d\rho_d\rho_{i,j}^n\big)\big(\rho_{i+1,j}^n - \rho_{i-1,j}^n\big) \\
&+ \Delta t'\big(\mp\Omega(\rho_{i,j}^n)^2(1-\rho_{i,j'}^n)(1-\rho_d) \mp \Omega_d(\rho_{i,j}^n)^2(1-\rho_{i,j'}^n)\rho_d \\
&\qquad \pm \Omega(\rho_{i,j'}^n)^2(1-\rho_{i,j}^n)(1-\rho_d) \pm \Omega_d(\rho_{i,j'}^n)^2(1-\rho_{i,j}^n)\rho_d\big)
\end{aligned} \tag{2.19}$$

Here the last four terms take negative (positive) and positive (negative) signs for lane A (B), respectively. The density profiles in the steady-state have been obtained by capturing the solution of the above discretized system in the limit $n\to\infty$, which ensures the occurrence of a steady-state. For the numerical solution, we have taken $L=1000$, $\Delta t'=0.0005$, $\Delta x = 1/L = 0.001$ for the computations, which satisfy the stability condition $|\frac{\Delta t'}{\Delta x}| \le 1$.

2.2.6 Monte Carlo simulation

To validate the outcomes of our theoretical mean-field approach, we simulate the two-channel model using Monte Carlo simulation (MCS) [74]. The random sequential update rule is used, which is the realization of the usual master equation in continuous time. We run the Monte Carlo simulation for $10^8 - 10^9$ time steps and first 5% steps are disregarded as transient The densities in both the lanes have been computed by taking time averages over an interval of $10L$. The lattice size is taken up to $L = 1000$. The following sections show that the results of theoretical mean-field approach give a good agreement with Monte Carlo simulation.

2.3 Results and Discussion

In this section, we provide a detailed discussion of the steady-state dynamics of the proposed model. The resulting phase diagrams, the effect of defect binding/unbinding constants, lane-changing rates, defect rate and the effect of system size are taken into account.

According to the extremal current principle [11] (equating the entrance as well as the exit current with bulk current), we define the critical entry rates $\alpha_c = \beta/(1-\rho_d)$ and $\alpha^* = 2J_{max}/(1-\rho_d)$, as well as the critical exit rate $\beta^* = 2J_{max}$, the phase boundaries are

$$\begin{aligned} &\alpha < \alpha_c; \alpha < \alpha^*(LD) \\ &\alpha > \alpha^*; \beta > \beta^*(MC) \\ &\alpha > \alpha_c; \beta < \beta^*(HD) \end{aligned} \tag{2.20}$$

Here, α^* and β^* are the coordinates of the triple point for the dynamically disordered system. The importance of formulating phase diagram lies in gaining intuitive insight of steady-state dynamics of the system. Fig. 2.2(a) indicates three distinct phases, namely low density phase (LD, LD), maximal current phase (MC, MC) and high density phase (HD, HD) where the first coordinate denotes steady-state phase in lane A and the second coordinate denotes steady-state phase in the lane B. The symmetry in the lane-changing rates cancels the lane-changing source terms with sink terms in the mean-field equations, which gives us two uncoupled ordinary differential equations representing two independent TASEPs with dynamic disorder [58,61]. This preserves the topology of the phase diagram of single-channel TASEP with dynamic disorder [91]. Moreover, due to symmetric coupling between

the lanes, the overlapping of particle densities in both lanes A and B is seen. The density profiles obtained from the results of continuum mean-field (CMF) estimates well with those of Monte Carlo simulation (MCS) shown in fig. 2.2(b), (c) and (d). A slight deviations in the mean-field approximations and Monte-Carlo simulation might be due to reason that mean-field theory and numerical scheme are approximations. This might lead to minor deviations in some parts of the phase space.

Further, it is found that the numerical scheme is valid for the values $\alpha \in [0, 1]$ and $\beta < 4J_{max}$, as clear from expressions of density for left and right boundary. Taking $\beta > 4J_{max}$, the value of parameter $\rho_j(L); j = A, B$, goes out of bounds ($\rho_j(L) < 0$). This is not a possibility in a real traffic situation. The phase diagram for $\beta > 4J_{max}$ is obtained from Monte Carlo simulation.

2.3.1 Shifting of phase boundaries

The study of considered problem is focused to examine the role played by stochastic defect in a two-channel TASEP model with site-wise dynamic disorder, we first attempt to analyze the effect of varying defect binding-unbinding rates (k_+ and k_-) by fixing other system parameters at $p_d = 1/3$, $\Omega = 0.1L$, $\Omega_d = 0.06L$ and $L = 1000$. The defect binding-unbinding rates are known to control defect density in the system, as we calculated earlier that $\rho_d = \frac{k_+}{k_+ + k_-}$.

The steady-state phase diagram for $k_+ = 0.2$ and $k_- = 0.6$, for defect density $\rho_d = 0.25$ in the system, is shown in Fig. 2.2(a). For a comparative study, a steady phase diagram is formulated by considering another set of defect binding-unbinding constants. Fig. 2.3 represents the phase diagram for $k_+ = 0.15$ and $k_- = 0.1$ giving defect density of $\rho_d = 0.6$ in the system. It is clear from fig. 2.2(a) and fig. 2.3 that there is no qualitative difference in phase diagrams, the number of phases also remain the same. The only noticeable difference is the shifting of the phase boundaries in the phase plane, leading to a variation in the size of the three phases. With an increase in the average defect density $\rho_d = k_+/(k_+ + k_-)$ from $(0.2)/(0.2 + 0.6) = 0.25$ to $(0.15)/(0.15 + 0.1) = 0.6$, there is an expansion of LD phase and shrinkage of HD phase. It is evident that with an increase in defect density over the lattice, more number of defects occupy lattice sites as compared to number of particles. As a consequence, the particles begin to cluster and the coupled system is observed to exhibit a low-density profile for an enlarged phase region and high-density region minimizes in the phase plane (α, β). The slight deviations in the analytical results and Monte Carlo simulations are accounted due

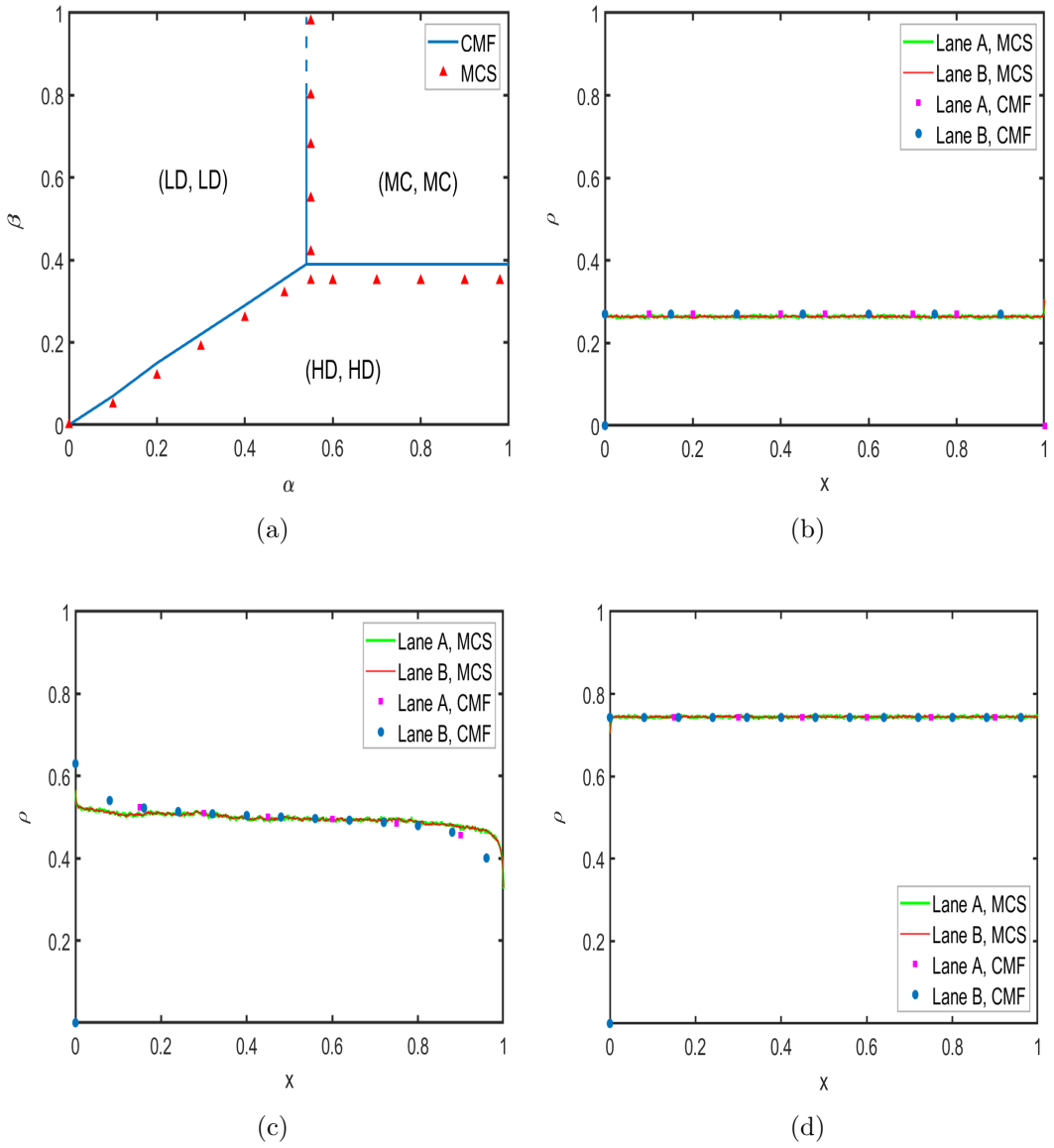

Figure 2.2: For $k_+ = 0.2,\ k_- = 0.6,\ p_d = 1/3,\ \Omega = 0.1L,\ \Omega_d = 0.06L$ (a) Steady-state phase diagram with three phases. The dashed line is the extrapolation of solid phase boundary between (LD-LD) and (MC-MC) phases. Density profiles for (b) (LD-LD)phase $\alpha = 0.3$, $\beta = 0.5$, (c) (MC-MC)phase $\alpha = 0.7$, $\beta = 0.6$ and (d) (HD-HD)phase $\alpha = 0.8$, $\beta = 0.2$.

to mean-field approximation which ignores the correlation between neighbouring sites on the lattice. The simple mean-field approach treats occupation between neighbouring lattice sites to be independent of each other. However, for slower defect dynamics ($k_+, k_- << 1$) there might be some particle-particle and particle-defect correlations present in the system.

Further, we have also investigated the steady phase diagram for a higher value of defect density ρ_d. For any combination of k_+ and k_- giving rise to $\rho_d = 0.9$, it has been observed that the phase diagram consists of only LD phase in $\alpha - \beta$ plane. This observation is supported by greater number of defects present on lattice sites, which reduces particle occupancy to a considerable extent, leaving the system to attain a low-density profile only. Hence, the steady-state of the coupled TASEP demonstrate only LD region in the phase plane. Due to simplicity, we omit providing phase diagram for $\rho_d = 0.9$.

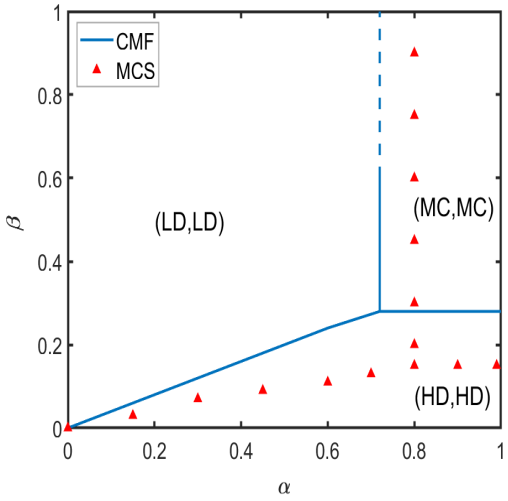

Figure 2.3: For $k_+ = 0.15$, $k_- = 0.1$, $\Omega = 0.1$, $\Omega_d = 0.06$, steady-state phase diagram with three phases.

2.3.2 Current Analysis

Next we explain the effect of k_+ and k_- rates on the flow rate of particles in the steady-state. The expression for current in LD and MC phase is given by

$$J = \begin{cases} \alpha(1-\rho_d)(1-\frac{\alpha(1-\rho_d)}{4J_{max}}) & , \alpha < \alpha^* \\ J_{max} & , \alpha \geq \alpha^* \end{cases} \tag{2.21}$$

Note that, from the expression in eqn. (2.21), the maximum current is independent of system size L. In order to derive parameter-free expression for current in LD phase, the current is expressed as function of normalised entrance rate $\hat{\alpha} = \frac{\alpha}{\alpha^*}$,

we get

$$\frac{J}{J_{max}} = \begin{cases} \hat{\alpha}(1-\hat{\alpha}) & , \hat{\alpha} < 1 \\ 1 & , \hat{\alpha} \geq 1 \end{cases} \tag{2.22}$$

The current J obtained from Monte Carlo simulation for different values of k_+, k_- is divided by J_{max}, and plotted as a function of α/α^* (for $\beta = 1$) in fig. 2.4(a). It is evident that the current in the system firstly rises monotonically up to $\alpha = \alpha^*$, beyond which it remains constant. The region $\alpha < \alpha^*$, $\beta = 1$ corresponds to LD phase, thereby giving $J < J_{max}$. As $\alpha = \alpha^*$, $J = J_{max}$ (transition from LD to MC phase) and for $\alpha > \alpha^*$ there is no further change in current (MC phase). Moreover, this pattern is independent of values of k_+ and k_- which is similar to the observation in single-channel TASEP with site-wise dynamic disorder [91].

Dominance of defect strength over k_+, k_- rates

Another important aspect in exploring the steady-state dynamics of the two-channel ddTASEP model is the strength of disorder represented by parameter p_d. In the TASEP system with no disorder, i.e., $p_d = 1$, and the considered model reduces to a homogeneous two-channel TASEP model under symmetric coupling. It is well reported in literature that under symmetric coupling environment, the homogeneous two-channel TASEP is analogous to its one-channel model. For $p_d > 1$, the defect is termed as fast defect because the particles hopping rate from defected site is more than the standard horizontal hopping rate over the lattice. Thus, we restrict to focus on the case where defect strength is less than p, i.e., $p_d < 1$. Clearly, a decrease in the value of p_d corresponds to an increase in defect strength. The steady-state behavior for distinct values of defect strength is analyzed by uniformly increasing the value of p_d from $p_d = 0$ to $p_d = 1$, fixing defect binding-unbinding rates. For a fixed value of $k_+ = 0.15$ and $k_- = 0.1$, with an increase in the value of p_d, $0 \leq p_d \leq 1$, the dynamic defects become weaker in strength. Thus, one can see that the maximum current in the system increases monotonically till it reaches the global maximum value of $J = 0.25$ which is same as the maximum current in a homogeneous TASEP. Fig. 2.4(b) shows the varying steady-state current with varying strength of the disorder. The effect of defect binding-unbinding rates is dominated by value of defect strength in the system as for any value of k_+ and k_-, particle tends to hop forward over the lattice depending upon the value of p_d. Further, the effect of defect (un-)binding constants on J_{max} is also examined. It is

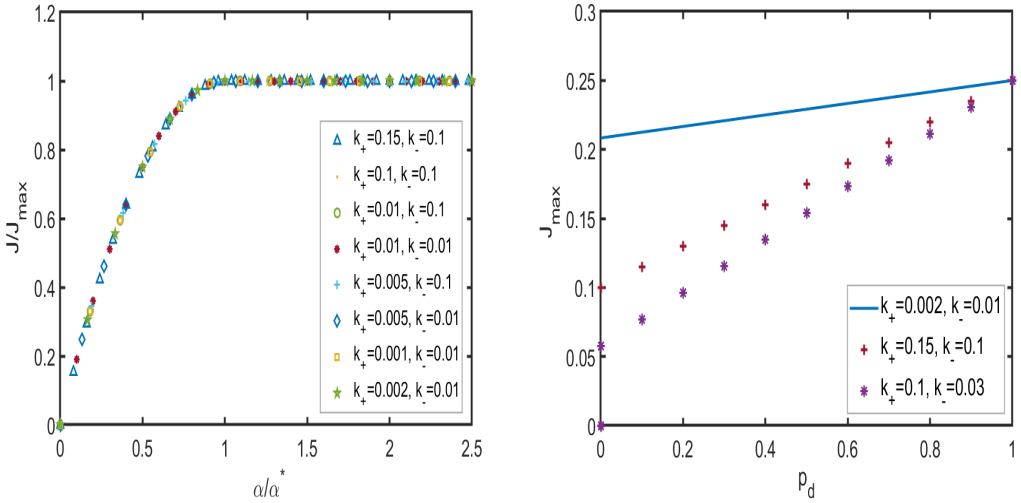

(a) (b)

Figure 2.4: (a) Re-normalized current J/J_{max} as a function of α/α^* for $\beta = 1$. (b) Maximum current J_{max} as a function of slow hopping rate p_d, for $L = 1000$ and varying k_+ and k_-.

observed that increasing the value of defect density (ρ_d) decreases the maximum current in the steady-state of the system as expected.

Current-density relation

Current-density relation (CDR) is examined to study the effect of defect density (ρ_d) and defect strength (p_d). Fig. 2.5 shows the CDR for a fixed value of defect density $\rho_d = 0.8$, with varying p_d value. The curve holds symmetry at the middle of x- axis i.e., around $\rho = 1/2$, similar to the one in standard TASEP model. From the figure, the following observations can be inferred. For weakest defect strength ($p_d = 1$), the particle hopping occurs with uniform rate. There is no significant effect of defect presence and the CDR acquires current same as in standard TASEP, $j_{max} = 0.25$. Upon a decrease in the p_d value from 1 to 0, the defects grows stronger due to which particles hop slower over the lattice. Therefore, the current decreases in the steady-state of the system.

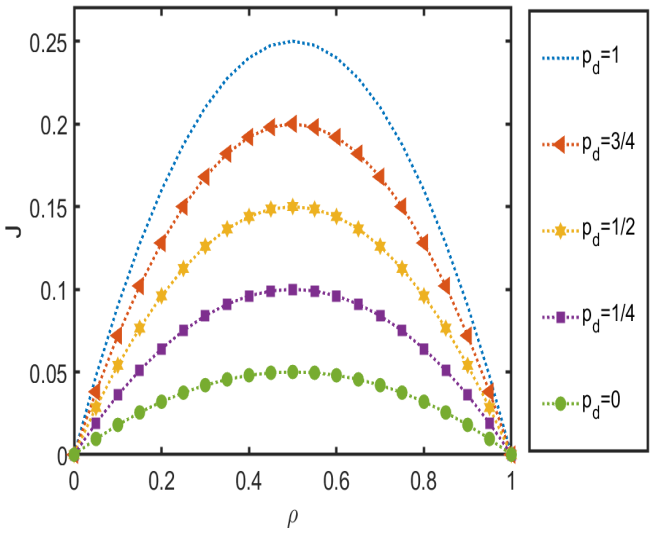

Figure 2.5: Particle current J as a function of particle density ρ for defect density $\rho_d = 0.8$ ($k_+ = 0.8$ and $k_- = 0.2$) and varying slow hopping rate p_d.

2.3.3 Effect of lane-changing rates

So far, we have investigated the effect of defect binding and unbinding constants on the system dynamics, but for fixed lane-changing rates $\Omega = 0.1$ and $\Omega_d = 0.06$. In this section, we study the effect of lane-changing rates on the steady-state system. No significant changes have been seen in phase diagram for any values of Ω which is due to the symmetric coupling environment. Also the lane-changing rate in the presence of defect (Ω_d) shows no considerable effect on stationary dynamics of the two-channel system. Similar observations have been reported in the literature for two-channel TASEP model in [58].

2.3.4 Finite-size effect

Finite-size effect occurs when the sample size of particles is insufficient to describe statistical illustration of the bulk behavior of a physical system. As a result, it is essential to undergo a reliable estimation of finite-size effect in many-particle systems in order to validate theoretical technique and to check accuracy of applied numerical scheme. To eliminate the possibility of any finite-size effect, we investigate the effect of system size on steady-state behavior of inhomogeneous system. In this direction, we have performed Monte Carlo simulation for different system size L= 100, 500 and 1000, which clearly is found to have no effect on the density profiles as shown in fig. 2.6, where the insets are results obtained from continuum

mean-field theory. It is found that the density profiles remain unchanged for all system sizes. Hence, we can infer that the model is independent of effect of any finite system size.

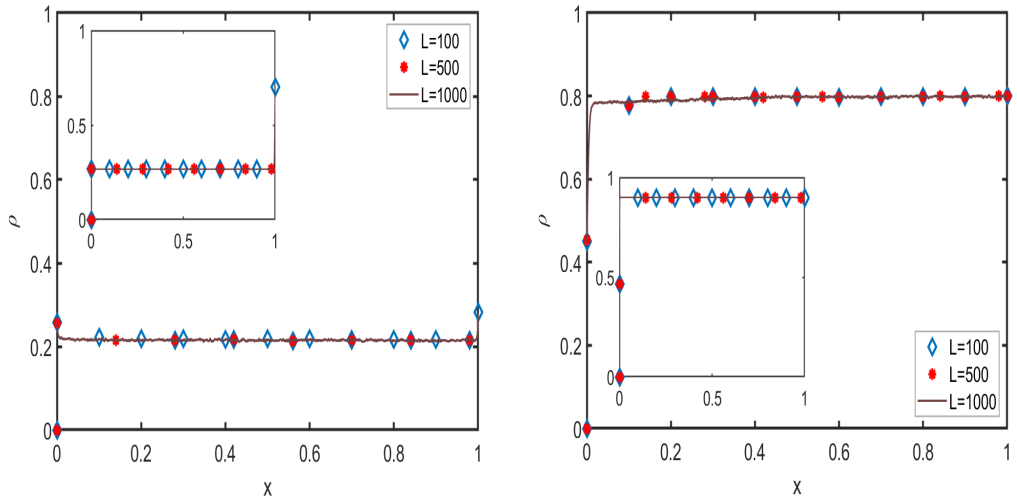

Figure 2.6: Density profiles for L=100, 500 and 1000, fixing $k_+ = 0.15$ and $k_- = 0.1$. The insets in both the figures are results obtained from continuum mean-field. (a) LD phase for $\alpha = 0.4$, $\beta = 0.3$ (b) HD phase for $\alpha = 0.7$, $\beta = 0.1$.

2.4 Conclusion

In this chapter, we have presented a detailed study of two-channel totally asymmetric simple exclusion process with dynamic disorder in both the lanes under symmetric coupling conditions. The case of unconstrained system with open boundary conditions is analyzed where a defect can bind and unbind to any lattice site irrespective of the presence and absence of particle.

Based on the investigation, one finds a rich topology of the steady-state phase diagram under different defect binding-unbinding rates. It is observed that for lower defect density, the stationary-state phase diagram turns out to be similar to its analogue in single-channel system. Nevertheless, the influence of dynamic disorder increases with an increase in its density over the lanes. As our main finding, it has been found that with an increase in the defect density over the lattice, the LD phase expands whereas the HD phase shrinks. Another important

observation is that for a considerable increase in defect density in the system, the steady-state phase diagram consists of only LD phase in $\alpha - \beta$ plane.

The effect of defect rates on the re-normalized current J/J_{max} is also examined. The steady-state current increases monotonically till it reaches a maxima and stabilizes for a further increase in normalised entrance rate. Furthermore, the effect of lane-changing rates on the system dynamics is thoroughly examined and found that due to symmetric coupling the topology of phase diagram in steady-state does not change much. No finite-size effects are observed on the steady-state density profiles.

In this chapter, we presented the effect of symmetric coupling in a two-channel dynamically disordered exclusion process. The following chapter covers the rich dynamics of the coupled system under asymmetric lane-changing rule.

Chapter 3

Asymmetric coupling in a two-channel ddTASEP

The comprehensive investigation of symmetrically coupled two-channel TASEP with dynamic disorder, as considered in last chapter, concludes that the two-channel ddTASEP model behaves similar to its single-channel counterpart. One can conclude that the steady-state behavior of ddTASEP with symmetric coupling is similar to single-channel ddTASEP. Nevertheless, we aspire to know if the same finding holds true for model with asymmetric coupling conditions also. The main difference in the study of current model and one discussed in the last chapter is in the lane-changing dynamics of the system. The symmetric coupling allows equal lane-changing between the lanes, in contrast, the asymmetric coupling deals with unequal rates of lane-changing. The study is motivated by cellular transport of motor proteins over microtubule filaments. At the times, due to structural deformity in the current filament, molecular motors may tend to jump asymmetrically between the chains. Apart from this, asymmetric lane-changing was employed in cellular automaton model in order to reduce accidents during lane-change in driving and overtaking lanes.

The aim of this chapter is to investigate the unexplored case of fully asymmetric coupling in a ddTASEP and draw a detailed description of non-equilibrium phenomena in steady-state. Further, we wish to analyze thoroughly the effect of system parameters, mainly defect and its strength, on the steady-state properties. The main idea in carrying out the analysis is the utilization of vertical cluster mean-field theory (VCMFT), which is found to be appropriate in describing the stationary state properties of the proposed model.

The chapter is organized as follows. The definition of model and its dynamical rules are given in section 3.1. The details of vertical cluster mean-field approach

and its utilization in deriving steady-state density profiles and phase diagram are discussed in section 3.2. The comparison of theoretical predictions with Monte Carlo simulation under fully asymmetric coupling environment is provided in section 3.3. In section 3.5, we briefly summarize the findings.

3.1 Model Description

3.1.1 Definition of the dynamical rules

We define a system of two parallel one-dimensional open lattice channels with the dynamic disorder (ddTASEP), denoted by lane A and lane B (see fig. 3.1). Each lattice has L sites and the identical particles move in a preferred direction. The particles obey hard-core exclusion principle in which each lattice site can be occupied by at most one particle. The dynamical rules for this model are the same as defined in section 2.1, except the following changes. The modified dynamical rules (for lane-changing only) are defined below.

1. Lane-changing rule: In the bulk ($1 < i < L$) of both lanes, a particle at site (i, j) has the following possibility for lane-changing only if the target site is particle free.

   (a) may shift to i^{th} site in other lane with a rate ω_A (lane changing rate from lane A to B) or ω_B (lane changing rate from lane B to A) if the target site is defect free. However, if the target contains a defect, the lane shifting rate is ω_{AD} (from lane A to B) or ω_{BD} (from lane B to A).

3.2 Theoretical analysis

3.2.1 Vertical Cluster Mean-Field Theory

This section discusses a theoretical approach to obtain the steady-state solution of the proposed TASEP model. Despite that the vertical cluster mean-field theory (VCMFT) neglects correlations between horizontal transitions, it is found to be the most effective and efficient method utilized to examine the role of asymmetric coupling. In the coupled two-channel homogeneous TASEP systems, the asymmetric lane interactions introduce significant vertical correlations and influence the steady-state properties of the system. Further, the inclusion of dynamic defects (as in our model) makes the corresponding model very complex to be solved exactly

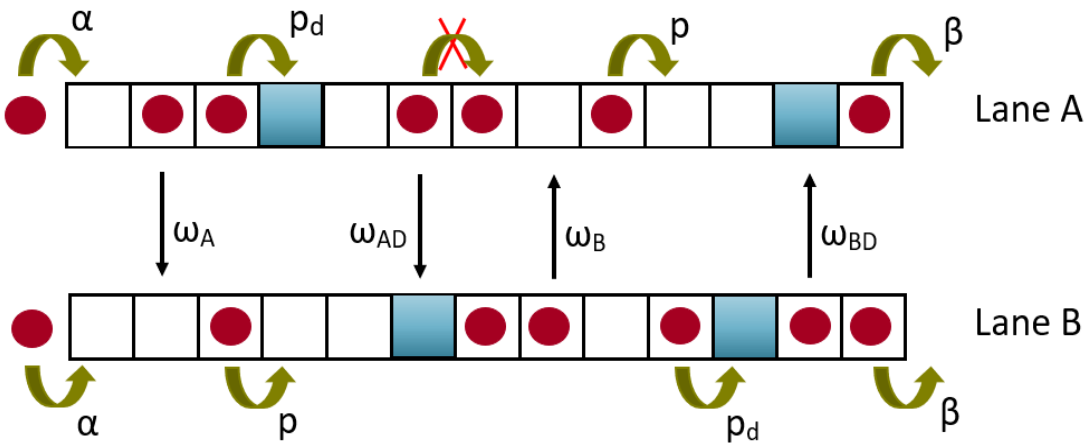

(a)

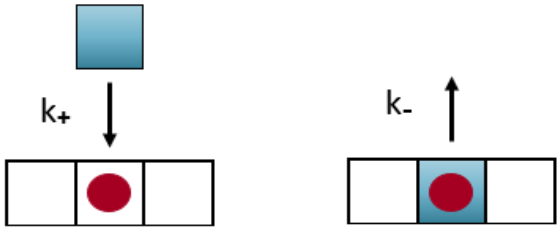

(b) (c)

Figure 3.1: (a) A schematic view of asymmetrically coupled two-channel TASEP with dynamic disorder. Circles describe particles and shaded squares are dynamic defects. An illustration of unconstrained defect dynamic (b) defect binding with rate k_+ and (c) defect unbinding with rate k_-.

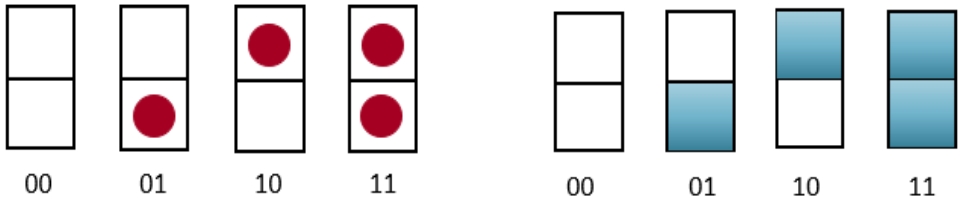

(a) (b)

Figure 3.2: Different possible configurations of a vertical cluster representing (a) particles and (b) defects in the system.

or using a simple mean-field approach. The VCMFT has been widely used in the past to study the steady-state behavior of many complex variants of TASEP as it makes up for some correlations in such systems [58, 59, 61, 106]. Below, we derive

the mathematical equations of the dynamically disordered coupled TASEP using VCMFT.

A vertical cluster at a site is described as a cluster of two sites, with one site from lane A and other from lane B. As we know, there are only two possible states for particle or defect occupancy for a lattice site, represented by 1 or 0. The four possible configurations for a vertical cluster depending upon the occupancy of the sites by particle are defined as: 11 for fully-filled vertical cluster (sites in both the lanes are occupied), 01 (10) for half-filled vertical cluster (exactly one of the two lanes occupied) and 00 for an empty vertical cluster (empty sites in both the lanes) as shown in fig. 3.2(a). The respective steady-state probabilities of a site are given by P_{11}, P_{01}, P_{10} and P_{00}. The corresponding vertical cluster probabilities for the occupancy of lattice sites by dynamic defects are denoted by Q_{11}, Q_{01}, Q_{10}, and Q_{00} (fig. 3.2(b)). The conservation of probability gives the following two conditions:

$$P_{00} + P_{01} + P_{10} + P_{11} = 1 \tag{3.1}$$

$$\text{and} \quad Q_{00} + Q_{01} + Q_{10} + Q_{11} = 1 \tag{3.2}$$

3.2.2 Master equations

In this section, we compute the master equations for temporal evolution of vertical cluster probabilities P_{11}, P_{01}, P_{10}, P_{00} and Q_{11}, Q_{01}, Q_{10}, Q_{00}. To compute the rate of change of probability of a vertical cluster with respect to time, all the possible configurations describing incoming to the cluster and outgoing from a cluster are identified and the respective gain and loss terms are formulated. A pictorial representation of gain and loss terms for fully-filled vertical cluster are shown in fig. 3.3 and 3.4 respectively. One can form the below written master equations for the bulk sites on the basis of these configurations.

$$\begin{aligned}
\frac{dP_{11}}{dt} &= P_{01}P_{10}(Q_{00}+Q_{10}) + p_d P_{01}P_{10}(Q_{01}+Q_{11}) + P_{11}P_{10}(Q_{00}+Q_{10}) \\
&+ p_d P_{11}P_{10}(Q_{01}+Q_{11}) + P_{10}P_{01}(Q_{00}+Q_{01}) + p_d P_{10}P_{01}(Q_{10}+Q_{11}) \\
&+ P_{11}P_{01}(Q_{00}+Q_{01}) + p_d P_{11}P_{01}(Q_{10}+Q_{11}) - P_{11}P_{00}(Q_{00}+Q_{01}) \\
&- p_d P_{11}P_{00}(Q_{10}+Q_{11}) - P_{11}P_{00}(Q_{00}+Q_{10}) - p_d P_{11}P_{00}(Q_{01}+Q_{11}) \\
&- P_{11}P_{10}(Q_{00}+Q_{10}) - p_d P_{11}P_{10}(Q_{01}+Q_{11}) - P_{11}P_{01}(Q_{00}+Q_{01}) \\
&- p_d P_{11}P_{01}(Q_{10}+Q_{11})
\end{aligned} \tag{3.3}$$

Similarly, the master equations describing the temporal evolution of clusters

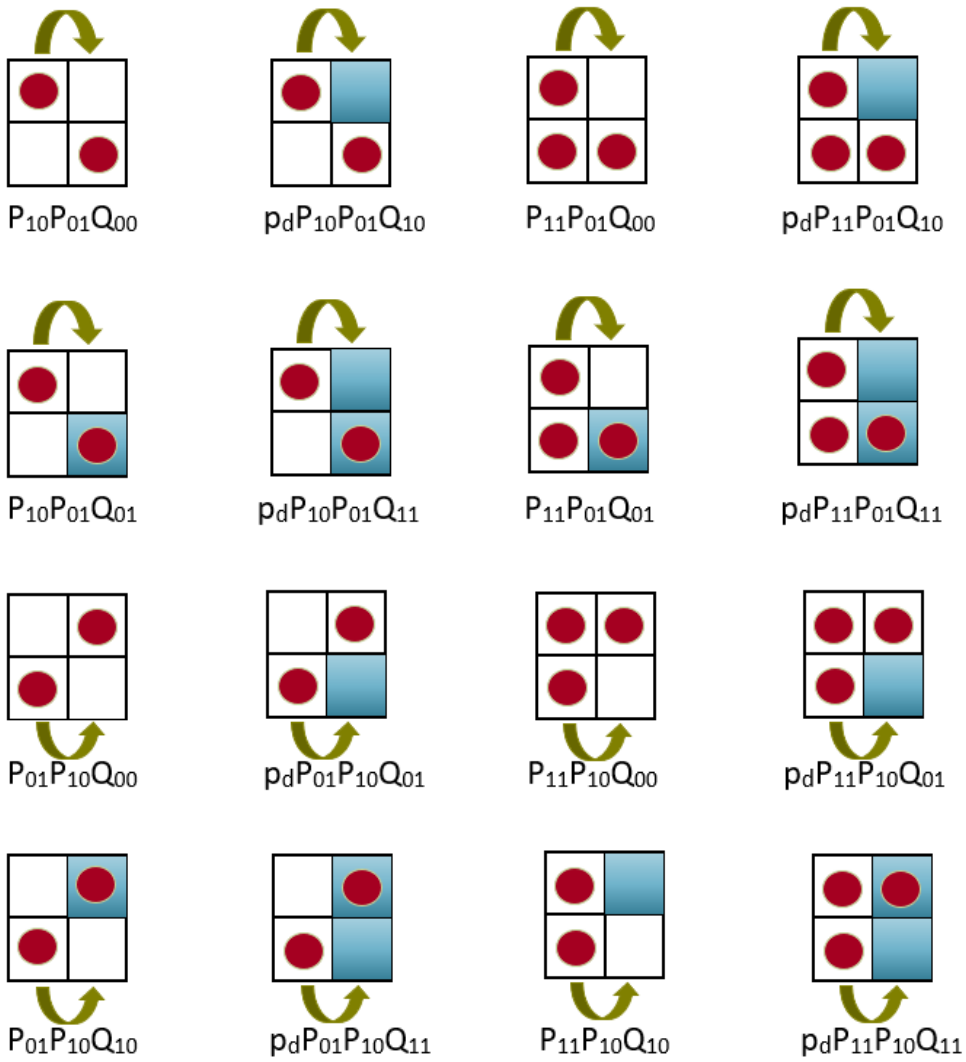

Figure 3.3: Gain terms: Different possible configurations incoming to probability P_{11}.

P_{01}, P_{10} and P_{00} are obtained as follows.

$$\begin{aligned}\frac{dP_{01}}{dt} &= P_{01}P_{00}(Q_{00}+Q_{10}) + p_dP_{01}P_{00}(Q_{01}+Q_{11}) + P_{11}P_{00}(Q_{00}+Q_{01}) \\ &+ p_dP_{11}P_{00}(Q_{10}+Q_{11}) + P_{11}P_{00}(Q_{00}+Q_{10}) + p_dP_{11}P_{00}(Q_{01}+Q_{11}) \\ &+ P_{11}P_{01}(Q_{00}+Q_{01}) + p_dP_{11}P_{01}(Q_{10}+Q_{11}) + \omega_A P_{10}(Q_{00}+Q_{10}) \\ &+ \omega_{AD}P_{10}(Q_{01}+Q_{11}) - P_{10}P_{01}(Q_{00}+Q_{01}) - p_dP_{10}P_{01}(Q_{10}+Q_{11}) \\ &- P_{11}P_{01}(Q_{00}+Q_{01}) - p_dP_{11}P_{01}(Q_{10}+Q_{11}) - P_{01}P_{00}(Q_{00}+Q_{10}) \\ &- p_dP_{01}P_{00}(Q_{01}+Q_{11}) - P_{01}P_{10}(Q_{00}+Q_{10}) - p_dP_{01}P_{10}(Q_{01}+Q_{11}) \\ &- \omega_B P_{01}(Q_{00}+Q_{01}) - \omega_{BD}P_{01}(Q_{10}+Q_{11})\end{aligned} \tag{3.4}$$

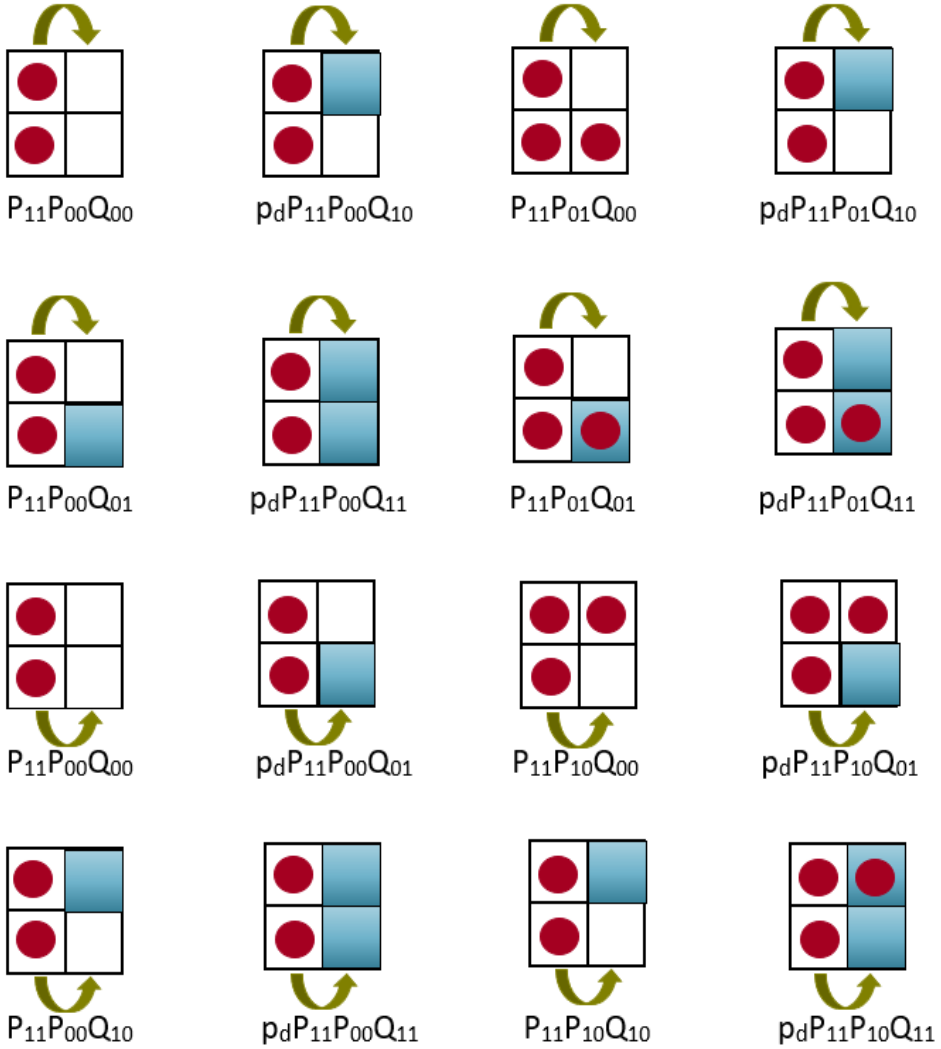

Figure 3.4: Loss terms: Different possible configurations outgoing from probability P_{11}.

$$
\begin{aligned}
\frac{dP_{10}}{dt} &= P_{10}P_{00}(Q_{00}+Q_{01}) + p_d P_{10}P_{00}(Q_{10}+Q_{11}) + P_{11}P_{00}(Q_{00}+Q_{01}) \\
&+ p_d P_{11}P_{00}(Q_{10}+Q_{11}) + P_{11}P_{00}(Q_{00}+Q_{10}) + p_d P_{11}P_{00}(Q_{01}+Q_{11}) \\
&+ P_{11}P_{10}(Q_{00}+Q_{10}) + p_d P_{11}P_{10}(Q_{01}+Q_{11}) + \omega_B P_{01}(Q_{00}+Q_{01}) \\
&+ \omega_{BD} P_{01}(Q_{10}+Q_{11}) - P_{01}P_{10}(Q_{00}+Q_{10}) - p_d P_{01}P_{10}(Q_{01}+Q_{11}) \\
&- P_{11}P_{10}(Q_{00}+Q_{10}) - p_d P_{11}P_{10}(Q_{01}+Q_{11}) - P_{10}P_{00}(Q_{00}+Q_{01}) \\
&- p_d P_{10}P_{00}(Q_{10}+Q_{11}) - P_{10}P_{01}(Q_{00}+Q_{01}) - p_d P_{10}P_{01}(Q_{10}+Q_{11}) \\
&- \omega_A P_{10}(Q_{00}+Q_{10}) - \omega_{AD} P_{10}(Q_{01}+Q_{11})
\end{aligned}
\tag{3.5}
$$

$$
\begin{aligned}
\frac{dP_{00}}{dt} &= P_{10}P_{00}(Q_{00}+Q_{01}) + p_d P_{10}P_{00}(Q_{10}+Q_{11}) + P_{10}P_{01}(Q_{00}+Q_{01}) \\
&+ p_d P_{10}P_{01}(Q_{10}+Q_{11}) + P_{01}P_{00}(Q_{00}+Q_{10}) + p_d P_{01}P_{00}(Q_{01}+Q_{11}) \\
&+ P_{01}P_{10}(Q_{00}+Q_{10}) + p_d P_{01}P_{10}(Q_{01}+Q_{11}) - P_{10}P_{00}(Q_{00}+Q_{01}) \\
&- p_d P_{10}P_{00}(Q_{10}+Q_{11}) - P_{01}P_{00}(Q_{00}+Q_{10}) - p_d P_{01}P_{00}(Q_{01}+Q_{11}) \\
&- P_{11}P_{00}(Q_{00}+Q_{01}) - p_d P_{11}P_{00}(Q_{10}+Q_{11}) - P_{11}P_{00}(Q_{00}+Q_{10}) \\
&- p_d P_{11}P_{00}(Q_{01}+Q_{11})
\end{aligned} \tag{3.6}
$$

Similarly, the master equations describing the temporal evolution of defect vertical cluster probabilities are described below.

$$\frac{dQ_{10}}{dt} = k_+ Q_{00} + k_- Q_{11} - k_- Q_{10} - k_+ Q_{10} \tag{3.7}$$

$$\frac{dQ_{00}}{dt} = k_- Q_{10} + k_- Q_{01} - 2k_+ Q_{00} \tag{3.8}$$

$$\frac{dQ_{11}}{dt} = k_+ Q_{10} + k_+ Q_{01} - 2k_- Q_{11} \tag{3.9}$$

$$\frac{dQ_{01}}{dt} = k_+ Q_{00} + k_- Q_{11} - k_- Q_{01} - k_+ Q_{01} \tag{3.10}$$

3.2.3 Steady-state solution

We analyze the steady-state dynamics of the system by solving

$$\frac{dP_{10}}{dt} = \frac{dP_{00}}{dt} = \frac{dP_{11}}{dt} = \frac{dP_{01}}{dt} = 0 \tag{3.11}$$

$$\frac{dQ_{10}}{dt} = \frac{dQ_{00}}{dt} = \frac{dQ_{11}}{dt} = \frac{dQ_{01}}{dt} = 0 \tag{3.12}$$

The symmetry in defect dynamics between both the lanes A and B gives $Q_{10} = Q_{01}$. In steady-state, the eqns. (3.7) and (3.8) gives expression for probabilities Q_{00} and Q_{11} in terms of Q_{10}.

$$Q_{00} = \frac{k_-}{k_+} Q_{10} \quad \text{and} \quad Q_{11} = \frac{k_+}{k_-} Q_{10} \tag{3.13}$$

Furthermore, substituting the expressions given by eqn. (3.13) into eqn. (3.2), we evaluate the steady-state defect probabilities in terms of defect binding (k_+) and

unbinding (k_-) rates.

$$Q_{10} = Q_{01} = \frac{k_+ k_-}{(k_+ + k_-)^2} \tag{3.14}$$

$$Q_{00} = \frac{k_-^2}{(k_+ + k_-)^2} \tag{3.15}$$

$$Q_{11} = \frac{k_+^2}{(k_+ + k_-)^2} \tag{3.16}$$

For simplicity, we denote $Q_{00} + Q_{01} = Q_{00} + Q_{10} = X$ and $Q_{01} + Q_{11} = Q_{10} + Q_{11} = Y$. The set of equations given by eqn. (3.11), due to particle-hole symmetry, reduces to the following system of equations.

$$\begin{aligned} 2P_{11}P_{00}(X + p_d Y) &= 2P_{01}P_{10}(X + p_d Y), \\ 2P_{11}P_{00}(X + p_d Y) &= 2P_{10}P_{01}(X + p_d Y) + P_{10}(\omega_A X + \omega_{AD} Y) \\ &\quad - P_{01}(\omega_B X + \omega_{BD} Y) \end{aligned} \tag{3.17}$$

which further leads to

$$P_{10} = P_{01} \frac{(\omega_B X + \omega_{BD} Y)}{(\omega_A X + \omega_{AD} Y)} \tag{3.18}$$

Equation (3.18) is valid when $\omega_A, \omega_{AD} \neq 0$. Clearly, X and Y are not both zero because $X + Y = 1$.

Now, we derive the particle density at the entrance and exit sites, denoted by $\rho_{1,A}$ ($\rho_{1,B}$) and $\rho_{L,A}$ ($\rho_{L,B}$) respectively. Clearly, $\rho_{1,A} = \rho_{1,B}$ and $\rho_{L,A} = \rho_{L,B}$ and let us write $\rho_{1,A} = \rho_{1,B} = \rho_1$ and $\rho_{L,A} = \rho_{L,B} = \rho_L$.

***At Entrance*:**

$$\begin{aligned} \frac{dP_{10}}{dt} &= \alpha P_{00}(Q_{00} + Q_{01}) + P_{11}P_{10}(Q_{00} + Q_{10}) + p_d P_{11}P_{10}(Q_{01} + Q_{11}) \\ &\quad + P_{11}P_{00}(Q_{00} + Q_{10}) + p_d P_{11}P_{00}(Q_{01} + Q_{11}) - P_{10}P_{00}(Q_{00} + Q_{01}) \\ &\quad - p_d P_{10}P_{00}(Q_{10} + Q_{11}) - P_{10}P_{01}(Q_{00} + Q_{01}) - p_d P_{10}P_{01}(Q_{10} + Q_{11}) \\ &\quad - \alpha P_{10}(Q_{00} + Q_{10}) \end{aligned} \tag{3.19}$$

$$\begin{aligned} \frac{dP_{00}}{dt} &= P_{01}P_{00}(Q_{00} + Q_{10}) + p_d P_{01}P_{00}(Q_{01} + Q_{11}) + P_{01}P_{10}(Q_{00} + Q_{10}) \\ &\quad + p_d P_{01}P_{10}(Q_{01} + Q_{11}) + P_{10}P_{00}(Q_{00} + Q_{01}) + p_d P_{10}P_{00}(Q_{10} + Q_{11}) \\ &\quad + P_{10}P_{01}(Q_{00} + Q_{01}) + p_d P_{10}P_{01}(Q_{10} + Q_{11}) - \alpha P_{00}(Q_{00} + Q_{01}) \\ &\quad - \alpha P_{00}(Q_{00} + Q_{10}) \end{aligned} \tag{3.20}$$

It is noteworthy that, at entrance site the vertical cluster probability $P_{01} = P_{10}$ as the dynamical rules excludes lane-changing at this site. The master equation

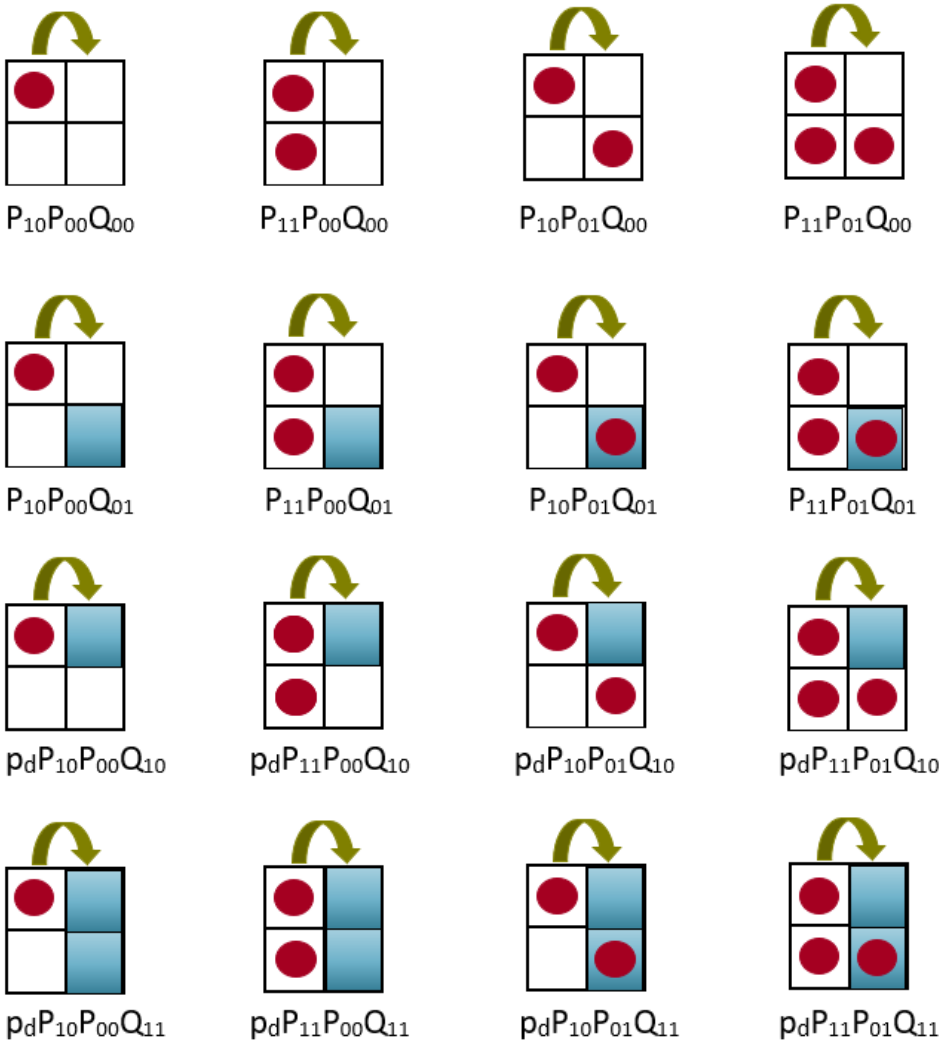

Figure 3.5: The horizontal particle transitions in the bulk of lane A.

for vertical cluster P_{11} can be derived using above equations along with eqn. (3.1). Solving eqns. (3.1), (3.19) and (3.20) in the steady-state of the system and using $P_{01} = P_{10}$, we get the following expressions for P_{00} and P_{01}.

$$P_{00} = \frac{((\alpha - 1)X - p_d Y)^2}{(X + p_d Y)^2} \quad \text{and} \quad P_{01} = \frac{\alpha X^2 - \alpha^2 X^2 + \alpha p_d XY}{(X + p_d Y)^2} \tag{3.21}$$

Hence, the average particle density at the first site of the lattice in each lane is

given by

$$\begin{aligned}\rho_1 &= 1 - P_{00} - P_{01} \\ &= 1 - \frac{((\alpha-1)X - p_d Y)^2}{(X+p_d Y)^2} - \frac{\alpha X^2 - \alpha^2 X^2 + \alpha p_d XY}{(X+p_d Y)^2} \\ &= \frac{\alpha X}{X+p_d Y}\end{aligned} \tag{3.22}$$

***At Exit*:**

$$\begin{aligned}\frac{dP_{10}}{dt} &= P_{10}P_{00}(Q_{00}+Q_{01}) + p_d P_{10}P_{00}(Q_{10}+Q_{11}) + P_{11}P_{00}(Q_{00}+Q_{01}) \\ &+ p_d P_{11}P_{00}(Q_{10}+Q_{11}) + \beta P_{11} - \beta P_{10} - P_{01}P_{10}(Q_{00}+Q_{10}) \\ &- p_d P_{01}P_{10}(Q_{01}+Q_{11}) - P_{11}P_{10}(Q_{00}+Q_{10}) - p_d P_{11}P_{10}(Q_{01}+Q_{11})\end{aligned} \tag{3.23}$$

$$\begin{aligned}\frac{dP_{00}}{dt} &= \beta P_{10} + \beta P_{01} - P_{10}P_{00}(Q_{00}+Q_{01}) - p_d P_{10}P_{00}(Q_{10}+Q_{11}) \\ &- P_{01}P_{00}(Q_{00}+Q_{01}) - p_d P_{01}P_{00}(Q_{10}+Q_{11}) - P_{11}P_{00}(Q_{00}+Q_{01}) \\ &- p_d P_{11}P_{00}(Q_{10}+Q_{11}) - P_{11}P_{00}(Q_{00}+Q_{10}) - p_d P_{11}P_{00}(Q_{01}+Q_{11})\end{aligned} \tag{3.24}$$

Solving the eqns. (3.1), (3.23) and (3.24) in the stationary-state of the system, we get the following expressions.

$$P_{00} = \frac{\beta^2}{(X+p_d Y)^2} \quad \text{and} \quad P_{01} = \frac{\beta(-\beta + X + p_d Y)}{(X+p_d Y)^2} \tag{3.25}$$

Hence, the average particle density at the last site of the lattice in each lane is given by

$$\begin{aligned}\rho_L &= 1 - P_{00} - P_{01} \\ &= 1 - \frac{\beta^2}{(X+p_d Y)^2} - \frac{\beta(-\beta + X + p_d Y)}{(X+p_d Y)^2} \\ &= 1 - \frac{\beta}{X+p_d Y}\end{aligned} \tag{3.26}$$

Further, we compute the system bulk current in one of the lanes (say lane A). Since it is known that current in the system is produced as a consequence of horizontal motion of particles and the vertical particle transition to other lane do not add to net flow rate. Therefore, the current for each lanes has been computed by considering horizontal transitions in respective lane. Fig. 3.5 shows the pictorial

representation of bulk current in lane A, denoted by $J_{bulk,A}$. Hence, we have

$$\begin{aligned} J_{bulk,A} &= P_{10}P_{00}(Q_{00}+Q_{01}) + p_d P_{10}P_{00}(Q_{10}+Q_{11}) + P_{11}P_{00}(Q_{00}+Q_{01}) \\ &\quad + p_d P_{11}P_{00}(Q_{10}+Q_{11}) + P_{10}P_{01}(Q_{00}+Q_{01}) + p_d P_{10}P_{01}(Q_{10}+Q_{11}) \\ &\quad + P_{11}P_{01}(Q_{00}+Q_{01}) + p_d P_{11}P_{01}(Q_{10}+Q_{11}) \\ &= P_{10}P_{00}(X+p_dY) + P_{11}P_{00}(X+p_dY) + P_{10}P_{01}(X+p_dY) \\ &\quad + P_{11}P_{01}(X+p_dY) \\ &= (P_{11}+P_{10})(1-P_{11}-P_{10})(X+p_dY) \end{aligned} \tag{3.27}$$

On the similar lines, the current for boundaries and bulk sites have been obtained which are given below.

$$\begin{aligned} J_{entr,A} &= \alpha(P_{01}+P_{00})X \\ J_{entr,B} &= \alpha(P_{10}+P_{00})X \\ J_{bulk,A} &= (P_{11}+P_{10})(1-P_{11}-P_{10})(X+p_dY) \\ J_{bulk,B} &= (P_{11}+P_{01})(1-P_{11}-P_{01})(X+p_dY) \\ J_{exit,A} &= \beta(P_{11}+P_{10}) \\ J_{exit,B} &= \beta(P_{11}+P_{01}) \end{aligned} \tag{3.28}$$

We now move towards our goal of the present study, in the upcoming section results have been provided for the case of fully asymmetric coupling between the lanes.

3.3 Results and Discussion

In this chapter, we focus on investigating the particular case of fully asymmetric coupling, in which lane-changing is allowed only from one lane to other. We consider both the coupling rates as non-zero ($\omega_A, \omega_B \neq 0$) while deriving model equations but the results are carried out only for fully-asymmetric case. The full asymmetry in the vertical transition rates means particles can shift from lane A to lane B with a non-zero rate ω_A or ω_{AD} (depending upon defect's existence) but shifting from lane B to lane A is prohibited ($\omega_B = \omega_{BD} = 0$).

Further, we analyze the steady-state behavior of the system which are mainly governed by four parameters: the defect binding-unbinding rates k_+ and k_-, the lane-changing rate ω_A and defect strength p_d. To analyze the role of each of these parameters in-depth, the phase diagrams and density profiles are generated, which compare our theoretical calculations with the computer simulation results. To tes-

tify the results derived from vertical cluster mean-field approach, the two-channel inhomogeneous model has been prompted with Monte Carlo simulation. In simulation, the random sequential update rules are used (discussed in previous chapters) for lattice length $L = 5000$. We run Monte Carlo simulation for $10^9 - 10^{10}$ time steps to be certain of occurrence of steady-state and also first 5% time steps are discarded as transient. Time averages over a $10L$ interval have been used to calculate the density in each lanes.

The vanishing of ω_B and ω_{BD} simplifies the system dynamics to a greater extent. One finds an interesting topological structure of the stationary phase diagram as will be discussed later. From eqn. (3.18), we have

$$P_{10} = 0 \tag{3.29}$$

which along with steady-state eqn. (3.17) gives $P_{11}P_{00} = 0$. The possible solutions for vertical cluster probabilities are discussed in the following cases.

- $P_{10} = P_{11} = 0$
- $P_{10} = P_{00} = 0$

Case 1:

In this case, we have $P_{10} = P_{11} = 0$, which infers that bulk of lane A is empty (i.e. $\rho_{bulk,A} = 0$) and non-zero particle current comes across lane B only. This leaves behind only P_{00} and P_{01} vertical cluster probabilities with the relation $P_{00} = 1 - P_{01}$. The simplified particle current expressions are given by

$$\begin{aligned} J_{entr,A} &= \alpha X & J_{entr,B} &= \alpha P_{00} X \\ J_{bulk,A} &= 0 & J_{bulk,B} &= P_{01}(1 - P_{01})(X + p_d Y) \\ J_{exit,A} &= 0 & J_{exit,B} &= \beta P_{01} \end{aligned} \tag{3.30}$$

The two-channel system with the dynamic disorder can be mapped onto a one-channel TASEP with dynamic disorder with effective entrance and exit rates as α_{eff} and β_{eff} respectively. In this one-channel system, particles are denoted by vertical cluster (01) and holes by vertical cluster (00). The effective entrance rate α_{eff} is different from α as there are two entrance currents in the system, whereas the effective exit rate is the same as β due to the fact that the lane A is empty, and particles exit from lane B only. It is well known from [91] that the corresponding one-channel TASEP with dynamic disorder has three phases, namely low-density (LD), high-density (HD), and maximal-current phase (MC). Our system also exists in three steady-state phases described by (0, LD), (0, HD) and (0, MC). The first

index in the label signifies that bulk of lane A is always empty, while the second index state is controlled by entrance and exit of the system.

(i) (0, LD): In low-density phase (0, LD), the bulk current is determined by entrance current utilizing which we can compute the effective entrance rate and current in the system, that is $J_{entr,A} + J_{entr,B} = J_{bulk,A} + J_{bulk,B}$.

From eqn. (3.30), we have

$$\alpha_{eff}(1 - P_{01})X = \alpha(2 - P_{01})X = P_{01}(1 - P_{01})(X + p_d Y) \tag{3.31}$$

Thus, the expression for half-filled vertical cluster probability (P_{01}) and the effective entrance rate (α_{eff}) are computed using eqn. (3.31) and are given by

$$P_{01} = \frac{(\alpha X + X + p_d Y) - \sqrt{\big((\alpha X + X + p_d Y)^2 - 8\alpha X(X + p_d Y)\big)}}{2(X + p_d Y)} \tag{3.32}$$

$$\begin{aligned} \alpha_{eff} &= P_{01}\frac{(X + p_d Y)}{X} \\ &= \frac{(\alpha X + X + p_d Y) - \sqrt{\big((\alpha X + X + p_d Y)^2 - 8\alpha X(X + p_d Y)\big)}}{2X} \end{aligned} \tag{3.33}$$

The (0, LD) phase occurs for $\alpha_{eff} < \alpha_c$ and $\alpha_{eff} < \alpha^*$, which leads to

$$\begin{aligned} \beta &> \frac{(\alpha X + X + p_d Y) - \sqrt{\big((\alpha X + X + p_d Y)^2 - 8\alpha X(X + p_d Y)\big)}}{2} \\ \alpha &< \frac{35X + 84 p_d Y}{204X + 288 p_d Y} \end{aligned} \tag{3.34}$$

with total current in the phase given by

$$J_{(0,LD)} = \alpha_{eff}(1 - \alpha_{eff})(X + p_d Y) \tag{3.35}$$

The detailed calculations for the existence of phase boundaries are provided in appendix B.

(ii) (0, HD): For the high density phase (0, HD), the exit current regulates the bulk current, which gives $P_{01}(1 - P_{01})(X + p_d Y) = \beta P_{01}$.

Thus, in this phase we can obtain the expression for half-filled vertical cluster probability

$$P_{01} = 1 - \frac{\beta}{X + p_d Y} \tag{3.36}$$

and the phase exists for $\alpha_c < \alpha_{eff}$ and $\beta < \beta^*$, which leads to

$$\begin{aligned} \beta &< \frac{(\alpha X + X + p_d Y) - \sqrt{\left((\alpha X + X + p_d Y)^2 - 8\alpha X(X + p_d Y)\right)}}{2} \\ \beta &< 2J_{max} \end{aligned} \tag{3.37}$$

with the steady-state current given by

$$J_{(0,HD)} = \beta(1 - \beta)(X + p_d Y) \tag{3.38}$$

(iii) (0, MC): The (0, MC) phase corresponds to maximal current in the bulk of lane B and exists for $\alpha^* < \alpha_{eff}$ and $\beta^* < \beta$. The vertical cluster probability and the bulk particle current in this phase are expressed as

$$P_{01} = \frac{3}{4}(X + p_d Y) \quad \text{and} \quad J_{(0,MC)} = P_{01}(1 - P_{01})(X + p_d Y) \tag{3.39}$$

Case 2:

Now, we consider the case in which the steady-state solution is described by $P_{10} = P_{00} = 0$. This implies $P_{01} + P_{11} = 1$ i.e., the bulk of lane B is completely filled, and non-zero particle current flows in lane A only. The expression for particle currents in the system are given below.

$$\begin{aligned} J_{entr,A} &= \alpha(1 - P_{11})X & J_{entr,B} &= 0 \\ J_{bulk,A} &= P_{11}(1 - P_{11})(X + p_d Y) & J_{bulk,B} &= 0 \\ J_{exit,A} &= \beta P_{11} & J_{exit,B} &= \beta \end{aligned} \tag{3.40}$$

Parallel to the previous case, here P_{11} are the effective particles and P_{01} are the effective holes in the system. Once more, the system can be mapped into a one-channel TASEP with dynamic disorder. As lane B is completely filled, no horizontal transition takes place which leads to entrance and bulk current in lane B as zero. Since there are two exit currents in the system, therefore the effective exit rate β_{eff} is different from β while the effective entrance rate (α_{eff}) remains the same as α. There are three possible steady-state phases for lane A known as low-density, high-density and maximal-current phase whereas lane B exists in

only one phase with maximum density. The phases in the system are collectively denoted by (LD, 1), (HD, 1) and (MC, 1) respectively. Here, 1 shows that bulk of lane B is completely filled.

(i) (LD, 1): Utilizing eqn. (3.40), the effective exit rate (β_{eff}) can be computed by equating the total bulk current to total entrance current. The identity $J_{entr,A} + J_{entr,B} = J_{bulk,A} + J_{bulk,B}$ reduces to

$$\alpha(1 - P_{11})X = P_{11}(1 - P_{11})(X + p_d Y) \tag{3.41}$$

Therefore, it can be easily shown that in this phase the probability of fully-filled vertical cluster P_{11} is given by:

$$P_{11} = \frac{\alpha X}{X + p_d Y} \tag{3.42}$$

The bulk current in the system is:

$$J_{(LD,1)} = \alpha(1 - \alpha)(X + p_d Y) \tag{3.43}$$

The low-density phase (LD, 1) exists for $\alpha < \alpha_c$ and $\alpha < \alpha^*$, which yields

$$\begin{aligned} \alpha &< \frac{(X + p_d Y + \beta) - \sqrt{\left((X + p_d Y + \beta)^2 - 8\beta(X + p_d Y)\right)}}{2X} \\ \alpha &< \frac{(X + p_d Y)}{2X} \end{aligned} \tag{3.44}$$

(ii) (HD, 1): The bulk current in (HD,1) phase satisfies $J_{exit,A} + J_{exit,B} = J_{bulk,A} + J_{bulk,B}$ which gives

$$\beta P_{11} + \beta = P_{11}(1 - P_{11})(X + p_d Y) \tag{3.45}$$

The particle density on lane A represented by cluster P_{11} and effective exit current (β_{eff}) are given by

$$P_{11} = \frac{(X + p_d Y - \beta) + \sqrt{\left((X + p_d Y + \beta)^2 - 8\beta(X + p_d Y)\right)}}{2(X + p_d Y)} \tag{3.46}$$

$$\beta_{eff} = \frac{(X + p_d Y + \beta) - \sqrt{\left((X + p_d Y + \beta)^2 - 8\beta(X + p_d Y)\right)}}{2} \tag{3.47}$$

The bulk current in the phase is expressed by

$$J_{(HD,1)} = \beta_{eff}(1-\beta_{eff})(X+p_dY) \tag{3.48}$$

For the existence of (HD, 1) phase, we obtained $\alpha_c < \alpha$ and $\beta_{eff} < \beta^*$, producing

$$\begin{aligned} \alpha &> \frac{(X+p_dY+\beta) - \sqrt{\big((X+p_dY+\beta)^2 - 8\beta(X+p_dY)\big)}}{2X}, \\ \beta &< \frac{X+p_dY}{6} \end{aligned} \tag{3.49}$$

(iii) (MC, 1): In the maximal-current phase (MC, 1), the current will be maximum in lane A and the phase exists for $\alpha^* < \alpha$ and $\beta^* < \beta_{eff}$. It can be shown that in this phase

$$P_{11} = \frac{3}{4}(X+p_dY) \quad \text{and} \quad J_{(MC,1)} = P_{11}(1-P_{11})(X+p_dY) \tag{3.50}$$

All the above phase boundaries can be obtained on the similar lines as described in appendix B. The steady-state characteristics of the proposed model are outlined in table 3.1.

Phase	Conditions of existence	Particle density	Current
(0, LD)	$\alpha_{eff} < \alpha_c$, $\alpha_{eff} < \alpha^*$	$\frac{\alpha_{eff}X}{X+p_dY}$	$\alpha_{eff}(1-\alpha_{eff})(X+p_dY)$
(0, HD)	$\alpha_c < \alpha_{eff}$, $\beta < \beta^*$	$1-\frac{\beta}{X+p_dY}$	$\beta(1-\beta)(X+p_dY)$
(0, MC)	$\alpha^* < \alpha_{eff}$, $\beta^* < \beta$	$\frac{3}{4}(X+p_dY)$	$P_{01}(1-P_{01})(X+p_dY)$
(LD, 1)	$\alpha < \alpha_c$, $\alpha < \alpha^*$	$\frac{\alpha X}{X+p_dY}$	$\alpha(1-\alpha)(X+p_dY)$
(HD, 1)	$\alpha_c < \alpha$, $\beta_{eff} < \beta^*$	$1-\frac{\beta_{eff}}{X+p_dY}$	$\beta_{eff}(1-\beta_{eff})(X+p_dY)$
(MC, 1)	$\alpha^* < \alpha$, $\beta^* < \beta_{eff}$	$\frac{3}{4}(X+p_dY)$	$P_{11}(1-P_{11})(X+p_dY)$

Table 3.1: Steady-state properties of each phase in a fully-asymmetric ddTASEP.

The phase boundary between (0, HD) and (LD, 1) phases can be obtained by joining origin to the point coordinates (α^*, β^*) in the phase plane [91]. In the region $\alpha > \alpha^*$ and $\beta > \beta^*$, the system exists in (MC, MC) state. The system satisfies maximal current conditions of (MC, 1) phase in the left bulk and those of (0, MC) phase in the right bulk. Fig. 3.6 shows the phase diagram separated

by phase boundaries for a particular set of system parameters. There may exist six stationary phases which might depend on the system parameter choice. The transition lines between (0, LD), (0, HD), (LD, 1) and (HD, 1) regions indicates first-order phase transitions and the rest of the transitions are second-order phase transitions. A qualitatively similar phase diagram exists for models studied in [59, 61] but a variation in the magnitude of particle density is observed in the present model. This variation can be attributed to the presence of dynamic defects over the lattice which influences particle density in the system.

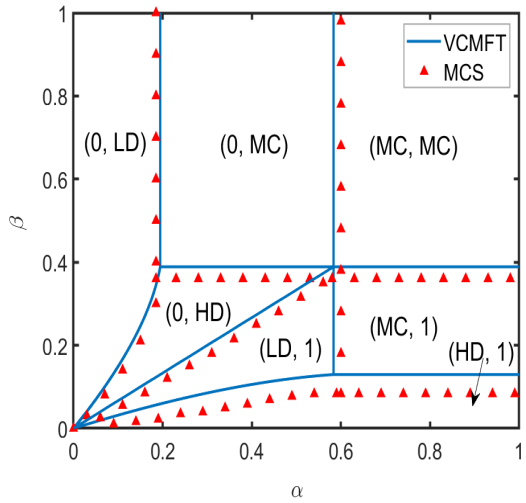

Figure 3.6: Steady-state phase diagram with seven different phases for $p_d = 1/3$, $k_+ = 0.4$, $k_- = 0.8$, $\omega_A = 1$ and $\omega_B = 0$.

Fig. 3.7(a-c) show density profiles corresponding to (0, LD), (0, HD) and (0, MC) phases. In the transient state of system, the asymmetric coupling tends to either shift particles from the lane A to lane B or forward hopping exits them from the right end of the lattice. In the steady-state of the system, lane A turns out to be empty and hopping of particles takes place in lane B only. This gives rise to a zero particle current in lane A and a non-zero current in lane B. Using particle-hole symmetry, the density profiles in fig. 3.7 (d-e) can be justified. It is important to mention that the phase boundaries in our model easily reduces to the boundaries obtained for its analogous homogeneous model (without defects) by substituting $X = 1$ and $Y = 0$ along with $j_{max} = 1/4$.

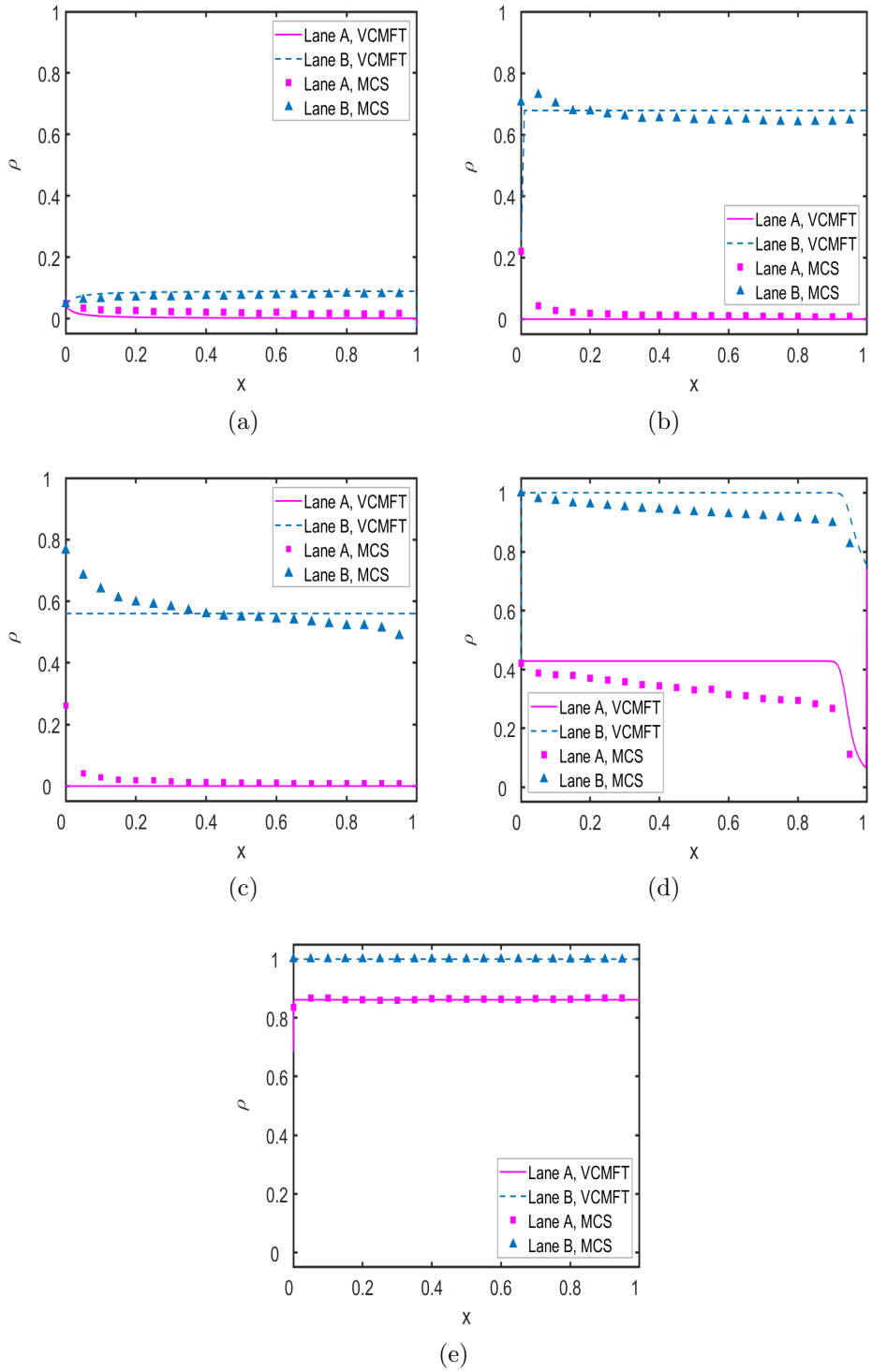

Figure 3.7: For $p_d = 1/3$, $k_+ = 0.4$, $k_- = 0.8$, $\omega_A = 1$, (a) (0, LD) phase for $\alpha = 0.05$, $\beta = 0.8$, (b) (0, HD) phase for $\alpha = 0.25$, $\beta = 0.25$, (c) (0, MC) phase for $\alpha = 0.3$, $\beta = 0.9$, (d) (LD,1) phase for $\alpha = 0.5$, $\beta = 0.2$, and (e) (HD, 1) phase for $\alpha = 0.8$, $\beta = 0.05$.

3.3.1 Effect of system parameters on the steady-state properties

This section discusses the effect of various system parameters: k_+, k_-, ω_A and p_d in analyzing the steady-state properties of our proposed model.

Effect of defect binding-unbinding rates

The defect binding and unbinding parameters (k_+, k_-) are known to control the defect density (Y) in the steady-state of the system. A change in the defect density affects particle density and particle current. It is found that, upon an increase in the defect density, a few stationary phases disappear as a result of the shifting of phase boundaries. Fig. 3.8 shows a phase diagram for the higher value of defect density $Y = 0.9$ ($k_+ = 0.9$, $k_- = 0.1$). The phases (0, LD), (0, HD), and (0, MC) significantly expands whereas (LD, 1) and (HD, 1) phases contracts and (MC, 1) and (MC, MC) phases completely disappear. This can be attributed to higher defect density on the lattice, which relatively decreases particle density on the lanes. Hence, the regions corresponding to higher density in any lane shrink or disappear. Note that the individual values of k_+ and k_- does not matter until we have $Y = 0.9$, still we get same steady-state behavior of the system.

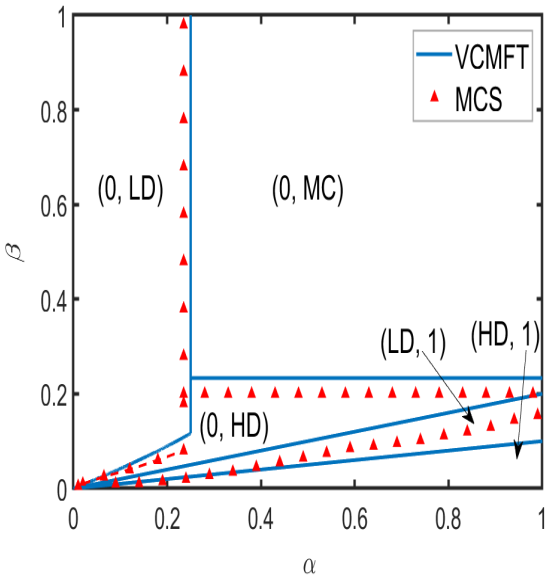

Figure 3.8: Phase diagram for $p_d = 1/3$, $k_+ = 0.9$, $k_- = 0.1$, $Y = 0.9$ and $\omega_A = 1$.

For very small values of defect density, it is observed that the steady-state phase diagram in our model turns out to be similar to the one presented in [59]. This

is because the system with lower values of defect density behaves similar to its homogeneous analogue.

Effect of lane-changing rate

The lane-changing rate is another crucial parameter in studying particle dynamics in the system. Theoretically, the expressions for particle cluster probabilities are independent of ω_A. Vertical cluster mean-field approach demonstrates that the findings are valid for all non-zero values of lane-changing rate ω_A. Fig. 3.9 shows a comparison of density in a particular phase (0, MC) for different values of ω_A through simulation. It can be seen that a variation in ω_A has no significant effect (neither qualitatively nor quantitatively) on the steady-state dynamics of the system. At instances, when the average particle density in lane A is 0 (i.e., lane A is vacant), no vertical transition between the lanes takes place and the role of coupling rate from lane A to lane B (ω_A) vanishes. On the other hand, when lane B is completely occupied (case 2), it can not accommodate any particle from lane A. These situations vanish the role of ω_A. A similar finding holds for other regions in the phase plane and is well validated through simulation. It is to note that the same observation is reported in literature also [59, 61, 106].

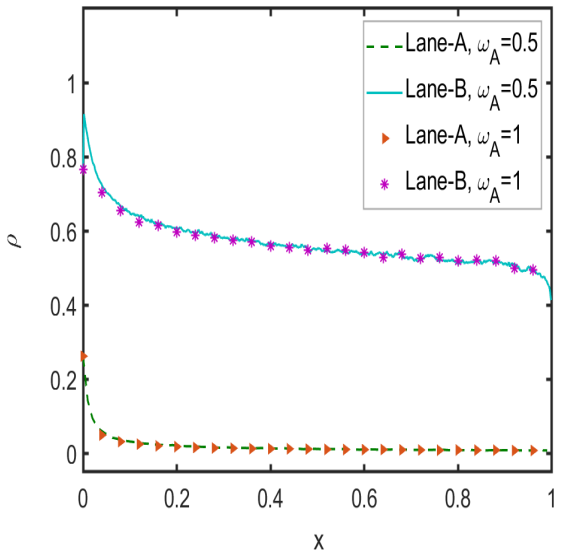

Figure 3.9: Density profile in (0, MC) region fixing $\alpha = 0.3$, $\beta = 0.9$, $p_d = 1/3$, $k_+ = 0.4$, $k_- = 0.8$ for $\omega_A = 0.5$ (lines) and $\omega_A = 1$ (markers).

Current analysis

The current-density relation (CDR) is analyzed in studying the effect of defect strength p_d. Fig. 3.10 shows the fundamental diagram for defect density $Y = 0.9$ and varying p_d in the system. The curve is found to be symmetric around $\rho = 1/2$, similar as in standard TASEP. For weak defect strength ($p_d = 1$), the particle forward hopping rate remains uniform in the bulk. Therefore, for $p_d = 1$, particles do not feel the presence of defects and the CDR emerges out same with $J_{max} = 0.25$ as in standard TASEP. With a decrease in the value of p_d from 1 to 0, defects become stronger and particles face difficulty in forward hopping over the lattice. Hence, the steady-state current decreases in the system. This observation is evident from the figure as well.

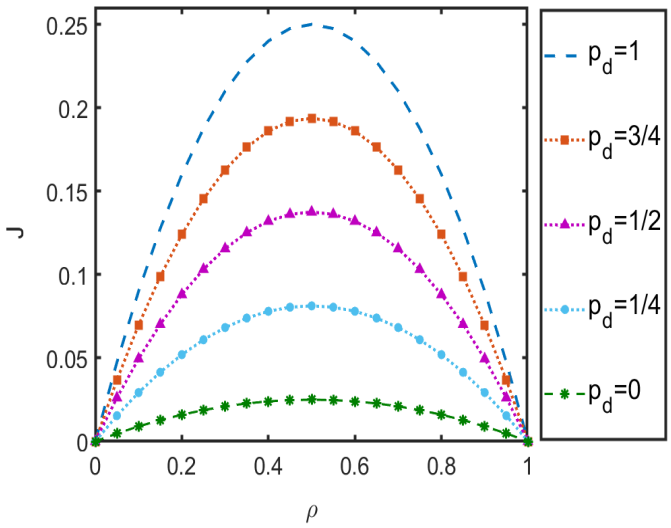

Figure 3.10: Particle current J as a function of particle density ρ for defect density $Y = 0.9$ ($k_+ = 0.9$ and $k_- = 0.1$) and varying slow hopping rate p_d.

3.4 Comparative analysis of symmetric and fully asymmetric coupling in a two-channel ddTASEP

This section lists the comparison of steady-state dynamics of effect of symmetric and fully asymmetric coupling in a two-channel ddTASEP model. The table 3.2 below shows the comparison in a list-wise manner.

Sr. No.	Symmetric coupling	Fully asymmetric coupling
1.	The system behaves as two parallel independent ddTASEPs	The system maps onto one-channel ddTASEP with effective entrance and exit rates
2.	The model is not exactly solvable whereas a numerical difference scheme is utilized.	The model can be solved exactly using vertical cluster mean-field theory.
3.	Steady phase diagram consist of maximum of three phases- (LD-LD), (HD-HD) and (MC, MC).	Steady phase diagram consist of maximum of seven phases- (0, LD), (0, HD), (0, MC), (LD,1), (HD, 1), (MC, 1) and (MC, MC).
4.	Equal density in each lane leads to overlapping of curves in density profiles.	Density in each lanes is unequal with one of the lanes either completely filled or empty.
5.	Due to symmetric coupling, the lane-changing source term cancels with sink terms leading to no significant effect on steady-state.	The fully asymmetry coupling leads to extreme situation of one of the lanes being wholly empty or completely filled, but a variation in coupling rates has no significant effect on system dynamics.
6.	An increase in ρ_d by varying k_+ and k_- rates, decreases particle current.	The observation is same as in symmetric coupling.

Table 3.2: Comparison of steady-state properties of symmetric and fully asymmetric coupling in two-channel ddTASEP.

3.5 Conclusion

The study in this chapter is an attempt to provide a theoretical model on the dynamics of a two-channel exclusion process with dynamic disorder under fully-asymmetric conditions. The key motivation is to analyze a more general two-channel system to describe the traffic dynamics in a more realistic way. The unconstrained defect dynamics are considered, in which defect occupancy is independent of particle presence at a site. To account for correlations emerging from inter-lane coupling, vertical cluster mean-field theory is utilized for exact calculations.

We have observed that horizontal transitions in the lanes have significant influence on stationary behavior of the system. The fully asymmetric coupling generates

complex steady-state behavior. The system maps to an effective one-channel exclusion process with dynamic disorder and exhibits seven different stationary phases. Interestingly, the steady-state results are found to be independent of variation in magnitude of non-zero lane-transition rate. Our main finding is the modification of phase boundaries with an increase in defect density over the lattice channels. The number of steady phases vary under different defect dynamics. A higher defect density is observed to decrease particle density in terms of cluster probabilities in the lanes. Hence, the phase boundaries translate with changes in the defect binding-unbinding rates.

Chapter 4

Particle creation and annihilation in a single-channel ddTASEP

4.1 Introduction

Till now, we have focused on dynamically disordered exclusion processes, in which number of particles in the system remains conserved. However, several real systems in the context of driven diffusive systems are generally subjected to particle non-conservation mechanism. Now, we shift our focus on studying the steady-state behavior of exclusion process models with particle non-conserving dynamics. Langmuir Kinetics (LK) is a mechanism in which particles from a bulk reservoir can attach to and detach from the lattice sites far from boundaries. The importance of investigating exclusion models in the existence of LK is present in its application in several real-life transport mechanisms with on-off process. One classic example of such systems is transport in vehicular traffic on highways, involves situations arising from on-off ramps by virtue of which a vehicle can attach to or leave a highway. Biological transport processes also typically involves directional progression of active species, which can reversibly or irreversibly associate and dissociate from a site.

The inclusion of LK in an exclusion model leads to particle non-conservation in the bulk which generates various interesting features in the steady-state. The rich and distinguishable non-equilibrium features of single-channel TASEP model with LK are phase coexistence, phase separation and localization of domain wall [72,74]. These characteristics are not observed in the exclusion models without LK. The incorporation of dynamic disorder in an open exclusion process model with LK may reveal interesting and novel features in the steady-state.

The chapter is organized as follows. The definition of model and its dynamical

rules are defined in section 4.2. The continuum mean field equations are derived in section 4.3. The numerical technique to solve continuum mean-field equations and Monte Carlo simulation are explained in section 4.4 of the chapter. This is followed by formulating steady-state phase diagrams and density profiles along with the validation from simulation in section 4.5. The shock dynamics and effect of various system parameters on it are discussed in section 4.6. The next section 4.7, concerns a brief investigation of finite-size effect. Lastly, in section 4.8, we summarize the outcomes and mention possible future studies.

4.2 Description of model and dynamical rules

We propose a system of one-dimensional open lattice channel with dynamic disorder and Langmuir kinetics having L sites (ddTASEP with LK). The particles are distributed under the hard-core exclusion principle, which means that each lattice site can either be vacant or occupied by exactly one particle. The evolution of the system from one state to another occurs according to the following dynamical rules.

(i) At the entrance i.e. $i = 1$, a particle can enter the lattice with a rate α provided $\tau_i = 0$ and $\nu_i = 0$.

(ii) At the exit i.e. $i = L$, a particle can leave the lattice with a rate β if $\tau_i = 1$ irrespective of $\nu_i = 0$ or 1.

(iii) In the bulk i.e. $i = 2, 3, \ldots, L-1$, if $\tau_i = 1$, then the particle at i^{th} site first tries to detach itself from the lattice with detachment rate ω_d and if it fails to detach then it hops forward to $(i+1)^{th}$ either with a rate p provided $\tau_{i+1} = 0$ and $\nu_{i+1} = 0$ or with a rate p_d, provided $\tau_{i+1} = 0$ and $\nu_{i+1} = 1$. On the other hand, if $\tau_i = 0$, a particle can attach to the lattice with attachment rate either ω_a if $\nu_{i+1} = 0$ i.e., target site is defect free or ω_{ad} if $\nu_{i+1} = 1$ i.e., target site has a defect.

A schematic representation of totally asymmetric exclusion process with dynamic disorder and Langmuir kinetics is shown in fig. 4.1.

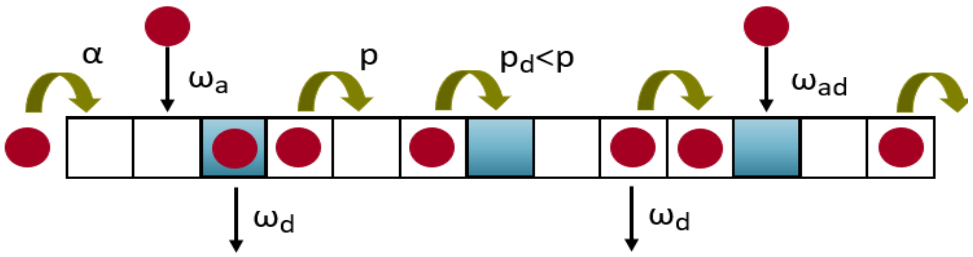

(a)

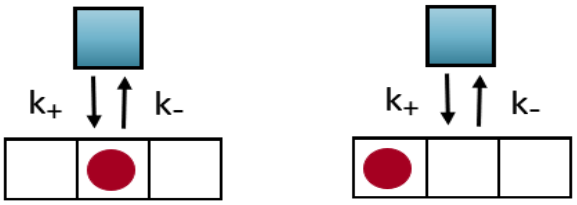

(b) (c)

Figure 4.1: (a) Schematic diagram of a single-channel TASEP with dynamic disorder and Langmuir kinetics. The dynamic defect is represented as a shaded site. Crossed arrows indicate forbidden transitions. Illustration of unconstrained defect dynamic (b) in the presence and (c) in the absence, of a particle at the target site.

4.3 Master equations

4.3.1 Particle density evolution

The temporal evolution of the average site occupation number $< \tau_i >$ for any site in the bulk i $(2 \leq i \leq L-1)$ is obtained from the following set of master equations.

$$\begin{aligned}\frac{d\langle\tau_i\rangle}{dt} &= p\langle\tau_{i-1}(1-\tau_i)(1-\nu_i)\rangle + p_d\langle\tau_{i-1}(1-\tau_i)(\nu_i)\rangle \\ &- p\langle\tau_i(1-\tau_{i+1})(1-\nu_{i+1})\rangle - p_d\langle\tau_i(1-\tau_{i+1})(\nu_{i+1})\rangle \\ &+ \omega_a\langle(1-\tau_i)(1-\nu_i)\rangle + \omega_{ad}\langle(1-\tau_i)(\nu_i)\rangle - \omega_d\langle\tau_i\rangle,\end{aligned} \tag{4.1}$$

where $\langle \ldots \rangle$ denotes the statistical average. Here, the first four terms on the right hand side represent particle forward hopping obeying hard-core exclusion principle and the last three terms describe the gain and loss terms arising due to particle

attachment and detachment. At the boundaries, the particle density evolves as

$$\begin{aligned}\frac{d\langle\tau_1\rangle}{dt} &= \alpha\langle(1-\tau_1)(1-\nu_1)\rangle - p\langle\tau_1(1-\tau_2)(1-\nu_2)\rangle \\ &\quad -p_d\langle\tau_1(1-\tau_2)(\nu_2)\rangle \qquad (4.2)\\ \frac{d\langle\tau_L\rangle}{dt} &= p\langle\tau_{L-1}(1-\tau_L)(1-\nu_L)\rangle + p_d\langle\tau_{L-1}(1-\tau_L)(\nu_L)\rangle - \beta\langle\tau_L\rangle \qquad (4.3)\end{aligned}$$

4.3.2 Defect density evolution

The defect density for any lattice site i ($i = 1,\ 2,\ 3, \ldots,\ L$) evolves corresponding to the following equation.

$$\frac{d\langle\nu_i\rangle}{dt} = k_+\langle 1-\nu_i\rangle - k_-\langle\nu_i\rangle \qquad (4.4)$$

4.3.3 Continuum mean-field equations

Factorizing the correlations as product of their averages using mean-field approximation, we get

$$\langle\tau_i\tau_{i+1}\rangle = \langle\tau_i\rangle\langle\tau_{i+1}\rangle \qquad (4.5)$$

Now, to obtain the continuum description of the model eqns. (4.1), (4.2), (4.3) and (4.4) by applying mean-field approximation given by (4.5). We coarse grain the discrete lattice with lattice constant $\epsilon = 1/L$ ($x \in [0,1]$) and replacing the binary discrete variable τ_i (ν_i) with a continuous variable ρ_i (ρ_d) $\in [0,1]$ to get the following equation

$$\begin{aligned}\frac{d\rho_i}{dt} &= p\rho_{i-1}(1-\rho_i)(1-\rho_{d_i}) + p_d\rho_{i-1}(1-\rho_i)\rho_{d_i} - p\rho_i(1-\rho_{i+1})(1-\rho_{d_i}) \\ &\quad - p_d\rho_i(1-\rho_{i+1})\rho_{d_i} + \omega_a(1-\rho_i)(1-\rho_{d_i}) + \omega_{ad}(1-\rho_i)\rho_{d_i} - \omega_d\rho_i\end{aligned} \qquad (4.6)$$

Using the following Taylor's series expansion by retaining the terms up to second order (for very large system i.e. $L >> 1$),

$$\rho_{i\pm1} = \rho_i \pm \frac{1}{L}\frac{\partial\rho_i}{\partial x} + \frac{1}{2L^2}\frac{\partial^2\rho_i}{\partial x^2} + O\Big(\frac{1}{L^3}\Big) \qquad (4.7)$$

we get

$$
\begin{aligned}
\frac{\partial \rho}{\partial t} =& p\left(\rho_i - \epsilon\frac{\partial \rho_i}{\partial x} + \frac{\epsilon^2}{2}\frac{\partial^2 \rho_i}{\partial x^2}\right)(1-\rho_i)(1-\rho_{d_i}) + p_d\left(\rho_i - \epsilon\frac{\partial \rho_i}{\partial x} + \frac{\epsilon^2}{2}\frac{\partial^2 \rho_i}{\partial x^2}\right)(1-\rho_i)\rho_{d_i} \\
& - p\rho_i\left(1-\rho_i - \epsilon\frac{\partial \rho_i}{\partial x} - \frac{\epsilon^2}{2}\frac{\partial^2 \rho_i}{\partial x^2}\right)(1-\rho_{d_i}) - p_d\rho_i\left(1-\rho_i - \epsilon\frac{\partial \rho_i}{\partial x} - \frac{\epsilon^2}{2}\frac{\partial^2 \rho_i}{\partial x^2}\right)\rho_{d_i} \\
& + \omega_a(1-\rho_i)(1-\rho_{d_i}) + \omega_{ad}(1-\rho_i)\rho_{d_i} - \omega_d\rho_i \\
=& \frac{\epsilon^2}{2}(p - p\rho_{d_i} + p_d\rho_{d_i})\frac{\partial^2 \rho_i}{\partial x^2} - \epsilon(p - p\rho_{d_i} + p_d\rho_{d_i})(1-2\rho_i)\frac{\partial \rho_i}{\partial x} \\
& + \omega_a(1-\rho_i)(1-\rho_{d_i}) + \omega_{ad}(1-\rho_i)\rho_{d_i} - \omega_d\rho_i
\end{aligned}
\tag{4.8}
$$

On the similar lines as in chapter 2, we re-scale the system parameters as follows.

$$
\Omega_a = \omega_a L, \Omega_{ad} = \omega_{ad} L \text{ and } \Omega_d = \omega_d L \tag{4.9}
$$

Eqn. (4.8), in terms of re-scaled variables becomes

$$
\begin{aligned}
\frac{\partial \rho_i}{\partial t'} =& \frac{\epsilon}{2}(p - p\rho_{d_i} + p_d\rho_{d_i})\frac{\partial^2 \rho_i}{\partial x^2} - (p - p\rho_{d_i} + p_d\rho_{d_i})(1-2\rho_i)\frac{\partial \rho_i}{\partial x} \\
& + \Omega_a(1-\rho_i)(1-\rho_{d_i}) + \Omega_{ad}(1-\rho_i)\rho_{d_i} - \Omega_d\rho_d
\end{aligned}
\tag{4.10}
$$

The system transitions are site independent as each site in bulk has equivalent dynamical rules, so we can drop the subscript i. The average density (ρ) as a function of time t' and space variable $x \in [0,1]$, governing the state of the system is depicted as

$$
\begin{aligned}
\frac{\partial \rho}{\partial t'} =& \frac{\epsilon}{2}(p - p\rho_d + p_d\rho_d)\frac{\partial^2 \rho}{\partial x^2} - (p - p\rho_d + p_d\rho_d)(1-2\rho)\frac{\partial \rho}{\partial x} \\
& + \Omega_a(1-\rho_)(1-\rho_d) + \Omega_{ad}(1-\rho)\rho_d - \Omega_d\rho_d
\end{aligned}
\tag{4.11}
$$

Similarly, the eqns. (4.2) and (4.3) in steady-state are translated to

$$
\rho(0) = \frac{\alpha(1-\rho_d)}{\rho_d p_d + (1-\rho_d)p}, \ \rho(1) = 1 - \frac{\beta}{\rho_d p_d + (1-\rho_d)p} \tag{4.12}
$$

with the particle current J given by

$$
J = [\rho_d p_d + (1-\rho_d)p]\ \rho(1-\rho) \tag{4.13}
$$

The defect evolution eqn. (4.4), representing the average defect density, in

continuum limit gives expression for defect density (ρ_d) as

$$\rho_d = \frac{k_+}{k_+ + k_-} \tag{4.14}$$

4.4 Steady-State solution and Monte Carlo Simulation

To compute the steady-state solution of the system, the left hand side of eqn. (4.11) vanishes and we need to solve the following equation along with the boundary conditions represented by eqn. (4.12). Since our system is complex due to the presence of dynamic disorder along with particle non-conserving dynamics, it is difficult to obtain the analytical solution of differential equation (4.11). The numerical techniques have been widely used in literature in order to get the approximate solution of such complex systems [70]. Note that, the same numerical technique- finite difference method, presented in chapter 2 is utilized in this chapter. The below described scheme is applied to eqn. (4.11) with the boundary conditions given by eqn. (4.12).

$$\begin{aligned}\rho_i^{n+1} = \rho_i^n + \frac{\epsilon}{2}\frac{\Delta t'}{\Delta x^2}\big(p - p\rho_d + p_d\rho_d\big)\big(\rho_{i+1}^n - 2\rho_i^n + \rho_{i-1}^n\big) + \frac{\Delta t'}{2\Delta x}\big(-p \\ + 2p\rho_i^n + p\rho_d - 2p\rho_i^n\rho_d - p_d\rho_d + 2p_d\rho_i^n\rho_d\big)\big(\rho_{i+1}^n - \rho_{i-1}^n\big) \\ + \Delta t'\big(\Omega_a(1-\rho_i^n)(1-\rho_d) + \Omega_{ad}(1-\rho_i^n)\rho_d - \Omega_d\rho_i^n\big)\end{aligned} \tag{4.15}$$

To ensure the occurrence of steady-state, the solution is captuerd in the limit $n \to \infty$. The aforementioned system yields a distinct steady-state solution and is obviously consistent.

We employed the same Monte Carlo simulation method in capturing the steady-state results as in chapter 2. The random sequential update rules are used for lattice length $L = 1000$. As we proceed in the chapter, the upcoming section shows the comparison of our theoretical findings of mean-field approximation with those of Monte Carlo simulation.

4.5 Steady-state phase diagrams and transitions

In this section, we explore the steady-state behavior of dynamically disordered TASEP with LK. The dynamics of the system are majorly governed by the following parameters: the defect binding rate k_+, the defect unbinding rate k_-, attachment rates Ω_a, Ω_{ad} and detachment rate Ω_d. To investigate the role of each of these

parameters in a comprehensive way, the results have been represented in the form of phase diagrams and density profiles obtained using numerical scheme on continuum mean-field equations which are further validated with Monte Carlo simulation. For the numerical solution, the values of $\Delta t' = 0.0005$, $\Delta x = 1/L = 0.001$ have been chosen which satisfy the stability condition $|\frac{\Delta t'}{\Delta x}| \leq 1$ [44]. In light of the various parameters involved in model, we conduct a thorough analysis of role of each parameter as follows.

It has been found in literature that for exclusion processes with particle non-conserving dynamics (LK), the stationary state dynamics of the system are characterized in terms of the binding constant [72].

Binding constant: It is determined as the ratio of attachment rate and detachment rate. Mathematically, it is given by

$$K = \frac{\omega_a}{\omega_d} = \frac{\Omega_a}{\Omega_d} \tag{4.16}$$

It is to note that the binding constant resembles the equilibrium constant in Langmuir isotherm [10]. Now we analyze in detail the role played by involved model parameters on the steady-state dynamics in the forth coming sections.

4.5.1 Effect of defect binding and unbinding rates

Since the goal of the problem is to analyze the role played by dynamic disorder in a single-channel dynamically disordered TASEP with LK, we first explore the effect of varying defect binding and unbinding rates (k_+ and k_-) by fixing other system parameters at $\Omega_a = 0.2$, $\Omega_{ad} = 0.1$, $p_d = 1/3$ and $L = 1000$. For a combination of defect binding-unbinding rates giving rise to very small value of defect density $0 \leq \rho_d \leq 0.15$, the current model behaves similar to a homogeneous single-channel TASEP with LK. For $\rho_d \geq 0.15$, the dynamic defects affects the steady-state dynamics considerably, as will be discussed in detail in the upcoming sections. Clearly, it is appropriate to focus on case where the presence of dynamic defects plays significant role of bottleneck in the system. It is observed that the steady phase boundaries shift continuously with varying defect density as more the number of defects on the lattice more hindrance is encountered by particles while hopping. Below, we discuss in depth the results for only those values of defect density, at which there are notable changes either in number or in nature of phases in steady-state. Based upon the values taken by binding constant, the upcoming discussion on steady system dynamics is divided into two parts $K = 1$ and $K \neq 1$.

Without the loss of generality, the attachment rate in the presence of defect at target site (Ω_{ad}) is taken as half the attachment rate in the absence of defect at target site (Ω_a) i.e., $\Omega_{ad} = \Omega_a/2$ throughout the upcoming chapters.

(a) $K = 1$

For simplicity, firstly we have explored the symmetric case in which the attachment and detachment rates of particles are taken as equal i.e, $\Omega_a = \Omega_d$.

Fig. 4.2 shows the phase diagram of the system for $\Omega_a = 0.2$, $k_+ = 0.4$, $k_- = 0.8$ and $\rho_d = 1/3$, which illustrates characterization of different phases in steady-state. One can see the existence of co-existing phases as a consequence of bulk transitions. The corresponding density and current profiles of each steady phase are shown in fig. 4.3 and 4.4 respectively. The defect binding and unbinding rates (k_+, k_-) are known to control defect density in the system, which further affects not only particle density in steady-state but also the steady current (J) in the system. Fig. 4.4(b) and 4.4(e) shows current for two phase coexisting regions LD-MC and MC-HD respectively. In LD-MC phase the current first increases and then at the transition point of LD to MC it reaches its maximum value. Similar observation is seen for HD-MC phase. The current profile (fig. 4.4(g)) has a transition point located at the position of shock in the plane.

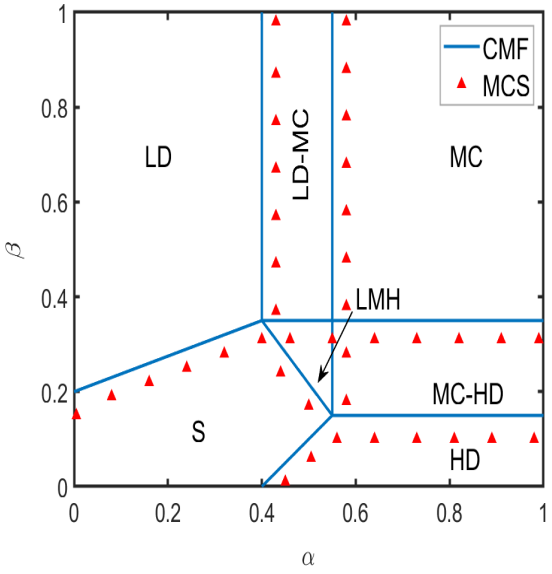

Figure 4.2: Steady-state phase diagram with seven different phases for $k_+ = 0.4$, $k_- = 0.8$, $\rho_d = 1/3$, $p_d = 1/3$, $K = 1$, $\Omega_a = 0.2$ and $\Omega_{ad} = \Omega_a/2$. The LMH region corresponds to LD-MC-HD.

Important features of stationary-state phase diagram for $\rho_d = 1/3$

- *Maximal current phase:* The upper right quadrant in the phase diagram ($\alpha \geq 0.55$, $\beta \geq 0.35$), the bulk density in the lane is independent of entrance and exit rates. Although, the boundary independent behavior of density profile is a dynamic of maximal current phase (MC), yet the current is not 1/4 as density in this phase is not 1/2. This decrease in system current is attributed to the presence of dynamic defect in the system. More the number of dynamic defects on the lattice, lesser will be particle hopping as hindrance in the forward hopping increases, hence lower the current in steady-state of the system. However, the magnitude of current is less than the one for maximal current region, we continue to name this particular region as maximal current phase (MC) to indicate the boundary independent behavior of single-channel system, as per convention used in the literature [30, 70, 91].

- *Co-existing phases:* Another characteristic of phase diagram is the appearance of co-existing phases. In such phases, a part of the density profile lies in any one of the phases included in LD, MC, HD or S, while its remaining part lies in the another phase. Such kind of density profiles are known as mixed profiles and the corresponding phase in known as co-existing phase. We separate the different phases in a density profile notation for this kind of phases by a dash ($-$). One example of a mixed density profile is demonstrated by fig. 4.3(e), in which left subsystem lies in MC phase and the right subsystem lies in HD phase. Another examples of mixed density profiles are shown in fig. 4.3(b) and 4.3(g) corresponding to LD-MC and S (i.e, LD-HD) phase. The bulk transitions in the phase plane lead to the existence of three phase coexistence region (LD-MC-HD) shown in fig. 4.3(f).

- *Phase transitions:* To gain a complete understanding of steady-state behavior of disordered system, it is necessary to explore some phase transitions. In fig. 4.2, in between the LD and HD phase regions, lies a region which has a density profile connecting LD profile to HD profile via domain wall. The profile with a density discontinuity at some point in the system is known as a shock profile and the corresponding region in the phase diagram is represented by shock (S). In such type of density profile, the current corresponding to the left and right solution matches and the strict monotonicity in current infers that the shock is localized in the system. Moreover, there is a shock phase in analogous single-channel homogeneous TASEP model with LK. This further implies that for small

defect density in the system, the topology of the phase diagram is similar as for the one with no defects ($\rho_d = 0$). The appearance of shock phase in a ddTASEP with LK is otherwise not noticed in single-channel and two-channel ddTASEP without LK [91].

Fig. 4.3(g) represents the type of a density profile in S phase for parameters $\alpha = 0.2$, $\beta = 0.1$. The boundaries of coexisting phase (S) are determined by varying α and β values, where the domain wall hits either the entrance or the exit of the system. For a fixed value of α, an increase in the value of β causes the rightwards motion of shock in the system, resulting in phase transition between S and LD phases. On the similar lines, remaining phase transitions in phase diagram can be understood by varying entrance and exit rates which gradually changes the magnitude of particle density. Note that all the phase transitions between different phases of phase diagrams are continuous also termed as second-order phase transitions and are characteristics of changes in density profiles.

Comparative analysis of steady-state phase diagram for different values of ρ_d

So far we have discussed the stationary-state dynamics and features like phase coexistence, maximal current phase etc, for weak dynamic defects (i.e., in terms of small values of ρ_d). Now we divert our focus to examine the effect of varying defect density on the stationary behavior of the system. In this direction, we gradually change the defect density by varying k_+, k_-, from small to moderate and then to high value, to check whether the same trend persists or not.

Fig. 4.5(a), shows the phase diagram for $k_+ = 0.15$, $k_- = 0.1$, $\rho_d = 0.6$, $\Omega_a = 0.2$ and $\Omega_{ad} = \Omega_a/2$. It can been seen that for moderate defect density ($\rho_d = 0.6$), the phase diagram is qualitatively and quantitatively different from that with small defect density (fig. 4.2). An important distinguishable observation is the shifting of phase boundaries in the phase plane which leads to elimination of HD phase on moving from small to moderate defect density. Clearly, with an increase in the defect density, more number of sites are being occupied by defects in comparison with particle occupancy. Hence, the number of particles in the steady-state reduces, which eliminates the occurrence of HD profile in the system and the LD phase appears over a larger region in the phase plane contrary to the case of $\rho_d = 1/3$. Hence, one can understand the shrinkage of rest of the regions in the phase diagram.

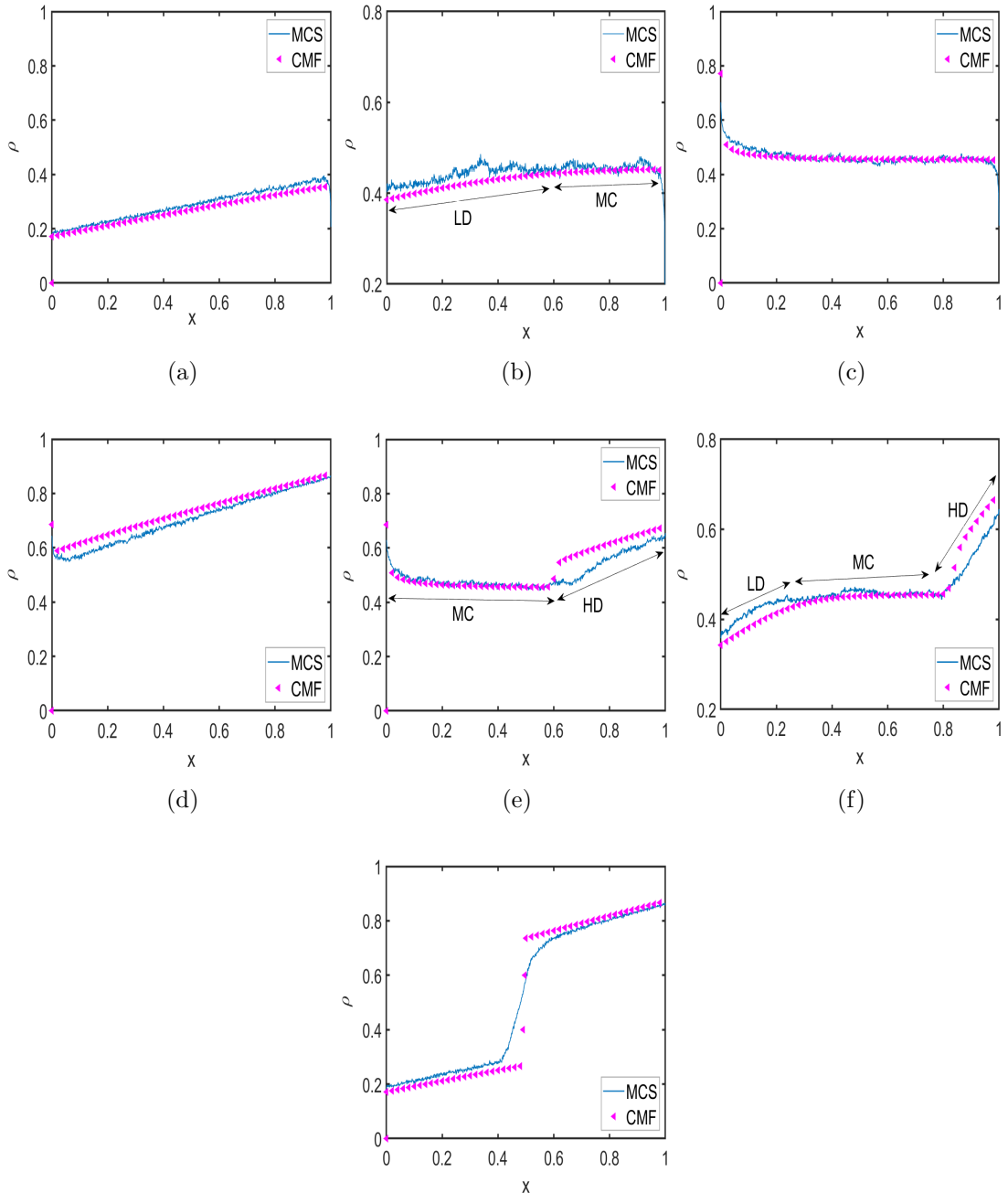

Figure 4.3: Density profiles for $p_d = 1/3$, $k_+ = 0.4$, $k_- = 0.8$, $\rho_d = 1/3$, $\Omega_a = 0.2$, $\Omega_{ad} = \Omega_a/2$ and $L = 1000$ (a) LD phase for $\alpha = 0.2$, $\beta = 0.8$, (b) LD-MC phase for $\alpha = 0.45$, $\beta = 0.9$, (c) MC phase for $\alpha = 0.9$, $\beta = 0.85$, (d) HD phase for $\alpha = 0.8$, $\beta = 0.1$, (e) MC-HD phase for $\alpha = 0.8$, $\beta = 0.25$, (f) LD-MC-HD phase for $\alpha = 0.4$, $\beta = 0.25$ and (g) S phase for $\alpha = 0.2$, $\beta = 0.1$.

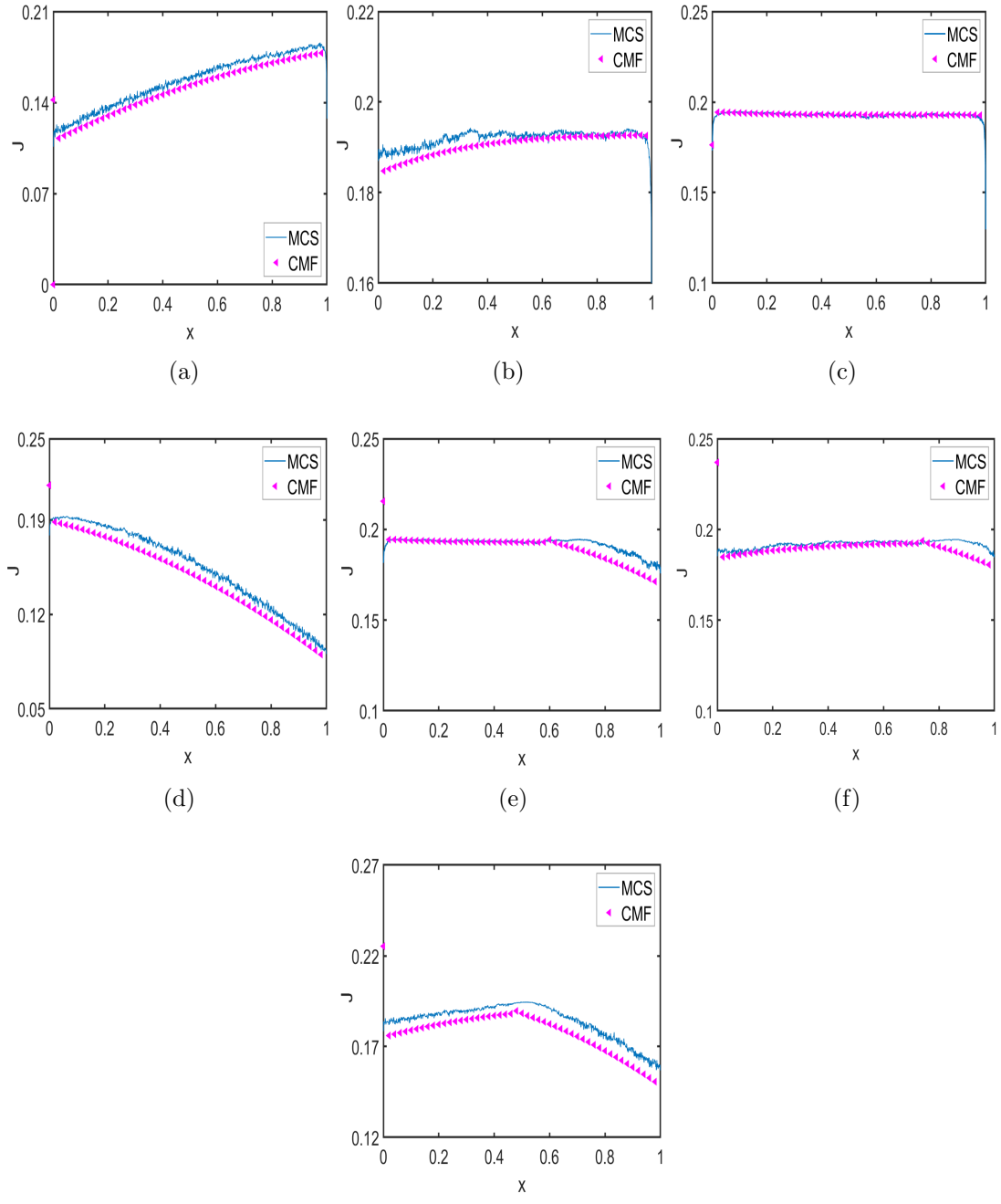

Figure 4.4: Current profiles for $p_d = 1/3$, $k_+ = 0.4$, $k_- = 0.8$, $\rho_d = 1/3$, $\Omega_a = 0.2$, $\Omega_{ad} = \Omega_a/2$ and $L = 1000$ (a) LD phase for $\alpha = 0.2$, $\beta = 0.8$, (b) LD-MC phase for $\alpha = 0.45$, $\beta = 0.9$, (c) MC phase for $\alpha = 0.9$, $\beta = 0.85$, (d) HD phase for $\alpha = 0.8$, $\beta = 0.1$, (e) MC-HD phase for $\alpha = 0.8$, $\beta = 0.25$, (f) LD-MC-HD phase for $\alpha = 0.4$, $\beta = 0.25$ and (g) S phase for $\alpha = 0.2$, $\beta = 0.1$.

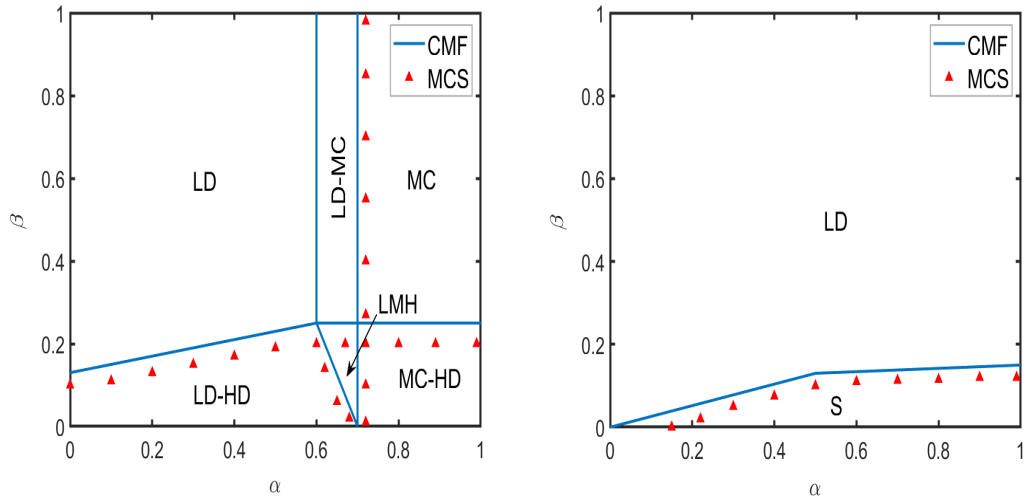

Figure 4.5: Phase diagram for $p_d = 1/3$, $K = 1$, $\Omega_a = 0.2$, $\Omega_{ad} = \Omega_a/2$, (a) $k_+ = 0.15$, $k_- = 0.1$ ($\rho_d = 0.6$) and (b) $k_+ = 0.9$, $k_- = 0.1$ ($\rho_d = 0.9$). The LMH region corresponds to LD-MC-HD.

On moving from moderate to high defect density in the system, the steady-state phase diagram becomes simplified leading to a reduction in number of phases. Fig. 4.5(b) shows the phase diagram for $k_+ = 0.9$, $k_- = 0.1$, $\rho_d = 0.9$, $\Omega_a = 0.2$ and $\Omega_{ad} = \Omega_a/2$. One can see from the figure that the phase diagram consists of only two steady-state phases namely LD and S. The higher number of defects present over the lattice replaces particles to a greater extent. As a result of which LD phase expands over a greater region and S phase exists over a very small region, as expected for a comparatively greater defect density. This observation is analogous to that for homogeneous single-channel TASEP with LK [72].

(b) $K = 3$

So far, we have explored the symmetric case in which the attachment rate (in the absence of defect) is equal to the detachment rate i.e., $K = 1$. But in real systems, generally the binding constant $K \neq 1$, which draws our attention towards the investigation of system dynamics for this case. Moreover, the methodology in using numerical technique is general and suitable to be applied for any value of K. The following discussion focuses on the situation where attachment and detachment rates are different, i.e., $\Omega_a \neq \Omega_d$.

Fig. 4.6 shows the phase diagram for $K = 3$. On comparing the phase diagram

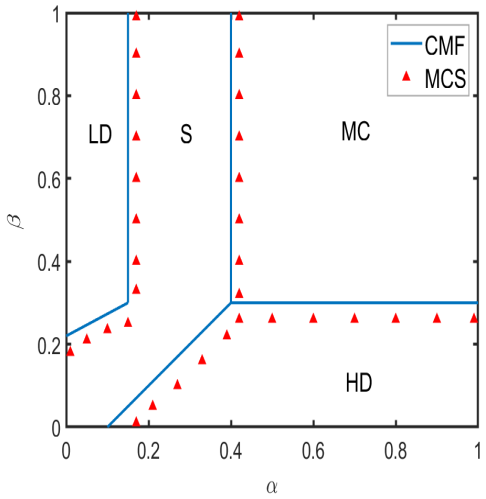

Figure 4.6: Steady-state phase diagram with four different phases for $k_+ = 0.4$, $k_- = 0.8$, $\rho_d = 1/3$, $p_d = 1/3$, $K = 3$, $\Omega_a = 0.2$ and $\Omega_{ad} = \Omega_a/2$.

for $K = 1$ and $K = 3$ (fig. 4.2 and fig. 4.6) with all other parameter values same, following observations can be listed.

(i) Clearly, the number of phases reduces in the steady-state of system upon increasing K. Only four phases are found for $K = 3$ which are LD, S, HD and MC phase. The coexisting phases LD-MC and MC-HD completely disappear. Due to an increase in the attachment rate in comparison to detachment rate, the particle density in each lane increases, resulting in shrinkage of LD phase and expansion of HD phase in the system. Similar observations have been reported in literature [70, 72].

(ii) Interestingly, the phase diagram is qualitatively similar to the one in homogeneous single-channel TASEP with LK [72]. One may notice the shifting of phase boundaries in steady phase diagram in comparison to the one for homogeneous model. This can be a consequence of presence of dynamic defects in the system.

(iii) The upper right quadrant in the phase diagram labelled as MC has the characteristics of boundary independent behavior of density profile, similar to the MC phase for $K = 1$. The magnitude of particle density in the phase is greater than the one in case of $K = 1$ due to higher particle attachment rate, but here also the current in MC phase is less than 1/4.

Fig. 4.7 shows the density profiles corresponding to four different regions in

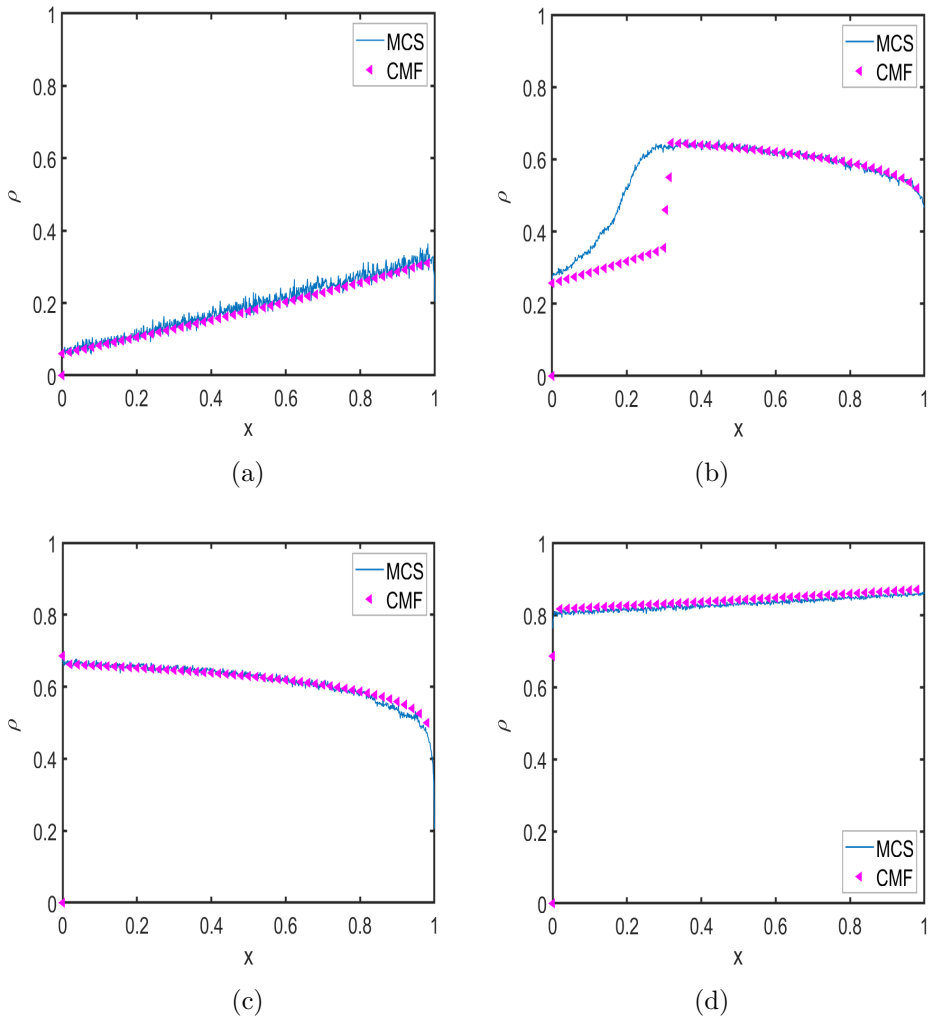

Figure 4.7: Density profiles for $p_d = 1/3$, $k_+ = 0.4$, $k_- = 0.8$, $\rho_d = 1/3$, $K = 3$, $\Omega_a = 0.2$, $\Omega_{ad} = \Omega_a/2$ and $L = 1000$ (a) LD phase for $\alpha = 0.07$, $\beta = 0.8$, (b) S phase for $\alpha = 0.3$, $\beta = 0.4$, (c) MC phase for $\alpha = 0.8$, $\beta = 0.9$, (d) HD phase for $\alpha = 0.8$, $\beta = 0.1$.

the phase diagram for $K = 3$ (fig. 4.6). It is inferred from fig. 4.7(c) for $K = 3$ that with an increase in the magnitude of particle density, there is a decrease in maximal current in the system.

To investigate the effect of varying defect density on the steady-state dynamics, phase diagram under different values of k_+ and k_- are plotted. Fig. 4.8 shows the phase diagram for $k_+ = 0.15$, $k_- = 0.1$ leading to $\rho_d = 0.6$ and $k_+ = 0.9$ and $k_- = 0.1$ giving $\rho_d = 0.9$ in the system. On comparing fig. 4.6 and 4.8(a), one of the significant observation is shifting of phase boundaries in the phase plane whereas qualitatively the phase diagrams remain the same. Also, the number

of phases remains identical. This effect is equivalent to that observed for same parameters under $K = 1$. Additionally, this effect is similar to the analogous model of dynamically disordered TASEP without non-conserving dynamics [72].

A further increase in the defect density in the system changes the structure of phase diagram. The phase diagram gets very much simplified comprising of only possible two stationary phases LD and S as shown in fig. 4.8(b). The S phase is observed to be expanded over a larger area in the phase plane which might be due to increase in the defect density in the system and larger value of binding constant K. The defects stay for a longer time in the system, consequently LD phase region also expands in comparison to the one for lower value of ρ_d.

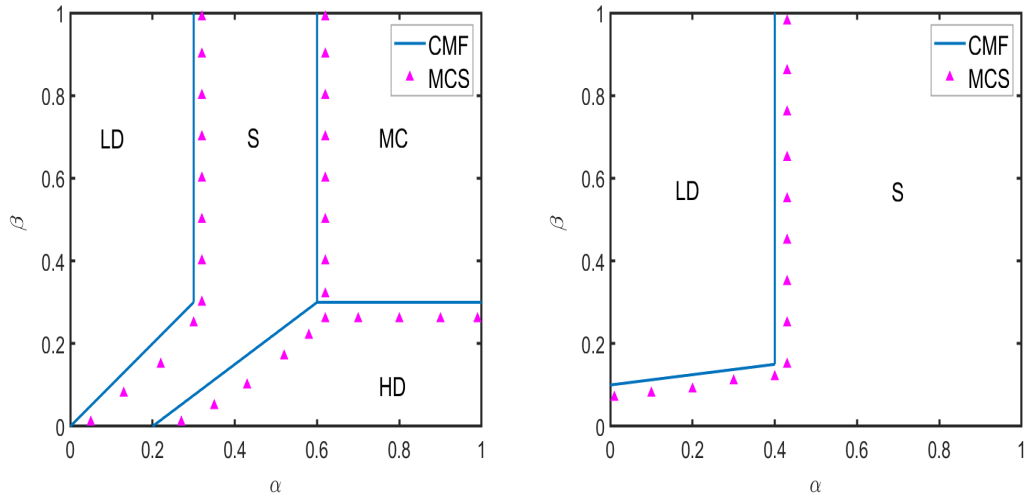

(a) (b)

Figure 4.8: Phase diagram for $p_d = 1/3$, $K = 3$, $\Omega_a = 0.2$, $\Omega_{ad} = \Omega_a/2$, (a) $k_+ = 0.15$, $k_- = 0.1$ ($\rho_d = 0.6$) and (b) $k_+ = 0.9$, $k_- = 0.1$ ($\rho_d = 0.9$).

4.5.2 Effect of variation in strength of dynamic defects

Another important system parameter controlling the defect dynamics is the slow forward hopping rate p_d. When there are no dynamic defects, i.e. $p_d = 1$, the current model reduces to a homogeneous single-lane TASEP with LK [72]. Although the defects have occupied lattice sites in accordance with their binding rate, yet their presence affecting the particle hopping is negligible as particles tend to hop with usual rate. For $p_d > 1$, one can assume a system with fast particle hopping which does not affects the steady-state dynamics as particles will exit faster from the lattice. Thus, we focus on the case with slower particle hopping rate in presence

of defect at target site i.e., $p_d < 1$.

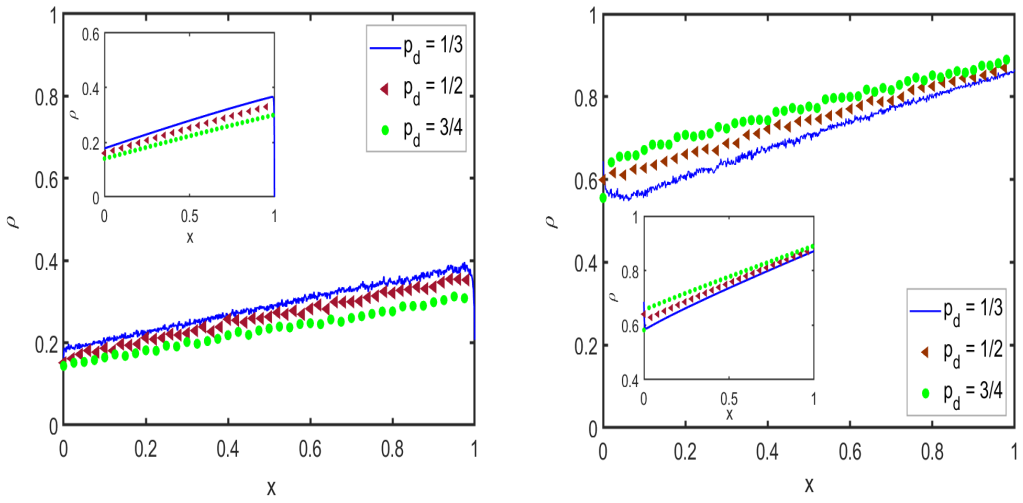

(a) (b)

Figure 4.9: Density profile for $K = 1$, $k_+ = 0.4$, $k_- = 0.8$ and varying pd, (a) $\alpha = 0.2$, $\beta = 0.8$ and (b) $\alpha = 0.8$, $\beta = 0.1$. The figures are results from MCS with the respective insets obtained from CMF.

A decrease in p_d is identical to an increase in the strength of the dynamic defect which further regulates particle density in the steady-state. To examine the steady-state dynamics for distinct strengths of defect, the value of p_d is gradually varied from $p_d = 1$ to $p_d = 0$. Fig. 4.9, shows the density profiles for LD and HD phase with three different values of p_d. There is only minor quantitative effect observed by varying the defect strength in the system. An increase in the magnitude of particle density ρ in LD phase (fig. 4.9(a)) and a decrease in the magnitude of particle density in HD phase (fig. 4.9(b)) has been found by increasing the defect strength from $p_d = 3/4$ to $p_d = 1/3$. Apart from these changes, there are no significant changes in the phase diagrams except for minor shifting in the phase boundaries in steady-state of the system.

Note that the observation follows for both the values of binding constant $K = 1$ and $K = 3$. It is observed that on varying slow hopping rate p_d there is qualitative minor change in the density profiles for $K = 3$, which is similar to that for $K = 1$.

4.5.3 Elimination of steady-state phases

Till this point, we have discussed the effects of various system parameters like defect rates, defect strength etc, for a fixed value of kinetic rate $\Omega_a = 0.2$ (attachment

rate). The analysis of stationary-state behavior of single-channel ddTASEP with LK allows one to deeply explore phase diagram for different values of Ω_a. In this section, we focus on exploring system dynamics by consistently varying Ω_a, which incorporates the particle non-conserving dynamics. Depending upon the value of Ω_a, the topological structure of the phase diagram changes at values $\Omega_a = 0.5$ and $\Omega_a = 1$.

(a) $K = 1$

For $0 < \Omega_a < 0.5$, the phase diagram (shown by fig. 4.2) consists of seven different phases. Upon increasing Ω_a till 0.5, the phase diagram simplifies, resulting in elimination of stationary phases. The LD and HD phases, observed for $\Omega_a = 0.2$, disappear leaving behind only five phases, shown in fig. 4.10(a). This result is analogous to that for homogeneous TASEP with LK [72]. Further, the bulk transitions lead to localization of shock in the system, and the LD, HD phases gradually eliminates.

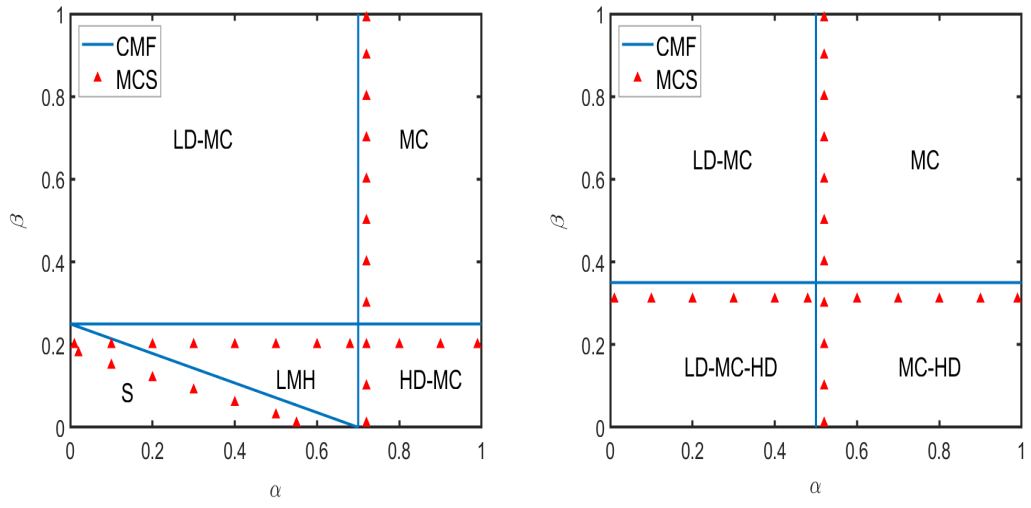

(a) (b)

Figure 4.10: Phase diagram for $k_+ = 0.4$, $k_- = 0.8$, $\rho_d = 1/3$, $p_d = 1/3$, $K = 1$, $\Omega_{ad} = \Omega_a/2$, (a) $\Omega_a = 0.5$ and (b) $\Omega_a = 1$. The LMH region corresponds to LD-MC-HD.

A further increase in Ω_a to 1, additionally simplifies the phase diagram with reduction of shock phase from the system (shown in fig. 4.10(b)). The region of LD-HD coexistence is replaced by three phase coexistence LMH. The regions of MC-HD and MC phase expands with the shifting of phase boundaries in the

system. Note that the effect of varying defect rates k_+, k_- is found to be similar for $\Omega_a = 0.5$ and $\Omega_a = 1$.

(b) $K = 3$

In addition to the analysis for the effect of varying kinetic rate, we also aim to investigate the case $K \neq 1$. As discussed earlier, for higher values of binding constant, more number of particles tend to attach as compared to particle detachment. This leads to a comparative higher particle density in the system than the one for equal kinetic rates ($K = 1$). The phase diagram for $K = 3$, $k_+ = 0.4$, $k_- = 0.8$, $\Omega_a = 0.2$ has been plotted in fig. 4.6. To better understand the nature of steady-state phases, we gradually change the values of controlling parameter Ω_a on a range of $\Omega_a = 0.2$ to $\Omega_a = 1$.

Upon increasing Ω_a, we observe a first change in the topological structure of the phase diagram at $\Omega_a = 0.5$. The phase diagram gets simplified leaving behind only three stationary phases- S, MC and HD. The LD phase shrinks progressively to a region close to β axis, while the other phase increase in size. The corresponding phase diagram has been shown in fig. 4.11(a), for $k_+ = 0.4$, $k_- = 0.8$. The effect of reduction of steady phase for higher values of attachment rate is equivalent to the one observed for the former case $K = 1$. Note that here also the shock gets localized in the bulk of the system.

Similarly, increasing Ω_a to higher values, the same topology change occurs. The phase diagram for $\Omega_a = 1$, keeping other system parameters the same, has been shown in fig. 4.11(b). However, one notices a very small change in the stationary phases, with the number of phases remaining the same. A minor shift in the phase boundary along the transition line between S and HD phase is found.

4.6 Shock dynamics

A shock is a discontinuity in bulk of the system connecting a low density profile on left to a high density profile on right. This type of discontinuity is known as upward shock. The understanding of steady-state solution using mean-field theory and numerical technique allows to study in detail the behavior of the domain wall upon a change in the system parameters. In this direction, we first explore the effect of defect density on shock and the results have been shown in fig. 4.12. It is clearly found that the shock moves from left towards right boundary upon increasing defect density on the lattice. This is due to the reason that the particle density lowers

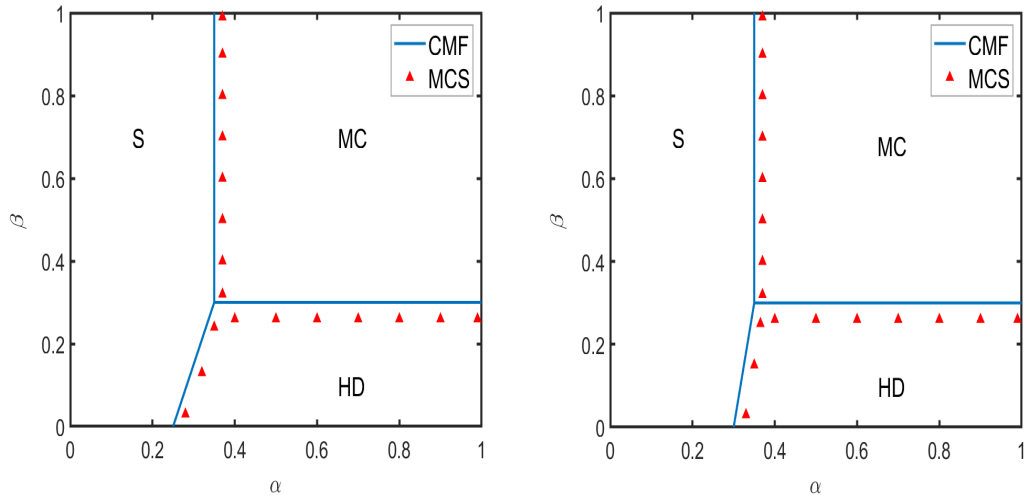

(a) (b)

Figure 4.11: Phase diagram for $k_+ = 0.4$, $k_- = 0.8$, $\rho_d = 1/3$, $p_d = 1/3$, $K = 3$, $\Omega_{ad} = \Omega_a/2$, (a) $\Omega_a = 0.5$ and (b) $\Omega_a = 1$.

with increasing density of defects in the system. Consequently, the HD phase is found to be eliminated whereas the LD phase expands. This observation can be validated from the phase diagrams (fig. 4.2 and 4.5). The trend has been found to be similar using Monte Carlo simulation and continuum mean-field approximation.

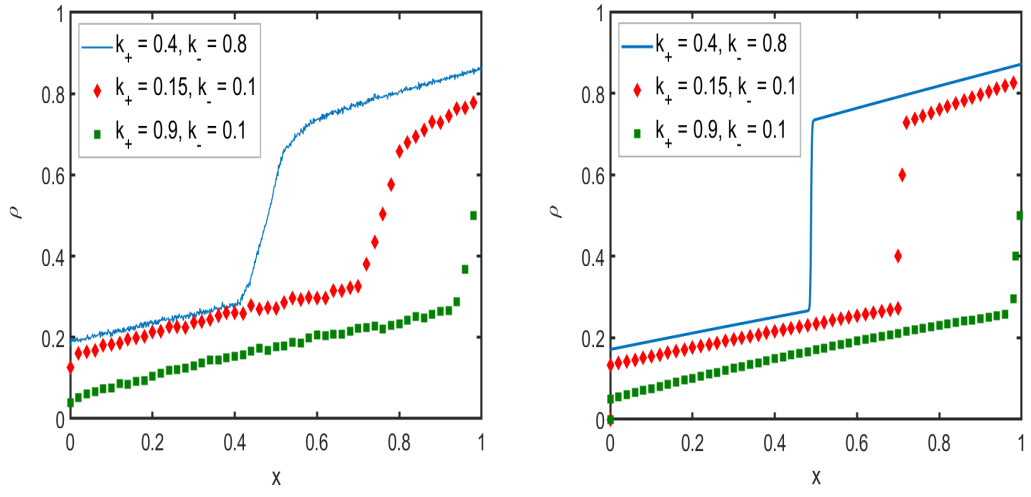

(a) (b)

Figure 4.12: Shock profile for $K = 1$, $\Omega_a = 0.2$, $p_d = 1/3$, $\alpha = 0.2$, $\beta = 0.1$ and varying k_+ and k_-. The results are captured using (a) Monte Carlo simulation and (b) continuum mean-field approximation.

Further, the effect of variation in the defect strength (p_d) has also been examined on shock profile. Fig. 4.13 shows the density profile for $\alpha = 0.3$, $\beta = 0.4$, $k_+ = 0.4$ and $k_- = 0.8$ with three different values of p_d, $p_d = 1/3, 1/2$ and $3/4$. A change in the shock position has been noticed upon varying p_d parameter. Lower the value of p_d stronger is the defect, more is the blockage of particles leading to an increase in the HD profile on lattice. Hence the shock continuously changes its position from right to left boundary of the system. Furthermore, Monte Carlo simulation and continuum mean-field approximation gives similar observation.

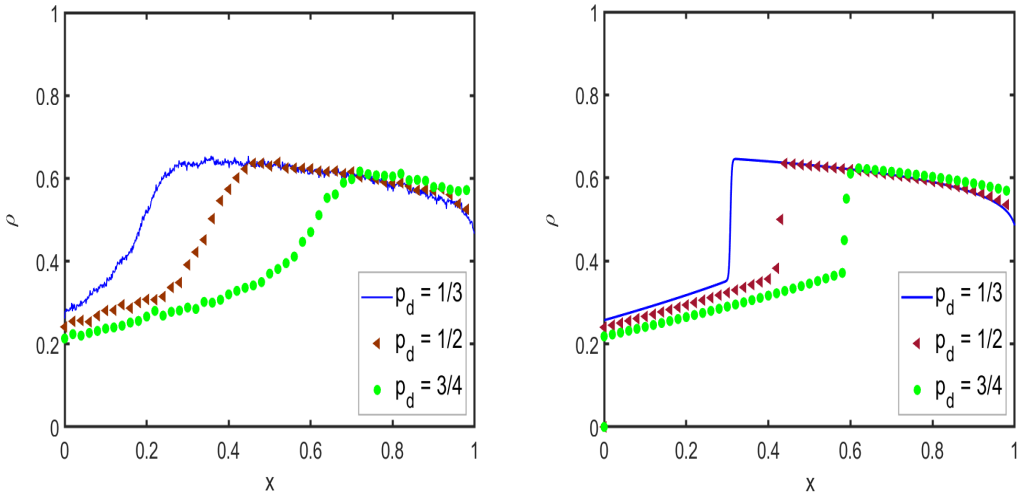

Figure 4.13: Shock profile for $K = 3$, $\Omega_a = 0.2$, $k_+ = 0.4$, $k_- = 0.8$, $\alpha = 0.3$, $\beta = 0.4$ and varying p_d. The results are captured using (a) Monte Carlo simulation and (b) continuum mean-field approximation.

4.7 Finite size effect

In order to inspect any finite size effect in the system, we attempt to analyze the effect of system size on our steady results. We found that the bulk solution is independent of size of lattice. The effect of system size has been analyzed on the density profiles for $\alpha = 0.2$, $\beta = 0.1$, $k_+ = 0.4$, $k_- = 0.8$, $K = 1$ as shown in fig. 4.14(a) and 4.14(b). It is clearly found that the results are not affected by system size. Moreover, the extensive Monte Carlo simulation have been carried out taking $L = 500, 1000, 5000$ and 10000 for different set of system parameters which evidently are found to have no significant effect on the density profiles. This observation is consistent with the findings reported in literature [72].

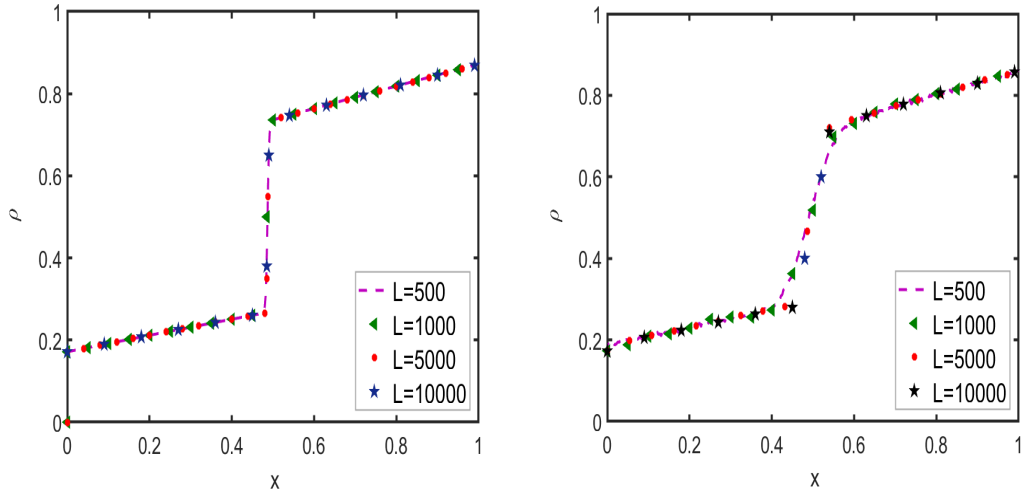

Figure 4.14: Effect of system size for $\alpha = 0.2$, $\beta = 0.1$, $k_+ = 0.4$, $k_- = 0.8$, $K = 1$, $\Omega_a = 0.2$, $\Omega_{ad} = \Omega_a/2$ and $L = 500, 1000, 5000$ and 1000. The results are obtained using (a) Monte Carlo simulation and (b) continuum mean field approximations.

4.8 Conclusion

The competing interplay between dynamic disorder and LK results in rich steady-state phase diagrams consisting of pure and coexisting phases. Another considerable outcome due to presence of LK dynamics is the appearance of steady-state shock which otherwise is not found in the single-channel ddTASEP without LK. The system is explored for two values of binding constant $K = 1$ and $K = 3$. The effect of binding constant Ω_a is examined on the phase diagrams and it is found that an increasing Ω_a reduces the number of phases in the system which is due to localization of shock in the bulk. Further, the defect binding/unbinding rates are observed to shift phase boundaries in the plane with number of phases remaining identical. Moreover, effect of variation in defect strength is observed on density profiles. It has been observed that with an increase in defect strength, the particle density in LD phase decreases whereas in HD phase the particle density increases. These mentioned findings are similar for both values of binding constant K. The shock dynamics are explored by varying defect density and the defect strength in the system. The shock moves from right to left upon increasing defect strength on the lattice. Also, the steady-state results are found to be independent of system size.

Here, we focused on a complete study of steady-state properties of single-channel

dynamically disordered TASEP system with LK under unconstrained conditions. The single-channel model can be generalized to a two-channel model that might uncover other interesting features of the steady-state behavior of the system. To check out its unrevealed aspects, let us move along the way towards the next chapter.

Chapter 5

Two-lane ddTASEP with Langmuir kinetics

5.1 Introduction

Lane changing appears to be an essential part of any traffic flow model. On highways, frequent lane changes may help to increase traffic capacity or they may worsen traffic flow. Apart from vehicular traffic, the field of biological transport also requires the investigation of effect of lane-changing by motor proteins while moving along parallel microtubule tracks. Moreover, due to finite processivity, the active motor proteins may attach to and detach from microtubule track into the cytoplasm.

So far, in the last chapter, we have explored the steady-state behavior of a single-channel ddTASEP with LK under different values of binding constant. In this chapter, we take up to analyse the role played by inter lane coupling in the steady behavior of a two-channel ddTASEP with LK. Furthermore, we aim to investigate the effect of attachment and detachment rates in the stationary state of the current model.

The chapter is organized as follows. In section 5.2 we define the mathematical model by its dynamical rules. The resulting continuum mean-field equations are derived in section 5.3. The next section 5.4 comprises the numerical scheme to solve continuum mean-field equations and the details of Monte Carlo simulation. In section 5.5 and 5.6, the density profiles, the phase diagrams and the effect of various system parameters have been examined to explore overall dynamics. In section 5.7, we conclude the findings of the present study.

5.2 Model

We define our present model in an open two-channel lattice with dynamic disorder and Langmuir kinetics (ddTASEP with LK), each with L sites, represented by A and B. The dynamic defects are considered to be stochastic. The system consists of identical particles distributed randomly under the hardcore exclusion principle, see fig. 5.1. The state of the system is defined by two different sets of the occupation numbers $\tau_{i,j}$ for particles and $\nu_{i,j}$ for defects at i^{th} site in j^{th} lane of the lattice, where $i = 1,\ 2,\ 3, ...,\ L; j = A,\ B$. Each occupation number is either 0 or 1, depending upon the absence or presence of particle or defect. For each time step, a lattice site (i, j); $(i = 1, 2, 3, ..., L;\ j = A, B)$ is chosen randomly according to random sequential update rules. The dynamic defect can bind and unbind with a rate k_+ and k_- respectively at any site in both the lane. We consider the unconstrained defect dynamics in which defect binding and unbinding are independent of particle occupancy at that site [91]. The particle hopping rules for this model are the same as defined in section 4.2, except the lane-changing rule in the bulk. In addition to bulk particle detachment and forward hopping, here particles may change the lane as per the below defined dynamical rule.

(i) For $1 < i < L$ (in the bulk), if $\tau_{i,j} = 1$ a particle at i^{th} site in j^{th} lane may

- shifts to an i^{th} site in another lane only if the target site is particle free, with a rate ω_A or ω_B if the target site is free from defect or with a rate ω_{AD} or ω_{BD} if target site contains a defect.

5.3 Master equations

5.3.1 Particle density evolution

This section is focused to compute the master equations illustrating the temporal evolution of the occupation probabilities $\tau_{i,j}$ and $\nu_{i,j}$ in bulk of both the lanes $(1 < i < L, j = A, B)$. The equations are as follows.

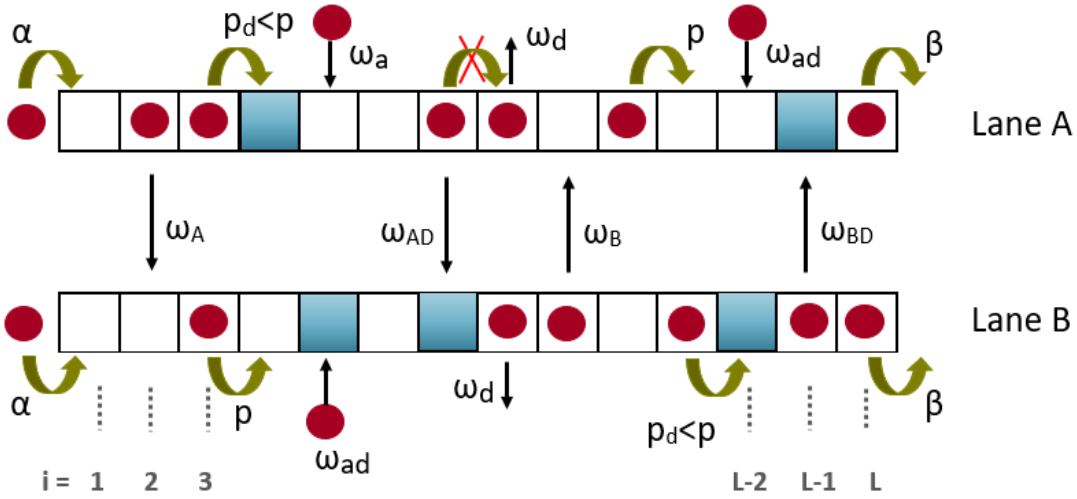

(a)

(b) (c)

Figure 5.1: (a) Schematic illustration of a two-lane TASEP with dynamic disorder and Langmuir kinetics. Shaded squares indicate the presence of dynamic defect and circles indicate particles. Crossed arrow indicate forbidden transition. An illustration of unconstrained defect dynamics (b) defect binding (c) defect unbinding, at the target site.

$$\begin{aligned}\frac{d\langle\tau_{i,j}\rangle}{dt} =& p\langle\tau_{i-1,j}(1-\tau_{i,j})(1-\nu_{i,j})\rangle + p_d\langle\tau_{i-1,j}(1-\tau_{i,j})(\nu_{i,j})\rangle \\ &- p\langle\tau_{i,j}(1-\tau_{i+1,j})(1-\nu_{i+1,j})\rangle - p_d\langle\tau_{i,j}(1-\tau_{i+1,j})(\nu_{i+1,j})\rangle \\ &+ \omega_a\langle(1-\tau_{i,j})(1-\nu_{i,j})\rangle + \omega_{ad}\langle(1-\tau_{i,j})(\nu_{i,j})\rangle - \omega_d\langle\tau_{i,j}\rangle \\ &\mp \omega_j\langle\tau_{i,j}\tau_{i+1,j}(1-\tau_{i,j'})(1-\nu_{i,j'})\rangle \mp \omega_{jD}\langle\tau_{i,j}\tau_{i+1,j}(1-\tau_{i,j'})(\nu_{i,j'})\rangle \\ &\pm \omega_{j'}\langle\tau_{i,j'}\tau_{i+1,j'}(1-\tau_{i,j})(1-\nu_{i,j})\rangle \pm \omega_{j'D}\langle\tau_{i,j'}\tau_{i+1,j'}(1-\tau_{i,j})(\nu_{i,j})\rangle,\end{aligned} \tag{5.1}$$

where $\langle ... \rangle$ denotes the statistical average. Note that when $j = A$, we have $j' = B$ and when $j = B$, $j' = A$. The first four terms on the right hand side represent particle hopping, the following three terms arise from particle non-conserving

dynamics, and the last four terms have a negative (positive) sign for lane A (B).

At boundaries, the evolution of particle density is in accordance with

$$\begin{aligned}\frac{d\langle\tau_{1,j}\rangle}{dt} = \quad & \alpha\langle(1-\tau_{1,j})(1-\nu_{1,j})\rangle - p\langle\tau_{1,j}(1-\tau_{2,j})(1-\nu_{2,j})\rangle \\ & -p_d\langle\tau_{1,j}(1-\tau_{2,j})(\nu_{2,j})\rangle, \qquad (5.2)\\ \frac{d\langle\tau_{L,j}\rangle}{dt} = \quad & p\langle\tau_{L-1,j}(1-\tau_{L,j})(1-\nu_{L,j})\rangle + p_d\langle\tau_{L-1,j}(1-\tau_{L,j})(\nu_{L,j})\rangle \\ & -\beta\langle\tau_{L,j}\rangle \qquad (5.3)\end{aligned}$$

5.3.2 Defect density evolution

The defect density for each lattice site $1 \leq i \leq L$ evolves as the following equation.

$$\frac{d\langle\nu_{i,j}\rangle}{dt} = k_+\langle 1-\nu_{i,j}\rangle - k_-\langle\nu_{i,j}\rangle \qquad (5.4)$$

5.3.3 Continuum mean-field equations

To derive the continuum mean-field equations, we factorize the correlations by using mean-field approximation given by

$$\langle\tau_{i,j}\tau_{i+1,j}\rangle = \langle\tau_{i,j}\rangle\langle\tau_{i+1,j}\rangle \qquad (5.5)$$

The continuum limit of our model is derived by coarse grainnig discrete lattice with lattice constant $\epsilon = 1/L$. Writing $x = (i-1)\epsilon$, we replace the binary discrete variables $\tau_{i,j}$ and $\nu_{i,j}$ with a continuous variables $\rho_{i,j}, \rho_{d_{i,j}} \in [0,1]$ and carry out Taylor's series expansion after retaining terms up to second-order, to obtain

$$\rho_{i\pm1,j} = \rho_{i,j} \pm \frac{1}{L}\frac{\partial\rho_{i,j}}{\partial x} + \frac{1}{2L^2}\frac{\partial^2\rho_{i,j}}{\partial x^2} + O\Big(\frac{1}{L^3}\Big) \qquad (5.6)$$

we get

$$\begin{aligned}
\frac{\partial \rho_{i,j}}{\partial t} =& \left(\rho_{i,j} - \epsilon\frac{\partial \rho_{i,j}}{\partial x} + \frac{\epsilon^2}{2}\frac{\partial^2 \rho_{i,j}}{\partial x^2}\right)(1-\rho_{i,j})(p(1-\rho_{d_{i,j}}) + p_d\rho_{d_{i,j}}) \\
&- \rho_{i,j}\left(1 - \rho_{i,j} - \epsilon\frac{\partial \rho_{i,j}}{\partial x} - \frac{\epsilon^2}{2}\frac{\partial^2 \rho_{i,j}}{\partial x^2}\right)(p(1-\rho_{d_{i,j}}) + p_d\rho_{d_{i,j}}) \\
&+ \omega_a(1-\rho_{i,j})(1-\rho_{d_{i,j}}) + \omega_{ad}(1-\rho_{i,j})\rho_{d_{i,j}} - \omega_d\rho_{i,j} \\
&\mp \rho_{i,j}\left(\rho_{i,j} + \epsilon\frac{\partial \rho_{i,j}}{\partial x} + \frac{\epsilon^2}{2}\frac{\partial^2 \rho_{i,j}}{\partial x^2}\right)(1-\rho_{i,j'})(\omega_j(1-\rho_{d_{i,j'}}) + \omega_{jD}\rho_{d_{i,j'}}) \\
&\pm \rho_{i,j'}\left(\rho_{i,j'} + \epsilon\frac{\partial \rho_{i,j'}}{\partial x} + \frac{\epsilon^2}{2}\frac{\partial^2 \rho_{i,j'}}{\partial x^2}\right)(1-\rho_{i,j})(\omega_{j'}(1-\rho_{d_{i,j}}) + \omega_{j'D}\rho_{d_{i,j}}) \\
\\
=& \frac{\epsilon^2}{2}(-p\rho_{dA} + p + p_d\rho_{dA})\frac{\partial^2 \rho_{i,j}}{\partial x^2} + \epsilon(-p + 2p\rho_A + p\rho_{dA} - 2p\rho_{dA}\rho_A \\
&- p_d\rho_{dA} + 2p_d\rho_{dA}\rho_A)\frac{\partial \rho_{i,j}}{\partial x} + \omega_a(1-\rho_{i,j})(1-\rho_{d_{i,j}}) \\
&+ \omega_{ad}(1-\rho_{i,j})\rho_{d_{i,j}} - \omega_d\rho_{i,j} \mp [\omega_j\rho_{i,j}^2(1-\rho_{i,j'})(1-\rho_{d_{i,j'}}) \\
&+ \omega_{jD}\rho_{i,j}^2(1-\rho_{i,j'})\rho_{d_{i,j'}} - \omega_{j'}\rho_{i,j'}^2(1-\rho_{i,j})(1-\rho_{d_{i,j}}) \\
&- \omega_{j'D}\rho_{i,j'}^2(1-\rho_{i,j})\rho_{d_{i,j}}]
\end{aligned} \tag{5.7}$$

On the similar lines as in chapter 2, we define the attachment and detachment rates as $\Omega_a = \omega_a L$, $\Omega_{ad} = \omega_{ad} L$ and $\Omega_d = \omega_d L$ and the lane-changing rates as $\Omega_A = \omega_A L$, $\Omega_B = \omega_B L$, $\Omega_{AD} = \omega_{AD} L$ and $\Omega_{BD} = \omega_{BD} L$. In terms of rescaled variables, eqn. (5.7) becomes

$$\begin{aligned}
\frac{\partial \rho_{i,j}}{\partial t'} =& \frac{\epsilon^2}{2}(-p\rho_{dA} + p + p_d\rho_{dA})\frac{\partial^2 \rho_{i,j}}{\partial x^2} + \epsilon(-p + 2p\rho_A + p\rho_{dA} - 2p\rho_{dA}\rho_A \\
&- p_d\rho_{dA} + 2p_d\rho_{dA}\rho_A)\frac{\partial \rho_{i,j}}{\partial x} + \Omega_a(1-\rho_{i,j})(1-\rho_{d_{i,j}}) \\
&+ \Omega_{ad}(1-\rho_{i,j})\rho_{d_{i,j}} - \Omega_d\rho_{i,j} \mp [\Omega_j\rho_{i,j}^2(1-\rho_{i,j'})(1-\rho_{d_{i,j'}}) \\
&+ \Omega_{jD}\rho_{i,j}^2(1-\rho_{i,j'})\rho_{d_{i,j'}} - \Omega_{j'}\rho_{i,j'}^2(1-\rho_{i,j})(1-\rho_{d_{i,j}}) \\
&- \Omega_{j'D}\rho_{i,j'}^2(1-\rho_{i,j})\rho_{d_{i,j}}]
\end{aligned} \tag{5.8}$$

In the absence of any spatial inhomogeneity, one can drop the subscript i. The nonlinear differential equations in terms of average densities ρ_A and ρ_B in both the lanes as functions of t' and the space variable $x \in [0,1]$, describing the steady-state of system, are given by

$$\frac{\partial}{\partial t'}\begin{bmatrix}\rho_A\\ \rho_B\end{bmatrix}+\frac{\partial}{\partial x}\quad\begin{bmatrix}(\frac{\epsilon}{2}p\rho_{dA}-\frac{\epsilon}{2}p-\frac{\epsilon}{2}p_d\rho_{dA})\frac{\partial\rho_A}{\partial x}+(p-p\rho_{dA}+p_d\rho_{dA})(\rho_A-\rho_A^2)\\ (\frac{\epsilon}{2}p\rho_{dB}-\frac{\epsilon}{2}p-\frac{\epsilon}{2}p_d\rho_{dB})\frac{\partial\rho_B}{\partial x}+(p-p\rho_{dB}+p_d\rho_{dB})(\rho_B-\rho_B^2)\end{bmatrix}$$

$$= S, \tag{5.9}$$

where

$$S=\begin{bmatrix}\Big(\Omega_a(1-\rho_A)(1-\rho_{dA})+\Omega_{ad}(1-\rho_A)\rho_{dA}-\Omega_d\rho_A-\Omega_A\rho_A^2(1-\rho_B)(1-\rho_{dB})\\ \quad-\Omega_{AD}\rho_A^2(1-\rho_B)\rho_{dB}+\Omega_B\rho_B^2(1-\rho_A)(1-\rho_{dA})+\Omega_{BD}\rho_B^2(1-\rho_A)\rho_{dA}\Big)\\ \Big(\Omega_a(1-\rho_B)(1-\rho_{dB})+\Omega_{ad}(1-\rho_B)\rho_{dB}-\Omega_d\rho_B+\Omega_A\rho_A^2(1-\rho_B)(1-\rho_{dB})\\ \quad+\Omega_{AD}\rho_A^2(1-\rho_B)\rho_{dB}-\Omega_B\rho_B^2(1-\rho_A)(1-\rho_{dA})-\Omega_{BD}\rho_B^2(1-\rho_A)\rho_{dA}\Big)\end{bmatrix}$$

The term S arises from the non-conservative terms formed by a combination of particle attachment-detachment kinetics and lane-changing transitions. Here, ρ_A and ρ_B denotes particle densities in lane A and lane B respectively. The defect density in both the lanes A and B are represented by ρ_{dA} and ρ_{dB}. Since, we employed similar defect dynamics in each lane which leads to equal defect density in the lanes. Therefore, in the forthcoming sections, we denote $\rho_{dA}=\rho_{dB}=\rho_d$.

Equations (5.2) and (5.3) in steady-state reduce to the following boundary conditions given by

$$\rho(0)=\frac{\alpha(1-\rho_d)}{\rho_d p_d+(1-\rho_d)p},\quad \rho(1)=1-\frac{\beta}{\rho_d p_d+(1-\rho_d)p} \tag{5.10}$$

along with the particle current J in the system is given by

$$J=\left[\rho_d p_d+(1-\rho_d)p\right]\,\rho_j(1-\rho_j),\text{ where j=A, B} \tag{5.11}$$

In steady-state, the average defect density represented in eqn. (5.4) gives

$$\rho_d=\frac{k_+}{k_++k_-} \tag{5.12}$$

5.4 Steady-state equations and numerical solution

In this section, we describe the numerical scheme to solve the coupled non-linear system obtained in eqns. (5.9) and (5.10). The details of Monte Carlo simulation are discussed to compute steady-state density profiles.

5.4.1 Steady-State equation

Since the study of system under transient state is no longer important as system behavior keeps on fluctuating with time. It is necessary to analyze the system behavior under steady-state which will persist hereafter. In steady-state, the time derivative term vanishes and one needs to solve the following equations with boundary conditions (eqn. 5.10).

$$
\begin{aligned}
&\frac{\partial \rho_A}{\partial t'} + \big(\frac{\epsilon}{2}p\rho_d - \frac{\epsilon}{2}p - \frac{\epsilon}{2}p_d\rho_d\big)\frac{\partial^2 \rho_A}{\partial x^2} + \big(p - 2p\rho_A - p\rho_d + 2p\rho_d\rho_A + p_d\rho_d \\
&- 2p_d\rho_d\rho_A\big)\frac{\partial \rho_A}{\partial x} = \Omega_a(1-\rho_A)(1-\rho_d) + \Omega_{ad}(1-\rho_A)\rho_d - \Omega_d\rho_A \\
&- \Omega_A\rho_A^2(1-\rho_B)(1-\rho_d) - \Omega_{AD}\rho_A^2(1-\rho_B)\rho_d + \Omega_B\rho_B^2(1-\rho_A)(1-\rho_d) \\
&+ \Omega_{BD}\rho_B^2(1-\rho_A)\rho_d, \\
&\frac{\partial \rho_B}{\partial t'} + \big(\frac{\epsilon}{2}p\rho_d - \frac{\epsilon}{2}p - \frac{\epsilon}{2}p_d\rho_d\big)\frac{\partial^2 \rho_B}{\partial x^2} + \big(p - 2p\rho_B - p\rho_d + 2p\rho_d\rho_B + p_d\rho_d \\
&- 2p_d\rho_d\rho_B\big)\frac{\partial \rho_B}{\partial x} = \Omega_a(1-\rho_B)(1-\rho_d) + \Omega_{ad}(1-\rho_B)\rho_d - \Omega_d\rho_B \\
&+ \Omega_A\rho_A^2(1-\rho_B)(1-\rho_d) + \Omega_{AD}\rho_A^2(1-\rho_B)\rho_d - \Omega_B\rho_B^2(1-\rho_A)(1-\rho_d) \\
&- \Omega_{BD}\rho_B^2(1-\rho_A)\rho_d
\end{aligned}
\tag{5.13}
$$

5.4.2 Numerical scheme

Equation (5.13) represents a complex system of second-order coupled ordinary differential equations which is difficult to solve analytically. We propose to find the steady-state solution by using a suitable numerical scheme. Moving parallel to the numerical scheme discussed in chapter 2 and 4, one can solve the system (5.13) directly by keeping the time derivative term in the system and acquiring the solution after a very long time ensuring the occurrence of steady-state. The numerical scheme is applied to model equation represented in eqn. (5.9) along with boundary

conditions, we get

$$\begin{aligned}\rho_{i,A}^{n+1} =&\rho_{i,A}^{n} + \frac{\epsilon}{2}\frac{\Delta t'}{\Delta x^2}\left(p - p\rho_{i,d}^{n} + p_d\rho_{i,d}^{n}\right)\left(\rho_{i+1}^{n} - 2\rho_{i}^{n} + \rho_{i-1}^{n}\right)\\ &+ \frac{\Delta t'}{2\Delta x}\left(p - p\rho_{i,d}^{n} + p_d\rho_{i,d}^{n}\right)\left(1 - 2\rho_{i}^{n}\right)\left(\rho_{i+1}^{n} - \rho_{i-1}^{n}\right)\\ &+ \Delta t'\big[\Omega_a(1-\rho_i^n)(1-\rho_{i,d}^n) + \Omega_{ad}(1-\rho_i^n)\rho_{i,d}^n - \Omega_d\rho_i^n\\ &\quad \mp \Omega_A(\rho_{i,A}^n)^2(1-\rho_{i,B}^n)(1-\rho_{i,d}^n) \mp \Omega_{AD}(\rho_{i,A}^n)^2(1-\rho_{i,B}^n)\rho_{i,d}^n\\ &\quad \pm \Omega_B(\rho_{i,B}^n)^2(1-\rho_{i,A}^n)(1-\rho_{i,d}^n) \pm \Omega_{BD}(\rho_{i,B}^n)^2(1-\rho_{i,A}^n)\rho_{i,d}^n\big]\end{aligned} \tag{5.14}$$

Further, to test the validity of the results given by continuum mean-field approximation, we stimulate the two-channel disordered model with Monte Carlo simulation (MCS). The random sequential update rules are used taking lattice length $L = 1000$.

The upcoming sections shows the comparison of our theoretical findings from mean-field approximation with those of Monte Carlo simulation. We discuss in detail the steady-state behavior of two-lane TASEP with dynamic disorder and LK through phase diagrams and density profiles. The density profiles and phase diagrams are obtained using a numerical scheme on the continuum mean-field equations and validated using Monte Carlo simulation. For numerical scheme, the values of $\Delta t' = 0.0005$, $\Delta x = 1/L = 0.001$ are chosen in order to satisfy the stability condition $|\frac{\Delta t}{\Delta x}| \leq 1$ [44].

In order to analyze the interplay between dynamic defect and interlane interactions, it is convenient to introduce the parameter namely coupling constant $C = \frac{\Omega_B}{\Omega_A},\ \Omega_A \neq 0$ [80]. The constant C represents strength of coupling between both the channels and the advantage of defining coupling constant is to study the effect of lane-changing parameters in a structured form. It is ample to analyse the case $0 \leq C \leq 1$ in respect of coupling constant. We restrict our discussion for only two values of C, $C = 1$ and $C = 0$ in this chapter. The influence of other major system parameters like the defect rates (k_+ and k_-), attachment and detachment rates (Ω_a, Ω_{ad} and Ω_d) is also considered in studying system in steady-state. To examine the role of particle non-conserving dynamics, termed as LK, it is appropriate to categorize steady-state system dynamics in respect of binding constant K defined as $K = \Omega_a/\Omega_d$ (defined in chapter 4) [72]. In the forthcoming sections, the role played by many involved system parameters in steady-state of our system is described.

5.5 Symmetric coupling (C=1)

Firstly, we discuss the case when coupling constant $C = 1$, which represents equal lane-changing rate from one lane to another, i.e., $\Omega_A = \Omega_B$ and $\Omega_{AD} = \Omega_{BD}$. For $C = 1$, the two-lane dynamically disordered TASEP with LK becomes symmetrically coupled. The symmetric coupling rates result in the cancelation of lane-changing source terms with sink terms in the mean-field equations which bring out two uncoupled ordinary differential equations representing two independent ddTASEPs with LK and therefore exhibits the steady-state dynamics similar to single lane dynamically disordered TASEP with LK (discussed in chapter 4). The steady-state phase diagram of a two-channel dynamically disordered TASEP with LK under symmetric coupling has been presented in fig. 4.2, which demonstrates the presence of co-existing phases such as LD-MC, MC-HD and LMH. In a region of phase plane lies a phase, with density discontinuity in the bulk, named as shock phase. The effect of varying various system parameters has also been discussed in detail with appropriate significance in the previous chapter. Now, we turn our attention to a comparatively challenging and unexplored case of asymmetric coupling, being discussed in the following part of the chapter.

5.6 Fully asymmetric coupling (C=0)

This section explains the steady-state system dynamics for $C = 0$, which is the case of fully asymmetric coupling conditions. In this situation, the particles are permitted to shift from lane A to lane B ($\Omega_A \neq 0$), but not from lane B to A ($\Omega_B = 0$). This particular case of coupling cannot be solved exactly and demand the use of numerical technique in finding the steady-state behavior of the system. The study is motivated by cellular transport by the motion of motor proteins over microtubule filaments. Sometimes, due to structural deformity in the current filament, the motor proteins may jump asymmetrically between the chains [107]. Another example is the multi-lane cellular automaton model, where asymmetric lane changing rules were employed to reduce accidents during lane change between driving and overtaking lanes [108].

We begin by dividing the analysis in two subparts such as (i) $K = 1$ and (ii) $K \neq 1$. Without the loss of generality, the attachment rate in the presence of defect at target site (Ω_{ad}) is taken as half the attachment rate in the absence of defect at target site (Ω_a) i.e., $\Omega_{ad} = \Omega_a/2$ throughout the chapter.

(a) K=1

Firstly, we explore the simpler case of symmetric attachment and detachment rates of particles i.e., $\Omega_a = \Omega_d = \Omega$. Figure 5.2 shows the phase diagram for $C = 0$, $k_+ = 0.4$, $k_- = 0.8$, $K = 1$, $\Omega_a = 0.2$, $\Omega_{ad} = \Omega_a/2$, $\Omega_A = 0.8$, $\Omega_{AD} = \Omega_A/3$, $\Omega_B = 0$ and $\Omega_{BD} = 0$. The solid lines corresponds to phase transitions captured from numerical solution of mean-field equations whereas the markers represent Monte Carlo simulation. The biased lane-changing rate produces rich and complex phase diagram which is classified into five stationary phases, namely (LD, LD), (LD, S), (S, HD), (S, S) and (LD, HD). Figure 5.3 shows three density profiles as well as corresponding current profiles for (S, S), (LD, S) and (LD, HD) phases. In (LD, LD) region, both the lanes are in low density; in region (LD, HD), lane A has a low density and lane B has a high density profile. In regions (LD, S), (S, HD) and (S, S) an appearance of shock is observed in the system. In (S, S) region, both the lanes have a shock profile in the bulk of the system. In (LD, S) and (S, HD) regions, a shock appears in lane B and lane A respectively. As seen from fig. 5.3(d), the current profile has a transition located at the position of shock in the plane. In (LD, HD) region, bulk particle current remains constant as depicted in fig. 5.3(f). This is in view of the fact that bulk of the system is defined by constant density in both lanes. Since, constant bulk density is a feature of maximal current phase in standard TASEP, however due to density difference in both lanes a maximal current of magnitude only 0.2 is achieved in the system.

Non-existence of a few steady-state phases

Importantly, it has been observed that particle density in lane B is always greater than the density in lane A, i.e., $\rho_B > \rho_A$. Besides, particle attachment and detachment beacuse of LK dynamics (occurring at equal rates as $\omega_a = \omega_d$), lane B receives more number of particles in comparison to lane A. Here, the coupling terms $\Omega_A \rho_A^2 (1 - \rho_B)(1 - \rho_d)$ and $\Omega_{AD} \rho_A^2 (1 - \rho_B)\rho_d$ in eqn. (5.9), emerging due to biased lane-changing rate, serves as source term for lane B and sink term for lane A. This leads to an imbalance in effective attachment and detachmnet rate in both the lanes. The effective attachment rate in lane A (B) becomes lower (higher) than an effective detachment rate in lane A (B). Moreover, the steady-state phase diagram structure for lane A as well as lane B turns out to be qualitatively similar as in one-channel TASEP with LK for more detachment ($K < 1$) and more attachment ($K > 1$) respectively [72, 79]. The relative variation in the number of particles in both lanes leads to the difference in steady-state particle density. A corresponding

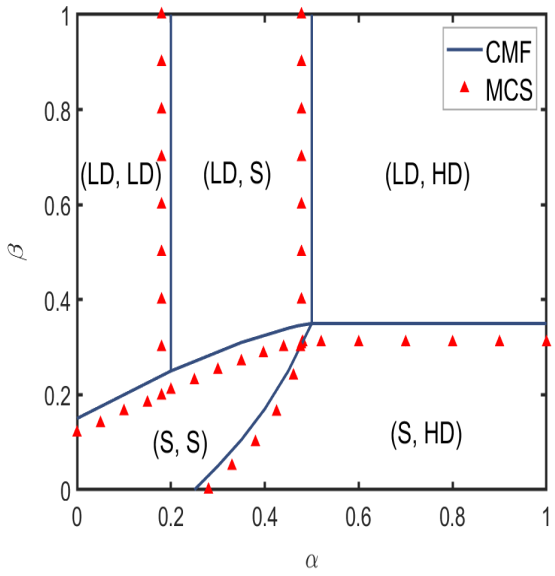

Figure 5.2: Phase diagram consisting five stationary phases for $p_d = 1/3$, $k_+ = 0.4$, $k_- = 0.8$, $\Omega_a = 0.2$, $\Omega_{ad} = \Omega/2$, $C = 0$, $\Omega_A = 0.8$, $\Omega_{AD} = \Omega_A/3$ and $L = 1000$.

density profile is shown in fig. 5.3(c). The particle density in (LD, HD) region is independent of change in boundary rates (α and β). Although this is a characteristic of density in the maximal current phase in homogeneous TASEP, they seem to define LD and HD profiles in lanes A and B because of density differences. Therefore, instead of naming the upper right quadrant in the phase diagram as (MC, MC), we name it as (LD, HD) region.

On comparing fig. 5.2 with the phase diagram in symmetrically coupled two-channel system (fig. 4.2), one observes that phase plane is majorly covered by (LD, HD) region in place of (MC, MC) phase noticed in symmetric coupling case. Moreover, the LD (HD) phase region expands and the HD (LD) phase region shrinks in lane A (B). This observation is explained as: the additional particles shifting from lane A to B (due to lane-changing rules) causes a relative lack (plenty) of particles in lane A (B). Consequently, we have $\rho_B > \rho_A$ which leads to non-existence of a few steady-state phases namely (S, HD), (HD, S) and (HD, LD).

Comparison of steady-state behavior with analogous homogeneous model

To study the effect of dynamic inhomogeneity on the steady-state behavior of our system, below we compare the stationary state phase diagram shown in fig. 5.2 with the one in analogous homogeneous model studied in [67]. The following observations can be inferred from the comparison.

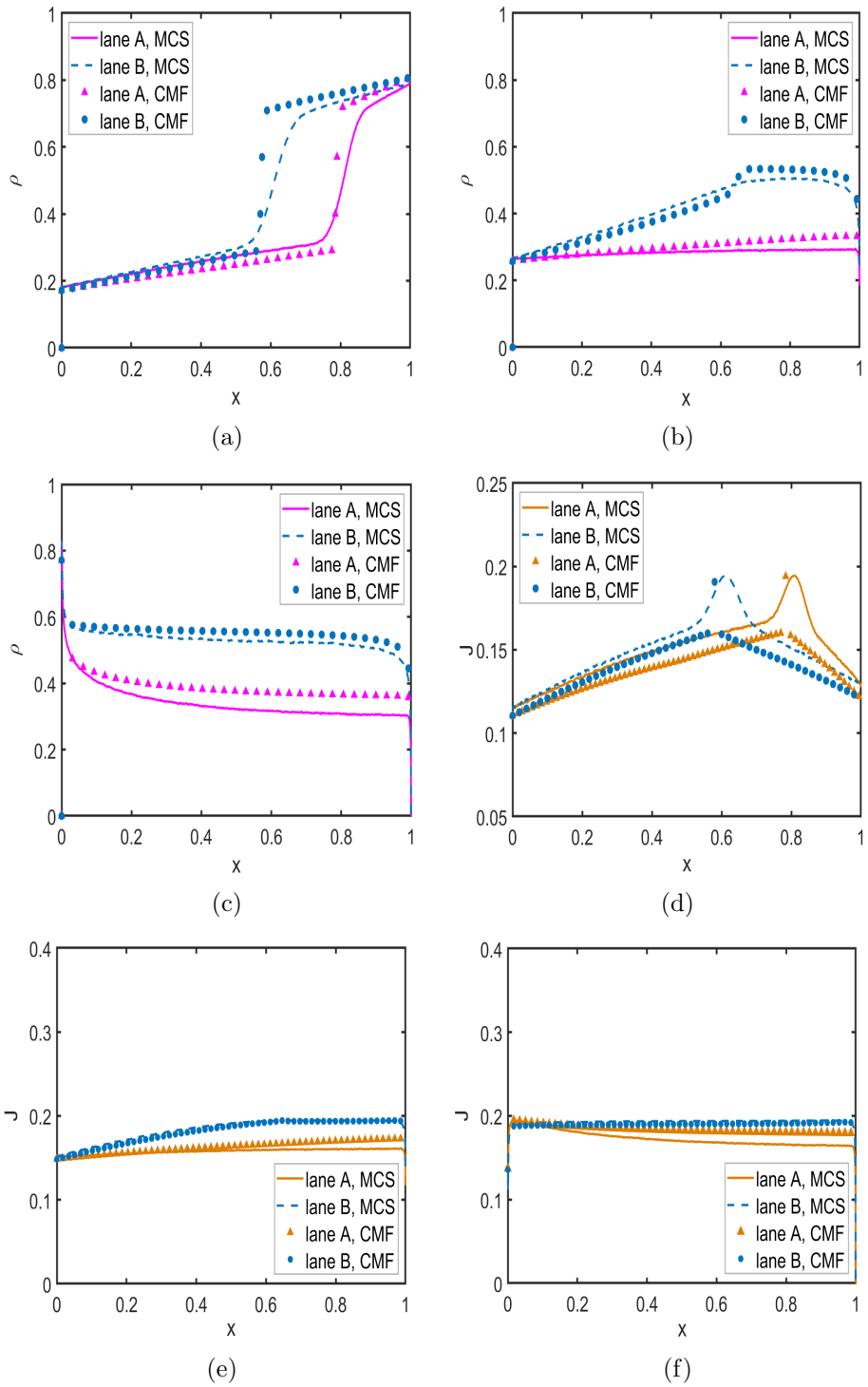

Figure 5.3: For $p_d = 1/3$, $k_+ = 0.4$, $k_- = 0.8$, $\Omega_a = 0.2$, $\Omega_{ad} = \Omega/2$, $\Omega_A = 0.8$, $\Omega_{AD} = \Omega_A/3$ and $L = 1000$ (a) (S, S) phase $\alpha = 0.2$, $\beta = 0.15$, (b) (LD, S) phase $\alpha = 0.3$, $\beta = 0.8$ and (c) (LD, HD) phase $\alpha = 0.9$, $\beta = 0.8$. Figures (d), (e) and (f) are the corresponding current profiles respectively.

(i) The phase diagram in present model is found to be qualitatively similar with the homogeneous model under fully asymmetric coupling conditions. The only difference is non appearance of (HD, HD) phase for given set of parameters which otherwise is observed for lower values of Ω_A. This observation can be justified as the effect of dynamic disorder in the lanes which leads to a relatively lower particle density in the lane A, in addition to particle shifting from lane A to lane B due to lane-changing rules and detachment due to LK dynamics. As a result, lane A does not have a region of high density in the phase plane.

(ii) Another difference is observed in the steady-state particle densities in the lanes. The density in different regions of phase diagram is found to be less in magnitude in comparison to the analogous model without disorder. This is attributed to the defects present randomly around the lattice which reduces bulk particle density in steady-state.

(b) K=3

The analytic methodology of utilizing numerical technique on mean-field equations is universal and appropriate for any value of K. Now, we discuss the steady-state dynamics for a case of unequal attachment and detachment rates, $\Omega_a \neq \Omega_d$, giving $K \neq 1$. We particularly discuss the case of value of binding constant $K = 3$. Figure 5.4 represents the phase diagram for $\Omega_a = 0.2$, $\Omega_{ad} = \Omega_a/2$, $\Omega_A = 0.8$, $\Omega_{AD} = \Omega_A/3$, $k_+ = 0.4$ and $k_- = 0.8$. On comparing the steady-state phase diagrams for $K = 1$ (Fig. 5.2) with $K = 3$ (Fig. 5.4), the following inferences can be drawn.

(i) Upon increasing K, the number of stationary-state phases remains the same in phase-plane while (LD, HD) phase expands.

(ii) The magnitude of particle density in each lane increases with an increase in value of K. This observation can be attributed to more particles attaching to each lane at higher value of K, as we have $\Omega_a = 3\Omega_d$ for $K = 3$.

5.6.1 Effect of lane-changing rate

The coupling strength has been a key parameter in studying a two-channels system, so it is essential to explore its role in our model also. It has been reported in literature that the higher values of lane-changing rates does not significantly affect the steady system dynamics of a two-channel TASEP, under symmetric coupling,

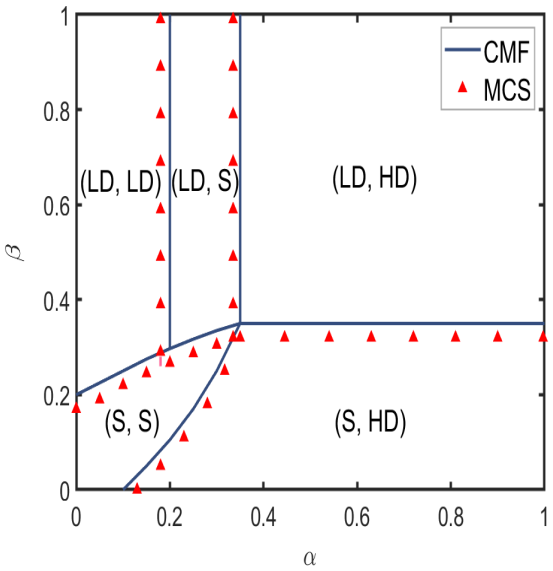

Figure 5.4: Steady-state phase diagram with five different phases for $k_+ = 0.4$, $k_- = 0.8$, $p_d = 1/3$, $K = 3$, $\Omega_a = 0.2$, $\Omega_{ad} = \Omega_a/2$, $\Omega_A = 0.8$ and $\Omega_{AD} = \Omega_A/3$.

with or without LK or inhomogeneity. Here, system de-couples in two-independent analogous single-channel TASEPs. Whereas, the case is different in our model due to presence of dynamic inhomogeneity. So, we explore the effect of strength of coupling on the steady-state dynamics of our suggested model under different values of binding constant.

(a) K=1

The exploration begins for different values of lane-changing rate from lane A to B i.e., Ω_A, while keeping other parameter values fixed. On increasing Ω_A, one of the noticeable observations is elimination of a few steady-state phases. Figure 5.5 shows the steady-state phase diagram for $\Omega_A = 80$ with only four phases. One can see elimination of (LD, LD) region in the phase-plane in comparison to fig. 5.2. Due to an increase in the value of Ω_A, more number of particles shift from lane A to lane B leading to a corresponding decrease (increase) in particle density in lane A (B). Therefore, due to a significant increase in particle density in lane B, it will no longer exhibits in LD phase and the (LD, LD) phase does not exists anymore. The shifting of particle from lane A to lane B at a higher order increases the density difference between the two lanes in steady-state. As a consequence, there is an expansion in the (LD, HD) region and shrinkage of all other remaining phases.

For $\Omega_A = 800$, a shift in the phase boundaries of different regions is noticed

where (S, S), (LD, S) and (S, HD) are confined to even small area in phase-plane. This happens due to higher order lane-changing rate which significantly decreases (increases) the particle density in lane A (B). For more higher values of Ω_A, the phase diagram is found to consist of (LD, HD) phase only. We skip providing phase diagrams for higher values of Ω_A.

In contrast, the proposed model has been investigated for lower values of lane-changing rate as well. It is observed that the phase diagram appears to be comparatively similar to that in single-lane ddTASEP with LK for $\Omega_A = 0.2$ (discussed in chapter 4). This can be physically explained as the system with lower values of lane-changing rates behaves like two parallel uncoupled ddTASEPs with LK which is the model studied thoroughly in the previous chapter.

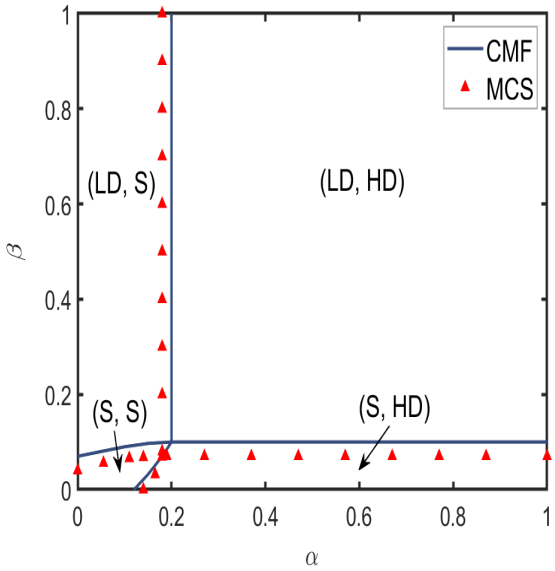

Figure 5.5: Phase diagram for $p_d = 1/3$, $k_+ = 0.4$, $k_- = 0.8$, $\Omega_a = 0.2$, $\Omega_{ad} = \Omega/2$, $\Omega_A = 80$, $\Omega_{AD} = \Omega_A/3$ and $L = 1000$.

Another lane-changing parameter involved in the system is Ω_{AD}, denoting lane-changing rate when defect is present at target site. Till now, the lane-changing rate in the presence of a defect at target site is taken as one-third of the lane-changing rate in absence of a defect at target site. Now, the effect of variation in magnitude of Ω_{AD} has been studied for three different cases: $\Omega_{AD} = \Omega_A/3$, $\Omega_A/2$ and $3\Omega_A/4$. Upon increasing the value of Ω_{AD} from $\Omega_A/3$ to $3\Omega_A/4$, the magnitude of density in lane A (B) decreases (increases). Further, the shock in the system moves towards right (left) along the lattice for lane A (B). This can be justified as an increase in the value of Ω_{AD}, more particles tend to shift from lane A to B which results in

shortage (excess) of particles in lane A (B).

(b) K=3

To investigate the effect of lane-changing rate, the stationary-state behavior of the system has been analyzed for another values of binding constant $K = 3$. Upon an increase in Ω_A, one significant observation is an increase in magnitude of difference between densities of lane A and lane B. However qualitatively the steady-state phase diagram remains the same. This observation is analogous to the one observed for $K = 1$. Moreover, the effect of lane-changing rate in the presence of defect at target site, Ω_{AD}, in steady-state is found to be similar as observed for $K = 1$.

5.6.2 Effect of Langmuir kinetics

Another parameter playing crucial role in controlling steady-state behavior of the TASEP model with LK is particle attachment rate Ω_a. Till this point, we have discussed effect of system parameters for a fixed value of attachment rate $\Omega_a = 0.2$. In order to investigate the steady-state behavior of the proposed model, we wish to analyze the effect of varying kinetic rates on the phase diagrams.

(a) K=1

Since this section explains system dynamics for $K = 1$, the effect of particle attachment rate is equivalent to particle detachment rate Ω_d. Upon increasing Ω_a, the non-conserving dynamics dominate whereas the effect of fully asymmetric coupling weakens in the steady-state of system. For large values of Ω_a, system can be thought as the one with almost no particle lane-changing. The more attachment of particles in both the lanes almost prohibits them to shift from lane A to lane B.

The steady-state of the system is observed for different values of attachment rate. For $\Omega_a = 2$ and keeping other system parameters the same, the topology of phase diagram changes. The phase diagram is observed to be qualitatively similar as in single-lane ddTASEP with LK (see fig. 4.10(b)). The only evident is a minor difference in particle densities in both lanes occurring due to negligible effect of asymmetric coupling.

On further increase in the value of $\Omega_a = 20$, the particle densities in both the lanes becomes equal leaving behind only (LD, LD) phase in the phase diagram. For higher values of Ω_a, the lane changing occurs negligibly whereas the LK dynamics dominate. The identical particle hopping rates in both lanes give rise to equal particle densities in each lane. Figure 5.6 shows a density profile for $\Omega_a = 20$,

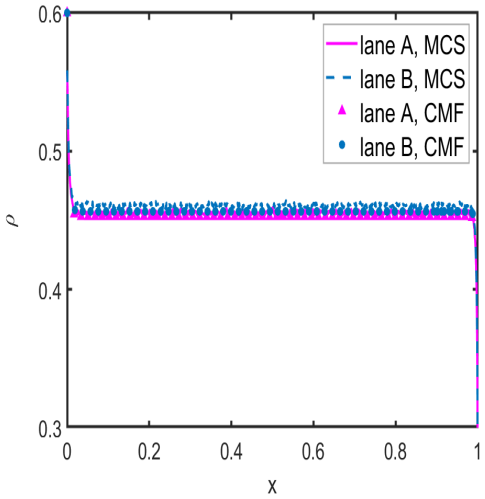

Figure 5.6: Density profile for $\alpha = 0.7$, $\beta = 0.7$, $p_d = 1/3$, $k_+ = 0.4$, $k_- = 0.8$, $\Omega_a = 20$, $\Omega_{ad} = \Omega/2$, $\Omega_A = 0.8$, $\Omega_{AD} = \Omega_A/3$ and $L = 1000$.

$\Omega_A = 0.8$ in which the value of particle density remains constant ($\rho \approx 0.4537$) throughout the plane. A similar effect continues for higher values of attachment rate $\Omega_a = 200$.

To study the effect of asymmetric coupling with increasing non-conserving rates, the steady-state behavior is examined for higher values of lane-changing and attachment rate. In particular, it has been observed that for $\Omega_a = 20$ and $\Omega_A = 80$, the density difference between two lanes increases leading to only (LD, HD) phase in the steady-state. Also, the bulk particle density remains constant throughout.

(b) K=3

Analogous to the investigation of effect of lane-changing rate, the present model is analysed for case $K \neq 1$ for the effect of Langmuir kinetic. For $\Omega_a = 2$ while keeping other set of parameter fixed, the phase diagram is found to be similar to that of one-lane ddTASEP with LK. A further increase in Ω_a ($\Omega_a = 20$), it has been found that the particle densities in both the lanes become equal and the phase diagram consist of (HD, HD) phase only. The density remains constant throughout the bulk with an approximate value of $\rho \approx 0.7105$ for given parameters. An increase in the particle density might be due to more number of particles getting attached to the lattice, as a result the particles stay for a longer time on the lattice. Similar trend continues for higher value of attachment rate Ω_a.

5.6.3 Current analysis

Figure 5.7 shows current-density relation (CDR) for defect density $\rho_d = 1/2$ and $\rho_d = 3/4$ respectively. Qualitatively, the fundamental diagram remains the same as for standard one-lane TASEP. The curve is found to be symmetric about $\rho = 1/2$. Further, the effect of defect strength p_d on particle current J has been examined. For $p_d = 1$, dynamic defects are the weakest as forward hopping rate remains constant in the bulk and hence for $p_d = 1$ (pink solid line) the CDR turns out to be same as in standard TASEP with $J_{max} = 1/4$. Despite of presence of dynamic defects, their influence on particle hopping at $p_d = 1$ is insignificant.

On comparing fig. 5.7(a) with fig. 5.7(b), it can be seen that with an increase in defect density from 1/2 to 3/4, the maximum current is reduced in the system for any given value of p_d. Additionally, the effect of variation in defect strength is examined and it is observed that with a decrease in value of p_d from 1 to 0, the defects become stronger causing more hindrance in the forward hopping of particles, which further decreases flow rate in the steady-state.

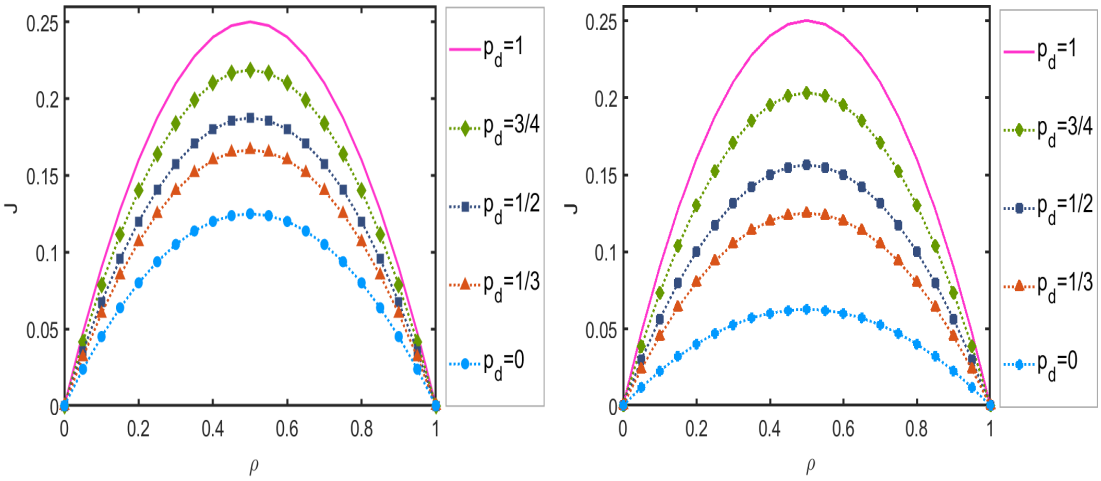

Figure 5.7: Current J as a function of particle density ρ for different values of slow hopping rate p_d. (a)$\rho_d = 0.5$ for $k_+ = 0.4$, $k_- = 0.4$ and (b)$\rho_d = 0.75$ for $k_+ = 0.6$, $k_- = 0.2$, and varying p_d.

Figure 5.8 shows the plot for particle current J as a function of defect strength p_d. For $\alpha = 0.8$, $\beta = 0.8$, $K = 1$, $\Omega_a = 0.2$, $\Omega_A = 0.8$ at middle of the lattice $(L/2)$ in lane A, J has been plotted by varying p_d between 0 to 1. As explained earlier, with an increase in value of p_d, the defects are weakening in strength, leading to an increase in J. As $p_d = 1$, J reaches its maximum value i.e., 0.24 (< 0.25). The

maximal current in the system is less than that of standard TASEP because of asymmetric lane-changing rates which reduces particle density in lane A. Further, the effect of defect density (ρ_d) on J is examined and found that with an increase in defect density (ρ_d), the current (J) decreases in the steady-state of the system. For any value of k_+ with $k_- = 0$, the defect density $\rho_d = k_+/(k_+ + k_-) = 1$. Here defects are not unbinding from the lattice, leading to a significant decrease in particle density in the lane. Hence, leading to a maximal current of only 0.12 in the steady-state of the system.

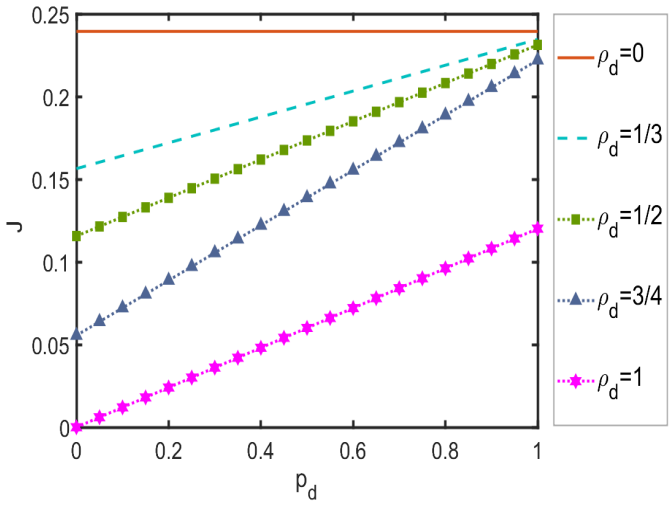

Figure 5.8: Current (J) as a function of defect strength (p_d) for $L = 1000$, $\alpha = 0.8$, $\beta = 0.8$, $\Omega_a = 0.2$, $\Omega_A = 0.8$, $K = 1$, $x = L/2$ and varying defect density ρ_d.

Figure 5.9 represents current J as a function of defect strength p_d for different values of K. An increase in K signifies more attachment of particles as compared to detachment which leads to high density on the lattice. This further results into reduction of free flow of particles, hence steady-state current decreases.

5.7 Conclusion

In this chapter, a detailed study of two-lane dynamically disordered exclusion process with Langmuir kinetics under symmetric as well as asymmetric coupling environment has been presented. Under symmetric coupling conditions, the two-lane ddTASEP with LK behaves similar to its analogue in one-lane. The symmetric coupling rates cancel lane-changing source term with sink term leaving behind two uncoupled ddTASEPs with LK. In the case of fully asymmetric coupling, the system is studied for two different values of binding constant ($K = 1$ and $K = 3$).

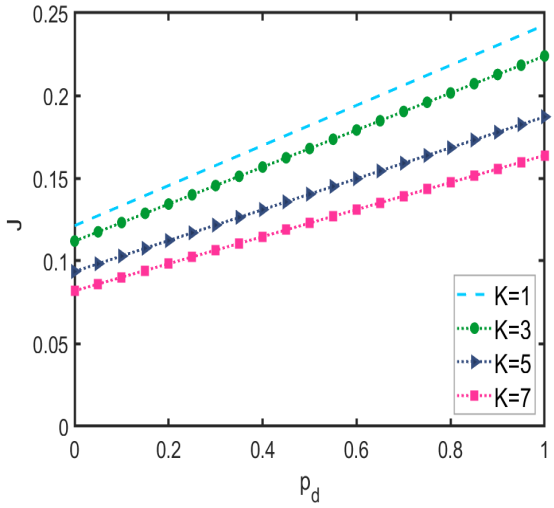

Figure 5.9: Current (J) as a function of defect strength (p_d) for $L = 1000$, $\alpha = 0.8$, $\beta = 0.8$, $\Omega_a = 0.2$, $\Omega_A = 0.8$, $K = 1$, $x = L/2$ and varying binding constant K.

A rich composition of phase diagram comprising five distinct phases is obtained. It is found that with an increase in lane-changing rate the number of steady-state phases reduces.

The fundamental diagram has been explored in order to investigate the effect of defect binding and unbinding constants. It is found that the maximum current in the system reduces with an increasing defect density. Further, the effect of attachment rate Ω_a has been studied and it is observed that for higher values of Ω_a, the effect of coupling between two lanes weakens whereas the the effect of LK dominates. These findings are observed for both the values of K.

To conclude, studying the interplay between Langmuir kinetics and coupling in lanes in the presence of dynamic disorder is important to get insight about real life transport processes. The observations in this study are also validated by performing extensive Monte Carlo simulation.

Chapter 6

Conclusion

In real-world transportation- either on roads or in living cells, of the greater concern in this century is the problem of congestion. The increasing population is one of the main causes of traffic congestion on the roadways. Scientists today are putting together constant efforts to deal with the growing congestion in this crowded world. The main goal of traffic engineers, physicists, and mathematicians from all over the globe is to create a smooth and efficient transport system. Analogous to vehicular transport, the problem of congestion also exists in natural biological transport occurring in living cells. The particular problem of congestion caused by dynamic defects is challenging to explore in transport systems.

The focus of this thesis is to interpret the complex inhomogeneous transport systems with dynamic disorder. Basically, we are interested in characterizing the collective features of such systems which are a particular type of non-equilibrium system. ASEP is considered to be the simplest and paradigmatic lattice gas model to investigate non-equilibrium driven diffusive systems in which the system particles represent the vehicles or motor proteins. Particularly, the systems with open boundaries have been considered where particles enter with a rate α from the left and exit with a rate β. The particles obey hard-core exclusion principle which prevents more than two particles from occupynig same lattice site. There also exists dynamic defects in the system which can stochastically bind and un-bind from a lattice site at certain rates.

The whole thesis revolve around studying the role of dynamic disorder in single-channel as well as two-channel ASEPs with and without LK. For theoretical investigation, we have adopted simple mean-field approximation theory and its variant-vertical cluster mean-field theory to derive continuum master equations. We have solved continuum equations using finite difference numerical scheme. To further validate the theoretical findings, we have run extensive Monte Carlo simulation us-

ing random sequential update rule which shows a good agreement with theoretical findings.

6.1 Summary of results

The very first model studied in this thesis is a two-channel exclusion process with site-wise dynamic disorder under symmetric (2) and asymmetric coupling environment (3). This study is an addition to the literature on disordered systems by analyzing a general coupled TASEP model. The dynamic defects follow unconstrained dynamics, which allows a defect to bind to a lattice site irrespective of particle presence. The model presented here well explains the biological process of gene transcription where the DNA-bound proteins act as a defect for transcription and slow down the RNA-polymerase. It has been discovered that under symmetric coupling conditions, the lane-changing source terms cancel with sink terms in the mean-field equations. This preserves the topology of the phase diagram of single-channel ddTASEP. Based on the investigation, we found a rich topology of the stationary-state phase diagram under distinct defect binding-unbinding rates. A thorough analysis has been performed for large system sizes which results in no finite-size effect in stationary state.

In chapter 3, we have derived phase diagrams and density profiles in steady-state of the model under fully asymmetric coupling environment. The system maps onto an effective one-channel exclusion process with dynamic disorder and exhibits rich phase diagram. The steady state phase boundaries depend upon a variation in defect density over the lattice. We have identified that horizontal transitions in the lanes have a significant influence on stationary behavior of the system which otherwise is observed to be independent of variation in magnitude of non-zero lane-transition rate. We made an attempt to yield a comprehensive depiction of the stationary behavior of a disordered two-channel exclusion process.

The second issue addressed in this thesis comprises the inclusion of Langmuir kinetics (LK) into a dynamically disordered TASEP model (4). LK dynamics allow particles to get attach to and detach from lattice bulk. The inclusion of LK, inspite of adding more realism into the model, brings along many mathematical challenges as well. The analysis is explicitly classified for two different values of binding constant (K). The competing interplay between dynamic disorder and LK discovers various non-equilibrium phenomena like phase coexistence and appearance of localised shock which otherwise are not found in ddTASEPs without LK.

The shock dynamics have been explored by varying defect density and the defect strength.

In chapter 5, we study the role played by dynamic disorder in a coupled two-channel exclusion process with LK. The model is inspired from real transport situation like periodic switching of traffic lights on roads and stochastic binding of motor proteins (namely histones) to microtubule. Further, the varying vehicle (motor protein) speed while changing its lane on highways (microtubule) encourages us to consider two different couplings- symmetric and asymmetric environments. Under symmetric coupling conditions, the two-lane ddTASEP with LK behaves similar to its analogue in one-lane. The symmetric coupling rates cancel lane-changing source term with sink term leaving behind two uncoupled ddTASEPs with LK. Under fully asymmetric coupling environment, the system is studied for two different values of binding constant $K = 1$ and $K = 3$. A rich composition of phase diagram comprising of five distinct phases is obtained. It has been observed that with an increase in lane-changing rate the number of steady-state phases reduces and the density difference between two lanes increases. The current-density relation has been explored to analyze the effect of defect dynamics. It is found that the maximum current in the system reduces with an increase in defect density. Further, it has been observed that for higher values of Ω_a, the effect of coupling between two lanes weakens whereas the effect of LK dominates. These findings are observed for both the values of K.

To our best efforts, we have attempted to capture the vital physical phenomena revealed by dynamically disordered transport systems, yet we still have an open room for advanced investigation. We hope to have conclusively described a strong relation between transport processes and statistical mechanics.

6.2 Future scope

Needless to say, in the studied models, we have overlooked some features of stochastic transport in complex systems. In particular, the dyynamical rules defined for our models does not fully capture the complexity of the interaction between vehicles on roads and molecular motors. It is possible to move towards incorporating particle-particle interactions into the models covered in this thesis and investigate the impact of particle-defect interactions also. A few studies [109, 110], in this direction, have been able to more realistically describe the transport systems. Another important aspects to take into consideration is an extended feature of particle

attach-detach effect termed as extended Langmuir kinetics (eLK) [111]. In eLK, the particle interactions are considered depending upon occupancy at lattice sites. The cluster mean-field theory might be easily implemented to analyse a more general disordered system in multi-lane TASEP and also to explore some rich dynamics in steady-state. We suspect to encounter more complex and informative stationary dynamics of the suggested phenomena. In this thesis, we focused on disordered TASEP models with open boundary conditions. The mean-field approach might be employed to explore some broad disordered systems under periodic boundaries which are known to exhibit generous properties in stationary state. Apart from these, one can think in other directions of more complex features and characteristics such as finite reservoir and transport on networks. Statistical physicists, traffic engineers are intrigued and immensely involved in exploring these vast areas of the field.

Bibliography

[1] Leah B Shaw, RKP Zia, and Kelvin H Lee. Totally asymmetric exclusion process with extended objects: a model for protein synthesis. *Physical Review E*, 68(2):021910, 2003.

[2] Kai Nagel. Particle hopping models and traffic flow theory. *Physical review E*, 53(5):4655, 1996.

[3] Carolyn T MacDonald, Julian H Gibbs, and Allen C Pipkin. Kinetics of biopolymerization on nucleic acid templates. *Biopolymers: Original Research on Biomolecules*, 6(1):1–25, 1968.

[4] Debashish Chowdhury, Ludger Santen, and Andreas Schadschneider. Statistical physics of vehicular traffic and some related systems. *Physics Reports*, 329(4-6):199–329, 2000.

[5] Victor J Blue and Jeffrey L Adler. Emergent fundamental pedestrian flows from cellular automata microsimulation. *Transportation Research Record*, 1644(1):29–36, 1998.

[6] David Chandler and Jerome K Percus. Introduction to modern statistical mechanics. *Physics Today*, 41(12):114–118, 1988.

[7] Debashish Chowdhury, Ludger Santen, and Andreas Schadschneider. Statistical physics of vehicular traffic and some related systems. *Physics Reports*, 329(4):199 – 329, 2000.

[8] V. Balakrishnan. *Elements of Nonequilibrium Statistical Mechanics*.

[9] JW Gibbs. Elementary principles in statistical mechanics; courier corporation: North chelmsford, ma, usa, 2014.

[10] Andreas Schadschneider, Debashish Chowdhury, and Katsuhiro Nishinari. *Stochastic transport in complex systems: from molecules to vehicles*. Elsevier, 2010.

[11] Vladislav Popkov and Gunter M Schütz. Steady-state selection in driven diffusive systems with open boundaries. *EPL (Europhysics Letters)*, 48(3):257, 1999.

[12] Vladimir Privman. *Nonequilibrium statistical mechanics in one dimension*. Cambridge University Press, 1997.

[13] Michael Plischke and Birger Bergersen. *Equilibrium statistical physics*. World scientific, 1994.

[14] Robert Zwanzig. *Nonequilibrium statistical mechanics*. Oxford university press, 2001.

[15] Carolyn T MacDonald and Julian H Gibbs. Concerning the kinetics of polypeptide synthesis on polyribosomes. *Biopolymers: Original Research on Biomolecules*, 7(5):707–725, 1969.

[16] Andreas Schadschneider. Traffic flow: a statistical physics point of view. *Physica A: Statistical Mechanics and its Applications*, 313(1-2):153–187, 2002.

[17] Manfred Schliwa and Günther Woehlke. Molecular motors: Switching on kinesin. *Nature*, 411(6836):424, 2001.

[18] Tom Chou and Greg Lakatos. Clustered bottlenecks in mrna translation and protein synthesis. *Physical review letters*, 93(19):198101, 2004.

[19] Reinhard Lipowsky, Janina Beeg, Rumiana Dimova, Stefan Klumpp, and Melanie J.I. Müller. Cooperative behavior of molecular motors: Cargo transport and traffic phenomena. *Physica E: Low-dimensional Systems and Nanostructures*, 42(3):649–661, 2010.

[20] Henry Hess and Viola Vogel. Molecular shuttles based on motor proteins: active transport in synthetic environments. *Reviews in Molecular Biotechnology*, 82(1):67–85, 2001.

[21] Julian H Gibbs. The kinetics of biopolymerization on nucleic acid templates. *Stochastic Processes in Chemical Physics*, 30:185, 2009.

[22] Jonathon Howard and RL Clark. Mechanics of motor proteins and the cytoskeleton. *Appl. Mech. Rev.*, 55(2):B39–B39, 2002.

[23] Anna-Lena Ström, Jozsef Gal, Ping Shi, Edward J Kasarskis, Lawrence J Hayward, and Haining Zhu. Retrograde axonal transport and motor neuron disease. *Journal of neurochemistry*, 106(2):495–505, 2008.

[24] K Schindowski, K Belarbi, and L Buee. Neurotrophic factors in alzheimer's disease: role of axonal transport. *Genes, brain and behavior*, 7:43–56, 2008.

[25] Sheldon Katz, Joel L Lebowitz, and Herbert Spohn. Nonequilibrium steady states of stochastic lattice gas models of fast ionic conductors. *Journal of statistical physics*, 34(3-4):497–537, 1984.

[26] Bruce Alberts. *Molecular biology of the cell*. Garland science, 2017.

[27] Anthony W Leung. *Systems of nonlinear partial differential equations: applications to biology and engineering*, volume 49. Springer Science & Business Media, 2013.

[28] Bernard Derrida, MR Evans, and David Mukamel. Exact diffusion constant for one-dimensional asymmetric exclusion models. *Journal of Physics A: Mathematical and General*, 26(19):4911, 1993.

[29] Bernard Derrida, Eytan Domany, and David Mukamel. An exact solution of a one-dimensional asymmetric exclusion model with open boundaries. *Journal of Statistical Physics*, 69(3-4):667–687, 1992.

[30] Anatoly B Kolomeisky, Gunter M Schütz, Eugene B Kolomeisky, and Joseph P Straley. Phase diagram of one-dimensional driven lattice gases with open boundaries. *Journal of Physics A: Mathematical and General*, 31(33):6911, 1998.

[31] Maury Bramson. Front propagation in certain one-dimensional exclusion models. *Journal of Statistical Physics*, 51(5):863–869, 1988.

[32] Steven A Janowsky and Joel L Lebowitz. Exact results for the asymmetric simple exclusion process with a blockage. *Journal of Statistical Physics*, 77(1-2):35–51, 1994.

[33] Goutam Tripathy and Mustansir Barma. Steady state and dynamics of driven diffusive systems with quenched disorder. *Physical review letters*, 78(16):3039, 1997.

[34] G Schütz and E Domany. Phase transitions in an exactly soluble one-dimensional exclusion process. *Journal of statistical physics*, 72(1-2):277–296, 1993.

[35] Bernard Derrida and MR Evans. Bethe ansatz solution for a defect particle in the asymmetric exclusion process. *Journal of Physics A: Mathematical and General*, 32(26):4833, 1999.

[36] Gunter M Schütz. Exactly solvable models for many-body systems far from equilibrium. In *Phase transitions and critical phenomena*, volume 19, pages 1–251. Elsevier, 2001.

[37] Bernard Derrida, Martin R Evans, Vincent Hakim, and Vincent Pasquier. Exact solution of a 1d asymmetric exclusion model using a matrix formulation. *Journal of Physics A: Mathematical and General*, 26(7):1493, 1993.

[38] Richard A Blythe and Martin R Evans. Nonequilibrium steady states of matrix-product form: a solver's guide. *Journal of Physics A: Mathematical and Theoretical*, 40(46):R333, 2007.

[39] Joachim Krug. Boundary-induced phase transitions in driven diffusive systems. *Physical review letters*, 67(14):1882, 1991.

[40] Paolo Pierobon, Mauro Mobilia, Roger Kouyos, and Erwin Frey. Bottleneck-induced transitions in a minimal model for intracellular transport. *Physical Review E*, 74(3):031906, 2006.

[41] Michael Kastner. Monte carlo methods in statistical physics: Mathematical foundations and strategies. *Communications in Nonlinear Science and Numerical Simulation*, 15(6):1589–1602, 2010.

[42] Kurt Binder, Dieter W Heermann, and K Binder. *Monte Carlo simulation in statistical physics*, volume 8. Springer, 1992.

[43] David J Earl and Michael W Deem. Monte carlo simulations. *Molecular modeling of proteins*, pages 25–36, 2008.

[44] Gordon D Smith, Gordon D Smith, and Gordon Dennis Smith Smith. *Numerical solution of partial differential equations: finite difference methods*. Oxford university press, 1985.

[45] Philip Greulich, Luca Ciandrini, Rosalind J Allen, and M Carmen Romano. Mixed population of competing totally asymmetric simple exclusion processes with a shared reservoir of particles. *Physical Review E*, 85(1):011142, 2012.

[46] Tobias Reichenbach, Erwin Frey, and Thomas Franosch. Traffic jams induced by rare switching events in two-lane transport. *New Journal of Physics*, 9(6):159, 2007.

[47] Anna Melbinger, Tobias Reichenbach, Thomas Franosch, and Erwin Frey. Driven transport on parallel lanes with particle exclusion and obstruction. *Physical Review E*, 83(3):031923, 2011.

[48] Rui Jiang, Katsuhiro Nishinari, Mao-Bin Hu, Yong-Hong Wu, and Qing-Song Wu. Phase separation in a bidirectional two-lane asymmetric exclusion process. *Journal of Statistical Physics*, 136:73–88, 2009.

[49] Qi-Hong Shi, Rui Jiang, Mao-Bin Hu, and Qing-Song Wu. Strong asymmetric coupling of multilane paseps. *Physics Letters A*, 376(40-41):2640–2644, 2012.

[50] Rui Jiang, Mao-Bin Hu, Yong-Hong Wu, and Qing-Song Wu. Weak and strong coupling in a two-lane asymmetric exclusion process. *Physical Review E*, 77(4):041128, 2008.

[51] Ekaterina Pronina and Anatoly B Kolomeisky. Spontaneous symmetry breaking in two-channel asymmetric exclusion processes with narrow entrances. *Journal of Physics A: Mathematical and Theoretical*, 40(10):2275, 2007.

[52] Martin R Evans, Yariv Kafri, Kate EP Sugden, and Julien Tailleur. Phase diagrams of two-lane driven diffusive systems. *Journal of Statistical Mechanics: Theory and Experiment*, 2011(06):P06009, 2011.

[53] Tetsuya Mitsudo and Hisao Hayakawa. Synchronization of kinks in the two-lane totally asymmetric simple exclusion process with open boundary conditions. *Journal of Physics A: Mathematical and General*, 38(14):3087, 2005.

[54] Vandana Yadav, Rajesh Singh, and Sutapa Mukherji. Phase-plane analysis of driven multi-lane exclusion models. *Journal of Statistical Mechanics: Theory and Experiment*, 2012(04):P04004, 2012.

[55] Richard J Harris and RB Stinchcombe. Ideal and disordered two-lane traffic models. *Physica A: statistical mechanics and its applications*, 354:582–596, 2005.

[56] Qing-Yi Hao, Rui Jiang, Chao-Yun Wu, Ning Guo, Bing-Bing Liu, and Yunxin Zhang. Theoretical analysis and computer simulation of dynamic processes for a driven diffusive two-lane system. *Physical Review E*, 98(6):062111, 2018.

[57] Vladislav Popkov and Ingo Peschel. Symmetry breaking and phase coexistence in a driven diffusive two-channel system. *Physical Review E*, 64(2):026126, 2001.

[58] Ekaterina Pronina and Anatoly B Kolomeisky. Two-channel totally asymmetric simple exclusion processes. *Journal of Physics A: Mathematical and General*, 37(42):9907, 2004.

[59] Ekaterina Pronina and Anatoly B Kolomeisky. Asymmetric coupling in two-channel simple exclusion processes. *Physica A: Statistical Mechanics and its Applications*, 372(1):12–21, 2006.

[60] Konstantinos Tsekouras and AB Kolomeisky. Parallel coupling of symmetric and asymmetric exclusion processes. *Journal of Physics A: Mathematical and Theoretical*, 41(46):465001, 2008.

[61] Arvind Kumar Gupta and Isha Dhiman. Coupling of two asymmetric exclusion processes with open boundaries. *Physica A: Statistical Mechanics and its Applications*, 392(24):6314–6329, 2013.

[62] Vladislav Popkov and Gunter M Schütz. Shocks and excitation dynamics in a driven diffusive two-channel system. *Journal of statistical physics*, 112:523–540, 2003.

[63] Yu-Qing Wang, Rui Jiang, Anatoly B Kolomeisky, and Mao-Bin Hu. Bulk induced phase transition in driven diffusive systems. *Scientific Reports*, 4(1):5459, 2014.

[64] Zhong-Pan Cai, Yao-Ming Yuan, Rui Jiang, Mao-Bin Hu, Qing-Song Wu, and Yong-Hong Wu. Asymmetric coupling in multi-channel simple exclusion processes. *Journal of Statistical Mechanics: Theory and Experiment*, 2008(07):P07016, 2008.

[65] Rui Jiang, Ruili Wang, and Qing-Song Wu. Two-lane totally asymmetric exclusion processes with particle creation and annihilation. *Physica A: Statistical Mechanics and its Applications*, 375(1):247–256, 2007.

[66] Isha Dhiman and Arvind Kumar Gupta. Effect of coupling strength on a two-lane partially asymmetric coupled totally asymmetric simple exclusion process with langmuir kinetics. *Physical Review E*, 90(1):012114, 2014.

[67] Arvind Kumar Gupta and Isha Dhiman. Asymmetric coupling in two-lane simple exclusion processes with langmuir kinetics: Phase diagrams and boundary layers. *Physical Review E*, 89(2):022131, 2014.

[68] Ruili Wang, Rui Jiang, Mingzhe Liu, Jiming Liu, and Qing-Song Wu. Effects of langmuir kinetics on two-lane totally asymmetric exclusion processes of molecular motor traffic. *International Journal of Modern Physics C*, 18(09):1483–1496, 2007.

[69] M Ebrahim Foulaadvand, Anatoly B Kolomeisky, and Hamid Teymouri. Asymmetric exclusion processes with disorder: Effect of correlations. *Physical Review E*, 78(6):061116, 2008.

[70] Isha Dhiman and Arvind Kumar Gupta. Collective dynamics of an inhomogeneous two-channel exclusion process: Theory and monte carlo simulations. *Journal of Computational Physics*, 309:227–240, 2016.

[71] Stefan Klumpp and Reinhard Lipowsky. Traffic of molecular motors through tube-like compartments. *Journal of Statistical Physics*, 113:233–268, 2003.

[72] A. Parmeggiani, T. Franosch, and E. Frey. Totally asymmetric simple exclusion process with langmuir kinetics. *Phys. Rev. E*, 70(4):046101, 2004.

[73] Vladislav Popkov, Attila Rákos, Richard D Willmann, Anatoly B Kolomeisky, and Gunter M Schütz. Localization of shocks in driven diffusive systems without particle number conservation. *Physical Review E*, 67(6):066117, 2003.

[74] Andrea Parmeggiani, Thomas Franosch, and Erwin Frey. Phase coexistence in driven one-dimensional transport. *Physical review letters*, 90(8):086601, 2003.

[75] Martin R Evans, Róbert Juhász, and Ludger Santen. Shock formation in an exclusion process with creation and annihilation. *Physical Review E*, 68(2):026117, 2003.

[76] Steven A Janowsky and Joel L Lebowitz. Finite-size effects and shock fluctuations in the asymmetric simple-exclusion process. *Physical Review A*, 45(2):618, 1992.

[77] Nikolay Mirin and Anatoly B Kolomeisky. Effect of detachments in asymmetric simple exclusion processes. *Journal of statistical physics*, 110(3-6):811–823, 2003.

[78] Sutapa Mukherji and Somendra M Bhattacharjee. Nonequilibrium criticality at shock formation in steady states. *Journal of Physics A: Mathematical and General*, 38(17):L285, 2005.

[79] Sutapa Mukherji and Vivek Mishra. Bulk and surface transitions in asymmetric simple exclusion process: Impact on boundary layers. *Physical Review E*, 74(1):011116, 2006.

[80] Isha Dhiman and Arvind Kumar Gupta. Two-channel totally asymmetric simple exclusion process with langmuir kinetics: The role of coupling constant. *Europhysics Letters*, 107(2):20007, 2014.

[81] Robert Juhasz. Weakly coupled, antiparallel, totally asymmetric simple exclusion processes. *Physical Review E*, 76(2):021117, 2007.

[82] Isha Dhiman and Arvind Kumar Gupta. Steady-state dynamics of an inhomogeneous two-channel tasep with langmuir kinetics. *International Journal of Modern Physics C*, 29(04):1850037, 2018.

[83] Isha Dhiman and Arvind Kumar Gupta. Origin and dynamics of a bottleneck-induced shock in a two-channel exclusion process. *Physics Letters A*, 380(24):2038–2044, 2016.

[84] Ruili Wang, Mingzhe Liu, and Rui Jiang. Local inhomogeneity in two-lane asymmetric simple exclusion processes coupled with langmuir kinetics. *Physica A: Statistical Mechanics and its Applications*, 387(2-3):457–466, 2008.

[85] Kang Qiu, Xianqing Yang, Wei Zhang, Dapeng Sun, and Yuemin Zhao. Density profiles in the totally asymmetric exclusion processes with both local inhomogeneity and langmuir kinetics. *Physica A: Statistical Mechanics and its Applications*, 373:1–10, 2007.

[86] Goutam Tripathy and Mustansir Barma. Driven lattice gases with quenched disorder: Exact results and different macroscopic regimes. *Physical Review E*, 58(2):1911, 1998.

[87] Philip Greulich and Andreas Schadschneider. Single-bottleneck approximation for driven lattice gases with disorder and open boundary conditions. *Journal of Statistical Mechanics: Theory and Experiment*, 2008(04):P04009, 2008.

[88] Yan Chai, Reinhard Lipowsky, and Stefan Klumpp. Transport by molecular motors in the presence of static defects. *Journal of Statistical Physics*, 135:241–260, 2009.

[89] Philip Greulich and Andreas Schadschneider. Phase diagram and edge effects in the asep with bottlenecks. *Physica A: Statistical Mechanics and its Applications*, 387(8-9):1972–1986, 2008.

[90] J Szavits-Nossan and K Uzelac. Totally asymmetric exclusion process with long-range hopping. *Physical Review E*, 74(5):051104, 2006.

[91] Bartlomiej Waclaw, Justyna Cholewa-Waclaw, and Philip Greulich. Totally asymmetric exclusion process with site-wise dynamic disorder. *Journal of Physics A: Mathematical and Theoretical*, 2019.

[92] Chikashi Arita, M Ebrahim Foulaadvand, and Ludger Santen. Signal optimization in urban transport: A totally asymmetric simple exclusion process with traffic lights. *Physical Review E*, 95(3):032108, 2017.

[93] Frank Jülicher and Robijn Bruinsma. Motion of rna polymerase along dna: a stochastic model. *Biophysical journal*, 74(3):1169–1185, 1998.

[94] Johan Paulsson. Models of stochastic gene expression. *Physics of life reviews*, 2(2):157–175, 2005.

[95] GM Schütz. Molecular motor traffic with a slow binding site. *Journal of Theoretical Biology*, 518:110644, 2021.

[96] JJ Dong, B Schmittmann, and RKP Zia. Towards a model for protein production rates. *Journal of Statistical Physics*, 128:21–34, 2007.

[97] Michael A Sørensen, CG Kurland, and Steen Pedersen. Codon usage determines translation rate in escherichia coli. *Journal of molecular biology*, 207(2):365–377, 1989.

[98] C Magnus Stenström, Haining Jin, Louise L Major, Warren P Tate, and Leif A Isaksson. Codon bias at the 3'-side of the initiation codon is correlated with translation initiation efficiency in escherichia coli. *Gene*, 263(1-2):273–284, 2001.

[99] Bruce Alberts, Alexander Johnson, Julian Lewis, Martin Raff, Keith Roberts, and Peter Walter. Molecular biology of the cell: Reference edition. 2007.

[100] Arvind Kumar Gupta and Isha Dhiman. Phase diagram of a continuum traffic flow model with a static bottleneck. *Nonlinear Dynamics*, 79(1):663–671, 2015.

[101] Charalambos Vlachopoulos, Michael O'Rourke, and Wilmer W Nichols. *McDonald's blood flow in arteries: theoretical, experimental and clinical principles*. CRC press, 2011.

[102] Tom Chou, K Mallick, and RKP Zia. Non-equilibrium statistical mechanics: from a paradigmatic model to biological transport. *Reports on progress in physics*, 74(11):116601, 2011.

[103] Francesco Turci, Andrea Parmeggiani, Estelle Pitard, M Carmen Romano, and Luca Ciandrini. Transport on a lattice with dynamical defects. *Physical Review E*, 87(1):012705, 2013.

[104] Mamata Sahoo, Jiajia Dong, and Stefan Klumpp. Dynamic blockage in an exclusion process. *Journal of Physics A: Mathematical and Theoretical*, 48(1):015007, 2014.

[105] Mamata Sahoo and Stefan Klumpp. Asymmetric exclusion process with a dynamic roadblock and open boundaries. *Journal of Physics A: Mathematical and Theoretical*, 49(31):315001, 2016.

[106] Qi-Hong Shi, Rui Jiang, Mao-Bin Hu, and Qing-Song Wu. Strong asymmetric coupling of two parallel exclusion processes. *Journal of Statistical Physics*, 142(3):616–626, 2011.

[107] Konstantinos Tsekouras and AB Kolomeisky. Inhomogeneous coupling in two-channel asymmetric simple exclusion processes. *Journal of Physics A: Mathematical and Theoretical*, 41(9):095002, 2008.

[108] Peter Wagner, Kai Nagel, and Dietrich E Wolf. Realistic multi-lane traffic rules for cellular automata. *Physica A: Statistical Mechanics and its Applications*, 234(3-4):687, 1997.

[109] Akriti Jindal, Anatoly B Kolomeisky, and Arvind Kumar Gupta. The role of dynamic defects in transport of interacting molecular motors. *Journal of Statistical Mechanics: Theory and Experiment*, 2020(4):043206, 2020.

[110] Akriti Jindal, Tripti Midha, and Arvind Kumar Gupta. Theoretical investigation of interacting molecular motors. In *Nonlinear Dynamics of Nanobiophysics*, pages 345–368. Springer, 2022.

[111] Hiroki Yamamoto, Shingo Ichiki, Daichi Yanagisawa, and Katsuhiro Nishinari. Two-lane totally asymmetric simple exclusion process with extended langmuir kinetics. *Physical Review E*, 105(1):014128, 2022.

Appendices

A

Since we know that in steady-state the system evolution is time independent and the time derivative term equates to zero. Therefore, eqn. (2.2) and (2.3) reduces to the following.

$$\alpha\langle(1-\tau_1)(1-\nu_1)\rangle - p\langle\tau_1(1-\tau_2)(1-\nu_2)\rangle - p_d\langle\tau_1(1-\tau_2)(1-\nu_2)\rangle = 0 \quad \text{(A.1)}$$

$$p\langle\tau_{L-1}(1-\tau_L)(1-\nu_L)\rangle + p_d\langle\tau_{L-1}(1-\tau_L)(\nu_L)\rangle - \beta\langle\tau_{L,j}\rangle = 0 \quad \text{(A.2)}$$

which reduces to the following

$$\alpha(1-\rho_1)(1-\rho_d) - p\rho_1(1-\rho_2)(1-\rho_d) - p_d\rho_1(1-\rho_2)(1-\rho_d) = 0 \quad \text{(A.3)}$$

$$p\rho_{L-1}(1-\rho_L)(1-\rho_d) + p_d\rho_{L-1}(1-\rho_L)(\rho_d) - \beta\rho_L = 0 \quad \text{(A.4)}$$

As we know $\rho_1 \approx \rho_2$ and $\rho_{L-1} \approx \rho_L$, hence we have

$$\rho_1(p(1-\rho_d) + p_d\rho_d) = \alpha(1-\rho_d) \quad \text{(A.5)}$$

$$(1-\rho_L)(p(1-\rho_d) + p_d\rho_d) = \beta \quad \text{(A.6)}$$

Hence, we get the expressions for particle density at the boundaries as

$$\rho_j(1) = \rho_1 = \frac{\alpha(1-\rho_d)}{p(1-\rho_d) + p_d\rho_d} \quad \text{(A.7)}$$

$$\rho_j(L) = \rho_L = 1 - \frac{\beta(1-\rho_d)}{p(1-\rho_d) + p_d\rho_d} \quad \text{(A.8)}$$

In the expression for current in eqn. (2.10)

$$J = \begin{bmatrix} (\frac{\epsilon}{2}p\rho_{dA} - \frac{\epsilon}{2}p - \frac{\epsilon}{2}p_d\rho_{dA})\frac{\partial\rho_A}{\partial x} & + & (p\rho_A - p\rho_A^2 - p\rho_{dA}\rho_A + p\rho_{dA}\rho_A^2 \\ & & +p_d\rho_{dA}\rho_A - p_d\rho_{dA}\rho_A^2) \\ (\frac{\epsilon}{2}p\rho_{dB} - \frac{\epsilon}{2}p - \frac{\epsilon}{2}p_d\rho_{dB})\frac{\partial\rho_B}{\partial x} & + & (p\rho_B - p\rho_B^2 - p\rho_{dB}\rho_B + p\rho_{dA}\rho_B^2 \\ & & +p_d\rho_{dB}\rho_B - p_d\rho_{dB}\rho_B^2) \end{bmatrix}$$

In the continuum limit, for a large system size (L), $\epsilon \to 0$ and the current in the system reduces to

$$J = \begin{bmatrix} (p\rho_A - p\rho_A^2 - p\rho_{dA}\rho_A + p\rho_{dA}\rho_A^2 + p_d\rho_{dA}\rho_A - p_d\rho_{dA}\rho_A^2) \\ (p\rho_B - p\rho_B^2 - p\rho_{dB}\rho_B + p\rho_{dA}\rho_B^2 + p_d\rho_{dB}\rho_B - p_d\rho_{dB}\rho_B^2) \end{bmatrix}$$

which further reduces to

$$J = [p(1-\rho_d) + p_d\rho_d]\rho_j(1-\rho_j), \text{ where j=A, B} \tag{A.9}$$

The eqn. (2.4) in steady-state reduces to the following expression.

$$k_+\langle 1-\nu_{i,j}\rangle - k_-\langle \nu_{i,j}\rangle = 0 \tag{A.10}$$

$$k_+(1-\rho_{d_{i,j}}) - k_-(\rho_{d_{i,j}}) = 0 \tag{A.11}$$

$$\rho_{d_{i,j}} = \frac{k_+}{k_+ + k_-} \tag{A.12}$$

B

The (0, LD) phase occurs for $\alpha_{eff} < \alpha_c$ and $\alpha_{eff} < \alpha^*$. Lets us first solve the inequality $\alpha_{eff} < \alpha_c$. We begin by substituting expressions on either side.

$$\frac{(\alpha X + X + p_d Y) - \sqrt{\big((\alpha X + X + p_d Y)^2 - 8\alpha X(X + p_d Y)\big)}}{2X} < \beta/X$$

$$\beta > \frac{(\alpha X + X + p_d Y) - \sqrt{\big((\alpha X + X + p_d Y)^2 - 8\alpha X(X + p_d Y)\big)}}{2} \tag{B.1}$$

The inequality $\alpha_{eff} < \alpha^*$, leads to

$$\frac{(\alpha X + X + p_d Y) - \sqrt{\big((\alpha X + X + p_d Y)^2 - 8\alpha X(X + p_d Y)\big)}}{2X} < 2J_{max}/X,$$

where $J_{max} = 7/36$, choosing X=2/3, Y=1/3

$$6((\alpha X + p_d Y) - X)^2 < 36((\alpha X + X + p_d Y)^2 - 8\alpha X(X + p_d Y))$$

$$X^2 - 12\alpha X^2 - 12 p_d XY < 36X^2 + 72\alpha X^2 + 72 p_d XY - 288\alpha X^2 - 288\alpha p_d XY$$

$$\alpha < \frac{35X + 84 p_d Y}{204X + 288 p_d Y}$$